LBL-13049
c.2

Lawrence Berkeley Laboratory

UNIVERSITY OF CALIFORNIA, BERKELEY

EARTH SCIENCES DIVISION

THE ROLES OF PORE PRESSURE AND FLUID FLOW IN THE HYDRAULIC FRACTURE PROCESS

Walter A. Palen and T.N. Narasimhan
(Ph.D. thesis)

June 1981

RECEIVED
LAWRENCE
BERKELEY LABORATORY

AUG 31 1981

LIBRARY AND
DOCUMENTS SECTION

TWO-WEEK LOAN COPY

This is a Library Circulating Copy which may be borrowed for two weeks. For a personal retention copy, call Tech. Info. Division, Ext. 6782

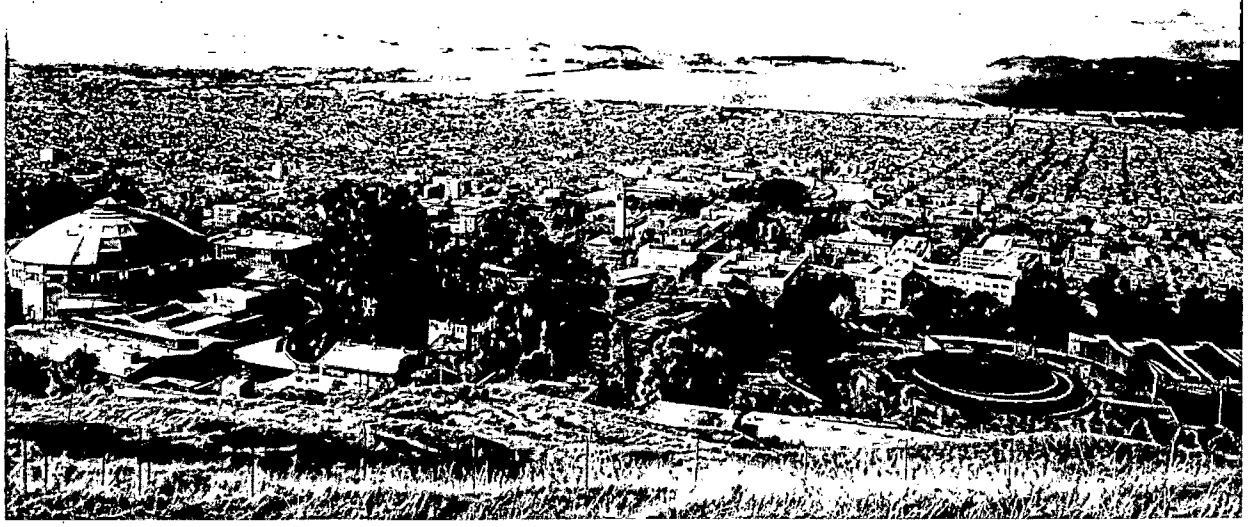

LBL-13049
c.2

Prepared for the U.S. Department of Energy under Contract W-7405-ENG-48

DISCLAIMER

This document was prepared as an account of work sponsored by the United States Government. While this document is believed to contain correct information, neither the United States Government nor any agency thereof, nor the Regents of the University of California, nor any of their employees, makes any warranty, express or implied, or assumes any legal responsibility for the accuracy, completeness, or usefulness of any information, apparatus, product, or process disclosed, or represents that its use would not infringe privately owned rights. Reference herein to any specific commercial product, process, or service by its trade name, trademark, manufacturer, or otherwise, does not necessarily constitute or imply its endorsement, recommendation, or favoring by the United States Government or any agency thereof, or the Regents of the University of California. The views and opinions of authors expressed herein do not necessarily state or reflect those of the United States Government or any agency thereof or the Regents of the University of California.

LBL-13049

THE ROLES OF PORE PRESSURE AND FLUID FLOW IN THE HYDRAULIC FRACTURE PROCESS

Walter A. Palen and T. N. Narasimhan

Earth Sciences Division
Lawrence Berkeley Laboratory
University of California
Berkeley, CA 94720

Ph.D. Thesis

June 1981

This work was supported by the Assistant Secretary for Conservation and Renewable Energy, Office of Renewable Technology, Division of Geothermal and Hydropower Technologies of the U. S. Department of Energy under Contract W-7405-ENG-48.

This report is an updated version of "The Roles of Pore Pressure and Fluid Flow in the Hydraulic Fracturing Process" by Walter A. Palen. The original was submitted in partial satisfaction of the requirements for the degree of Doctor of Philosophy in Engineering in the Graduate Division of the University of California, Berkeley, on May 23, 1980.

ABSTRACT

The process of hydraulic fracturing is important in many geo-science related applications including: petroleum reservoir stimulation, geothermal energy extraction, in-situ coal gasification, and in-situ measurement of tectonic stresses. Previous work done in the field of hydraulic fracturing has resulted in a variety of approximate expressions for estimating the fracture length and aperture as a function of time and other process variables. These approximations either ignore fluid flow in the reservoir or assume a constant one-dimensional leakage of fluid from the fracture faces. Other restrictions in the previous approximations include constant pumping rate, purely elastic dependence of the fracture aperture on fracture length, and fracture lengths that greatly exceed the fracture height, the latter ignoring the initial growth period.

A model is proposed in this work for analyzing the fracture growth with time, by considering fluid flow in the system and deformation due to pore pressure in the fracture. The model includes the response of the mechanical connections in the system, i.e. the surface pumps, wellbore tubing, and packer cavity. A thermodynamic energy balance based on a Griffith crack criterion is introduced and used in the model to

control the rate of fracture growth. This highly non-linear problem necessitates the use of a numerical approach.

The model uses a successive series of numerical meshes, each representing a discrete stage of fracture growth. The use of the meshes is first validated against known analytic solutions. The model is then applied to simulate small scale hydraulic fracture (mini-fracture) experiments conducted by the US Geological Survey in the Monticello field in South Carolina. This model study indicates that fracture growth and the measured surface pressure is very sensitive to the resiliency of the fracture walls to applied pore pressure, indicated by the value of fracture stiffness coefficient, a_v. The fracture growth is also found to be greatly influenced by the rock properties including the permeabilty, k, and specific surface energy coefficint, γ.

The use of a mesh acceleration factor in the model enables the growth of very large fractures to be simulated. The results of the study indicate that the fracture growth has two distinct phases: (i) the first is an extremely rapid expansion coinciding with a correspondingly sharp decrease in pressure. This is due to a sudden release of compressional energy from the fluid in the pressurized wellbore tubing. This could cause fracture penetration of upper and lower formations if the energy release occurs very rapidly. However, the use of higher fluid viscosities, variable pumping rates, and smaller wellbore tubing may control this energy release and the unstable fracture growth. (ii) the second phase of the overall growth is considered to be stable, i.e. the wellbore pressure gradually increases as the fracture extends. This pressure increase is due both to the pressure gradient along the fracture and to the increased fluid necessary to offset leakage to the formation. The stable growth period is interrupted by periodic quasi-stable behavior

characterized by short spurts of fracture extension followed by periods of relative quiescence. This behavior is a reflection of the rapid decline and subsequent increase of the energy required to create new fracture surface.

The overall growth rate of the fracture aperture approaches the analytical prediction of a square root with time relationship only after lengths exceeding 250 m. This indicates that the approximate equations may only be used after a fracture has propagated a very considerable length from the wellbore. Thus, these approximations are unreliable for predicting the behavior of shorter fractures or for analyzing early time pressure transients which may be the only direct reflection of the system behavior near the wellbore.

TABLE OF CONTENTS

PAGE

LIST OF FIGURES xi

LIST OF TABLES xiv

I. INTRODUCTION 1

Hot Dry Rock Energy 1

Oil and Gas Reservoir Stimulation 2

In-situ Coal Gasification 3

Other Hydraulic Fracturing Applications 4

The Role of Fracture Analysis 6

Intent of the Present Work 7

Format and Organization 7

II. BASIC CONSIDERATIONS AND PREVIOUS WORK 10

Historical Perspective and Definition 10

Breakdown Pressure 11

Estimating Breakdown Pressure : Fracture Gradients . . 17

Fracture Orientation 19

Field Observations of Fracture Extension 23

Fracturing in Cased Wells 24

Fracturing Fluids 25

Temperature Effects on Fracture Extension 27

Fracture Closure 28

Fracture Proppants 29

Fracture Design 30

Fluid Loss Coefficient 31

page

Fracture Geometry Parameters 32

Extension Pressure 37

Analysis of Constant Geometry Systems 37

Infinite Fracture Conductivity 39

Steady State Fracture Flow Behavior 41

Type Curve Analysis 42

The Effect of Fracture Skin on an Infinite Conductivity Fracture 45

Finite Conductivity Fractures 46

Calculation of Fracture Orientation 47

Pressure Dependent Permeability 48

Chapter Summary 49

III. MODEL DEVELOPMENT 50

A. Limitations of the Analytical Models 50

Fixed Length Fractures 50

Growing Fractures 51

B. Numerical Approach 52

Aspects of IFDM Formulation 53

Previous Computer Codes 56

Solution Techniques 56

C. Meshes Used in the Fixed Fracture Length Simulations . . 57

General Considerations 57

Deformable ("Breathing") Fracture 59

Fractures With Fixed Geometry 62

D. Meshes Used in the Growing Fracture Simulations 65

General Considerations 65

Computational Aspects of Fracture Extension 66

page

Rectangular Mesh Extension Factor 67

Growing Fracture : Mechanical Connections 68

Fracture Element Mesh 71

Circular Fracture Reservoir Mesh 73

Rectangular Fracture Reservoir Mesh 75

E. Fracture Extension Criteria 79

Introduction 79

Stress Intensity Factors 80

Griffith's Fracture Criterion 81

Extension Criteria and Model Considerations 82

A Modified Griffith Energy Concept : System Boundary . 84

Minimum Extension Pressure 85

Application of the Energy Criteria 86

Development of the Internal Energy Terms 86

Use of Fracture Stiffness in the Energy Calculation . 89

Chapter Summary 93

IV. RESULTS AND DISCUSSION 96

A. Fixed Geometry Fracture 96

Simulation Parameters 97

Finite Conductivity Fractures 99

Wellbore Storage Effects 102

Effects of Fracture Skin 104

Comments on the Validation Studies 108

Variation in Fracture Storage 109

Unequal Wing-Length 110

Choked Fractures 113

page

Deformable Fractures 114

Summary of the Fixed Geometry Fracture Solutions . . . 116

B. Growing Fracture Validation : The Monticello Experiment 118

Well Test System 119

Use of Monticello Data for Validation 123

Monticello Validation - First Cycle Simulation 125

Monticello Validation - Consecutive Cycles 128

Consecutive Cycle Simulation Results 129

C. Monticello Data : Parameter Evaluation 133

Effects of the Variation in Fracture Stiffness 133

Effects of Variation in Initial Aperture 135

Effect of Varying the Minimum Earth Stress 137

Effect of Variation in Formation Permeability. 139

Effect of Variation in the Surface Energy Coefficient 140

Conclusions from the Monticello Simulations 142

D. Model Applications to Growth of Rectangular Fractures . 145

Numerical Effects of the Scale Factor 145

Initial Fracture Growth and the Effects of Tubing Size 151

E. Rectangular Fracture Growth - Parameter Study. 155

Effects of Fracture Stiffness. 156

The Effects of Viscosity 163

Super Frac Simulations 169

Fracture Control : Variation in Flow Rate 172

Summary of the Rectangular Hydraulic Fracture Simulations 175

Future Work 176

page

V. SUMMARY AND CONCLUSIONS 178

VI. NOMENCLATURE 181

REFERENCES 185

APPENDICES 192

A. Derivation of the Fluid Leakoff Coefficient 192

B. Kiel's Equations 192

C. Nordgren's Equations 193

D. Gringarten's Solutions 194

E. Development of the Integral Finite Difference Method 194

LIST OF FIGURES

Figure		page
1.	Representations of HDR, MHF, and In-situ Coal Gasification Applications	5
2.	Examples of Vertical and Horizontal Hydraulic Fractures	12
3.	Stress Orientations in the Formation and at the Wellbore	20
4a.	Elliptical Cross Section and Uniform Pressure Distribution	33
4b.	Corrected Cross Section and Polynomial Pressure Distribution	33
5.	Representation of a Well Intercepting a Single Vertical Fracture	40
6.	Volume Element Representation Used in IFDM Formulation	55
7.	Fracture Element Representations	61
8.	Mesh Used in Fixed Fracture Length Simulations	63
9.	Growing Fracture Tubing Element Representation	69
10a.	Circular Fracture Mesh	72
10b.	Rectangular Fracture Mesh	72
11a.	Circular Reservoir Mesh Element	74
11b.	Circular Reservoir Mesh Plane View	74
12a.	Rectangular Reservoir Mesh Overview	76
12b.	Rectangular Reservoir Mesh - Expanded View	77
13.	Representation of an Arbritrary Thermodynamic Volume	87
14a.	Potential Energy Stored in an Elastic Spring	90
14b.	Potential Energy Stored in an Elastic Fracture	90
15.	Log - Log Plot of P_{wD} vs T_{Df} for Various Values of C_r	100
16.	The Effect of Wellbore Storage	103
17.	The Effect of Fracture Skin	106

Figure		page
18.	Skin Factor Analysis - Variation in Skin Thickness	107
19.	The Effect of Fracture Storage	111
20.	The Effect of Unequal Wing Length	112
21.	The Effect of a Choked Region on the Pressure Drawdown	115
22.	The Effect of a Deformable 'Breathing' Fracture	117
23.	Monticello Data Example (after Zoback)	120
24.	Monticello 2-4-1 Surface Pressure vs. Time	124
25.	Monticello 2-7-1 Surface Pressure vs. Time	127
26.	Subsequent Cycles in the Monticello Data	130
27.	Monticello Simulation Results - Comparison of Field Data vs. Simulation	131
28.	The Effect of the Fracture Stiffness on the Monticello Simulation	134
29.	The Effects of the Initial Aperture on the Monticello Simulation	136
30.	The Effect of the Minimum Earth Stress on the Monticello Simulation	138
31.	The Effect of Formation Permeability on the Monticello Simulation	141
32.	The Effect of the Surface Energy Coefficient on the Monticello Simulation	143
33.	The Effect of the Mesh Extension Factor on the Initial Fracture Growth	147
34.	Pressure vs. time and x_f vs. time for a Rectangular Hydraulic Fracture	150
35.	The Effect of Tubing Size on Unstable Fracture Growth	153
36a.	Log-log Plot of x_f vs. time, $Q = 4 \cdot 10^{-3}$ m^3/sec, $\mu = 2.34 \cdot 10^{-3}$ Pa-sec	157
36b.	Log-log Plot of x_f vs. time, $Q = 8 \cdot 10^{-3}$ m^3/sec, $\mu = 2.34 \cdot 10^{-3}$ Pa-sec	158

Figure		page
37a.	Log-log Plot of x_f vs. time, $Q = 4 \cdot 10^{-3}$ m^3/sec, μ = .01 Pa-sec	164
37b.	Log-log Plot of x_f vs. time, $Q = 8 \cdot 10^{-3}$ m^3/sec, μ = .01 Pa-sec	165
38a.	Log-log Plot of x_f vs. time, $Q = 4 \cdot 10^{-3}$ m^3/sec, μ = 0.1 Pa-sec	166
38b.	Log-log Plot of x_f vs. time, $Q = 8 \cdot 10^{-3}$ m^3/sec, μ = 0.1 Pa-sec	167
39a.	Log-log Plot of x_f vs. time, $Q = 4 \cdot 10^{-3}$ m^3/sec, μ = 1.0 Pa-sec	170
39b.	Log-log Plot of x_f vs. time, $Q = 8 \cdot 10^{-3}$ m^3/sec, μ = 1.0 Pa-sec	171
40a.	Log-log Plot of x_f vs. time, variable flow rates, $a_v = 10^{-10}$ Pa^{-1}, μ = 0.1 Pa-sec	173
40b.	Log-log Plot of x_f vs. time, variable flow rates, $a_v = 5 \cdot 10^{-10}$ Pa^{-1}, μ = 0.1 Pa-sec	174

LIST OF TABLES

Table		page
1.	Parameters Used in Fixed Fracture Simulations	98
2.	Parameters Used In Monticello Studies	122
3.	Parameters Used in Rectangular Fracture Studies	146
4.	Summary of Calculated Apertures for Rectangular Fractures	160
5.	Fracture Growth vs Time Calculations, $a_v = 2{\cdot}5{\cdot}10^{-10}\ Pa^{-1}$	162

I. INTRODUCTION

Increased demand for domestic energy supplies has led to a corresponding interest in geothermal energy, synthetic fuel production, and stimulation of conventional but low productivity fossil fuel reservoirs. All of these sources are located within the Earth's crust and methods currently used for their production can be thought of as geo-resource extraction. One technique that is being used to assist in this extraction process is the method of hydraulic fracturing. Hydraulic fracturing, briefly, entails the overpressurization of a sealed section of a borehole until a crack is formed in the rock which propagates as a planar fracture. The following are a few examples of either current or envisioned applications of the hydraulic fracturing concept.

Hot Dry Rock Energy

One of the less conventional methods of extracting geothermal energy is the concept of the hot-dry-rock (HDR) system. In conventional geothermal systems the convecting medium for transferring the available thermal energy to surface conversion facilities is the in-situ geothermal fluid, usually brine or superheated steam. So far the existing and planned geothermal facilites have been located in areas that have both high subsurface temperatures and large volumes of associated heated fluids. Thus conventional systems depend on the location of geothermal fluid reservoirs. However, such reservoirs represent only a small fraction of the recoverable geothermal energy in this country.

The hot-dry-rock concept does not require the presence of an in-situ fluid reservoir but is dependent only on the presence of a high geothermal gradient, i.e. > 30° C/km or > 2.5 heat flow units (h.f.u.), and an adequate supply of a working fluid, such as water. The scheme basically

consists of drilling into impermeable rock that is sufficiently hot for power generation, creating a fracture by hydraulic fracturing, and then completing a circulation system by intercepting the fracture with another well (Murphy, et al., 1977). Laboratory studies (Hunsbedt, et al., 1978) indicate that for such a subsurface heat exchanger to operate at maximum thermal efficiency the rock faces must be as least 60 meters in radius. This large surface area is needed due to the fact that the sweep efficiency in such a system is low because of the low thermal diffusivity of the impermeable granite used in the models and in projected field applications. In theory, a knowledge of the dimensions of the fracture and its location and orientation would be necessary in order to evaluate the response of the system and to complete the circulation loop. In practice however this has not been accomplished. The demonstration HDR project administered by the Department of Energy through the Los Alamos Scientific Laboratory has proven, at present, to be uneconomic due to the large circulation impedance of the system. The failure has been attributed to the inability to orient the second well with the created fracture (Spilhaus 1979) and the high thermal drawdown. Current plans are to test larger fracture systems or a multiple fracture system where an inclined well may form many parallel fractures for a greater reservoir surface area and longer project lifetimes (Cummings, et al., 1979). The feasibility of creating such a system has been demonstrated in petroleum applications (Strubhar, et al., 1975).

Oil and Gas Reservoir Stimulation

Hydraulic fracturing has been used extensively in the petroleum industry to help stimulate low productivity fields since the conceptual introduction of the method in 1949 (Krueger 1973). In these early treatments a well was pressured with petroleum based fluids until a fracture

was initiated downhole. Sand was usually placed in the wellbore during treatment to "prop" the fracture open so it would not close during production. Injection rates were typically 20-30 barrels a minute. Successful stimulation occured in well over 50% of the treated wells.

Current practices in the petroleum industry are to stimulate extremely low permeability oil and gas fields that had previously been thought of as uneconomic. Trends have been towards larger fracture treatments at greater formation depths and pressures (Holditch and Ely 1973). The term massive hydraulic fracturing (MHF) is used to describe a fracturing technique designed to expose a very large surface area of low permeability (< .1 md) formation to enhance flow to the wellbore (Agarwal, et al., 1979). The technique is applied for example to the thick, tight gas reservoirs in Texas, Louisiana, and Colorado. A MHF technique may require the injection of 12,000 barrels of fracturing fluid and up to 500 tons of sand proppant at injection rates upwards of 75 barrels per minute. Such an effort is thought to create vertical fractures of up to 6000 ft in total length with a maximum propped width of .05 - .15 in. (Gidley, et al., 1979). However, none of these measurements has been repeatedly verified from fields tests. Successful stimulations have been reported in .05 - .005 md. gas formations using MHF at costs of over one-quarter of a million dollars per well, in 1977 dollars (Fast, et al., 1977). The economics of such a project depend heavily in the degree of fracture penetration in the reservoir as well as the resultant fracture width, w, and permeability k_f. If the designed values were not obtained due to a variety of parameters involved in the MHF application then the usefulness of the technique cannot be guaranteed.

In-situ Coal Gasification

While emphasis on coal production has been on shallow surface mining

and slurry type transportation of the coal in solid form, a new concept has been developed on the in-situ use of coal in coal gasification.

Coal gasification is a way to substitute high B.T.U. coal derived gas for increasingly scarce supplies of natural gas. The process envisioned involves the location of a thick seam of coal, at depth, and establishment of a highly porous, permeable connection in the bed between two or more boreholes. Water, oxygen, and catalysts are injected through the channels and with in-situ combustion, coal gas is formed and circulated to the surface. Methods used to create the desired permeability and porosity have included chemical explosives, reverse combustion, and hydraulic fracturing (Dinsmoor, et al., 1978). However, success of the proposal involves creation of the flow path at the bottom of the seam. Currently the fracture mechanisms involved do not seem sufficiently controllable by the industry to guarantee this fracture placement and other methods may be used to create the flow channels.

Representations of the HDR concept, petroleum reservoir stimulation, and in-situ coal gasification appear in Figure 1.

Other Hydraulic Fracturing Applications

Hydraulic fracturing is currently being used in the Athabasca Oil Sands in Alberta, Canada (Dusseault 1979). Here depths have been no greater than 600 meters and the possibility of surface penetration exists with the use of proposed MHF techniques. The unconsolidated nature of these sands also poses problems for conventional design practices that are based on the behavior of fractures in elastic media. The need for controlling fracture growth in these and other sensitive formations is paramount for successful application of the technique.

In the field of geoscience and induced seismicity there has been increased interest in the use of hydraulic fracturing for small scale,

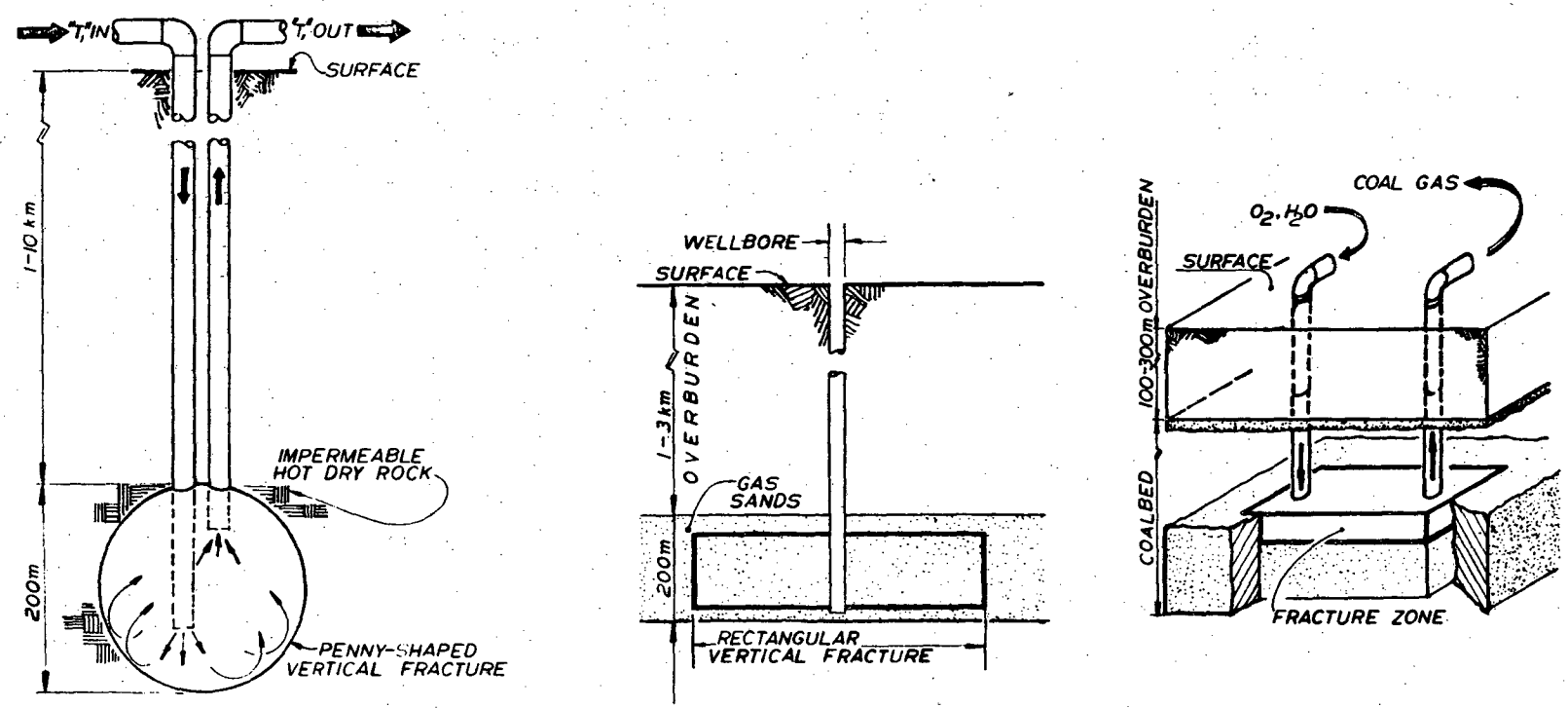

Figure 1 Representations of HDR, MHF, and In-situ Coal Gasification Applications

or "mini-fracture" operations. These mini-fracture operations are used to determine the minimum earth stresses in areas of tectonic activity such as the San Andreas fault zone in California (Zoback 1979). The information is revealed through a careful analysis of the pressure transients observed in the wellbore during the fracturing process. A thorough understanding of these earth stresses may play in important part in understanding and charting the mechanisms involved in earthquake prediction.

The Role of Fracture Analysis

Underlying all these recovery schemes is the need for a quantitative understanding of the hydraulic fracturing process and analysis of the behavior of hydraulically fractured wells (or natural fractures) in permeable and impermeable formations. Accurate prediction of the magnitude of the fluid pressures and fluid volumes required to create and extend hydraulic fractures would help to insure adequate surface equipment and subsurface connections. The roles of fluid viscosity and compressibility on the pressures and dimensions of the fracture (the critical dimensions being the characteristic length, x_f, or radius, r_f, and the width, w) are important in the volumetric calculations of the total fluid injection, equipment rating, and size of the proppants used in the design. The effect of pumping rate on fracture growth and orientation is also very important especially in the design of in-situ stress measurements and fracture control in sensitive formations.

In post fracture analysis, an understanding of the fluid flow in the fracture-reservoir system is necessary in the evaluation of the success of a fracture job. This can be easily achieved in practice through application of typical pressure buildup or drawdown tests. A description of the numerous factors involved in the completion of a

hydraulic fracturing operation and their effects on the well test data will help in analysis of these tests so that the fracture geometry and fracture damage may be estimated. Fracture damage will be defined in terms of a fracture skin (formation damage adjacent to the fracture surface) or in terms of a low permeability region in the fracture itself called a choked region. An understanding of the formation response to increased fracture permeability may permit the use of transient data from observation wells to help determine fracture orientation and length.

Intent of the Present Work

The problem undertaken in this work will be to investigate the behavior of the fracture systems described above. The purpose then will be to develop a conceptual model for the hydraulic fracturing process. The model in conjunction with a highly flexible numerical method will enable analysis of the geometry and rate of propagation of a growing fracture. The work will also treat the problem of a stabilized or fixed geometry fracture that intercepts a wellbore. The model will be used to generate type curves that will illustrate possible variations in drawdown behavior in response to conventional and new parameters such as the choked fracture defined above. Only systems involving vertical hydraulic fractures will be extensively treated.

Format and Organization

The work is divided into three main parts. The first part (Chapter II) consists of a literature review. In this part the mechanisms of hydraulic fracturing are summarized with emphasis on fracture mechanics, field applications, and on the factors that influence fracture growth. This part is also concerned with the application of pressure transient analysis which appears to be the only available technique that can reveal information about the nature of the fracture-reservoir system.

The second main part (Chapter III) presents the development of the model and its incorporation in the computer program HYDFR. Consideration of limiting assumptions in the analytical work presented in the literature review chapter has emphasized the use of a numerical solution technique. The Integral Finite Difference Method formulation used is briefly introduced along with comments on the advantages of a direct solution technique used in this work. The chapter presents the development of a mathematical representation of the static and growing fracture systems with a detailed description of the meshes used. Two classical approaches of fracture extension are analysed with emphasis on Griffith's energy theory. The equation for total system energy is derived and the resultant strain energy calculation refined for use in the computer program. This calculation and a minimum pressure requirement become the basis for the fracture extension criteria. The chapter concludes with a discussion of the limitations of this type of numerical approach.

The last main part (Chapter IV) will present the results and discussion. Solutions for the pressure drawdown of a well intercepting a single finite conductivity vertical fracture will be presented and compared with the analytical solution of Cinco-Ley and Samaneigo (1978). The predicted response of the pressure drawdown incorporating the effects of wellbore storage, permeability damage in the formation, permeability damage in the fracture, variation of fracture storage capacity, and of stress sensitive formations are also presented. The results of the growing hydraulic fracture simulations are compared with field data conducted in mini-fracture experiments conducted in the Monticello Field in South Carolina. The effects of the formation strength, minimum earth stress, and specific surface energy requirements on the simulations are also described. The creation of large vertical hydraulic fractures is

discussed. A parametric study is performed to ascertain the effects on the rate of fracture growth by varying controllable surface factors such as fluid viscosity, pumping rate, and fluid loss additives. The chapter will conclude with an analysis of the properties of the rock formation on the stability of hydraulic fracture growth, and suggest further refinements in extending the model capability.

A further section will provide a summary of the present work. An appendix is included that will assist the interested reader in following the details of the second and third chapters.

II. BASIC CONSIDERATIONS AND PREVIOUS WORK

Historical Perspective and Definition

The concept of hydraulic fracturing is one of the major developments of petroleum engineering. Before 1950, acidizing was frequently used for increasing well productivity, but was generally ineffective in non-reactive sandstone formations. The method of hydraulic fracturing was patented by Farris in 1950 (Krueger, 1973) and has since been employed extensively in the oil industry for formation stimulation and by geophysicists to estimate in-situ earth stresses. Hydraulic fracturing basically entails, in simplest form, the pressurization of a sealed or packed off section of a wellbore by the injection of fluid from surface pumps. Once the formation has broken or fractured due to the overpressurization of the wellbore, the fracture may penetrate deeply into the formation with continued fluid injection. This is the extension phase of the process. After completion of this procedure and the removal of the associated equipment, the well is produced to remove the fracturing fluids, (referred to as the clean up period) and returned to normal production.

Considerable attention had been focused on understanding this by analyzing inadvertent hydrofracturing during water flood operations, the use of high density drilling muds, and squeeze cementing. Up until the mid 1950's the process was attributed to a physical lifting of the overburden as a result of overpressurization along either pre-existing bedding planes or by the creation of a horizontal fracture. The first major attempt at explaining the actual mechanics of hydraulic fracturing is attributed to M. King Hubbert (Hubbert and Willis, 1957). Hubbert pointed out that most fracture pressures recorded were significantly less than the lithostatic stress (overburden weight). Hubbert demonstrated

that the major stress field in the formation consisted of unequal principal stresses and in areas of normal faulting (tectonically relaxed zones) the least stress would be horizontal. Thus it was possible for a vertical hydraulic fracture to form at pressures much less than that due to the overburden. The difference between a vertical fracture (fracture plane parallel with the wellbore) and a horizontal fracture (fracture plane normal to wellbore and assumed parallel with the earth's surface) is illustrated in Fig. 2. Hubbert was the first to quantify the fact that the fracture orientation was related to the state of stress in the ground at the point of fracture initiation.

Breakdown Pressure

Hubbert showed (with an experimental apparatus consisting of sand boxes) that vertical faults (normal faults with respect to the applied horizontal stress) would be created if the horizontal stress was gradually eliminated with constant vertical stress applied to the sand. Thus he proposed that a hydraulic fracture would occur when conditions in the wellbore were such that the minimum component of stress in the wellbore region was reduced to zero. Hubbert then demonstrated with the use of Mohr's diagrams and isotropic elastic theory, that an equation for calculation of the wellbore rupture pressure could be developed for a rock impermeable to the fluid. The generalized form of this expression has been derived by Cleary (1979) as

$$\alpha_3 P_b - \alpha_4 P_o - \alpha_1 S_h + \alpha_2 S_H = T_o \qquad (1)$$

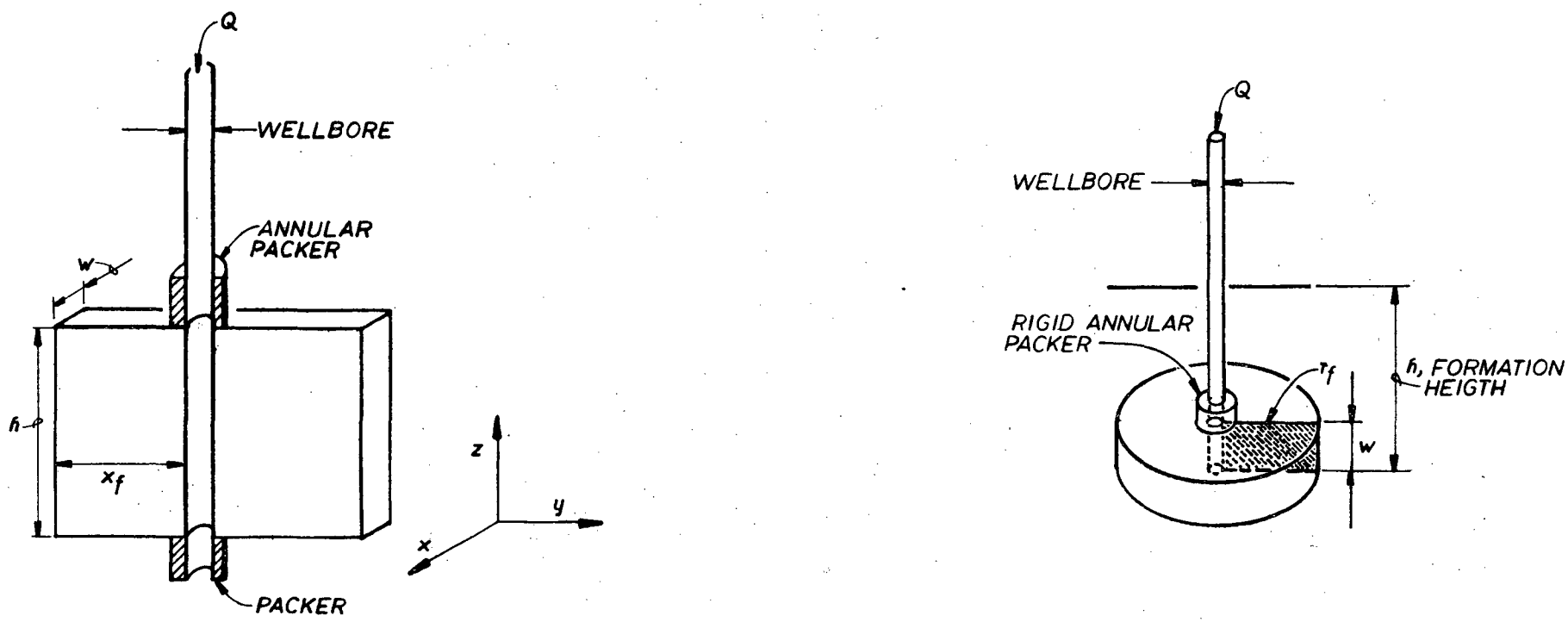

Figure 2 Examples of Vertical and Horizontal Hydraulic Fractures

where (α_i), $i = 1, 2, 3, 4$ are stress related coefficients

P_b is the breakdown pressure,

T_o is the tensile strength of the formation,

S_h, S_H are the minimum and maximum horizontal stresses and

P_o is the initial pore pressure.

For pure elastic behavior $\alpha_1 = 3$ $\alpha_2 = \alpha_3 = 1$, $\alpha_4 = -1$ and the equation reduces to the Hubbert and Willis (1957) equation

$$P_b = 3S_h - S_H - P_o + T_o \qquad (2)$$

Hubbert and Willis assumed the maximum principal stress, S_V, to be vertical such that S_h, S_H, S_V are all orthogonal.

The value of 3 for α_1 was shown by Hubbert to be that value which would reduce one of the major compressive stresses to zero. For values above $\alpha_1 = 1$ (equal stresses in the horizontal direction) it was shown that the tangential stress component σ_θ at the wellbore face becomes zero in a direction normal to S_h as pressure in the wellbore is increased. Thus P_b can range from a value of zero ($S_H/S_h = 3$) to a value of $2S_h$ ($\alpha_1 = 1$) depending on the ratio of S_H/S_h (the far field stress ratio) and the magnitudes of T_o and P_o. In general, a rock has a definite tensile strength, but Hubbert reasoned that for a sufficiently large section of wellbore the intersected formation would have many joints in which $T_o = 0$. In most competent formations $T_o > 0$ and a fracture will never be self-generating in a wellbore (as would happen if $S_H \geqslant 3S_h$).

The concept of initiating a fracture in a 2-dimensional elastic medium ignores the possible creation of a horizontal fracture as the fluid pressure acts only in a radial (horizontal) direction. However in the sealed interval of a wellbore it is possible that an axial force may

be generated due to fluid pressure acting on the packers and/or the bottom of the well. In such cases a horizontal fracture may be initiated and the breakdown pressure becomes

$$P_b = S_V + T_o - P_o \tag{3}$$

The effect of the fluid in the wellbore permeating into the formation will have a significant effect on the breakdown pressure as has been observed repeatedly in the field (Howard and Fast, 1970). In this case the stress field is found by superimposing the three principal tectonic stresses, the stress field caused by the pressurized wellbore, and the fluid pressure created by flow of fracturing fluid into the reservoir (Haimson and Fairhurst, 1970). Their resultant calculations for breakdown pressure for a porous formation, designated by the superscript p as P_b^p, would be especially applicable to stimulation work in some geothermal reservoirs or in oil reservoirs. In these situations the rock permeability, k, could be fairly high and large fluid invasion would be expected near the wellbore. This effect could also be created by very low pumping rates which would also permit fluid invasion before breakdown. Haimson's formula for P_b^p for a vertical fracture is

$$P_b^p = \frac{T_o + 3S_h - S_H - P_o}{2 - a\left(\frac{1-2\nu}{1-\nu}\right)} \tag{4}$$

where ν is the Poisson's ratio and

$$a = \left(1 - \frac{C_r}{C_b}\right)$$

in which C_r is the bulk compressibility of the solids and C_b is the bulk compressibility of the porous rock.

Equation (4) is the same as (2) except for the term in the denominator. If in very stiff formations ν is bounded by 0.5 and the coefficient a by 1.0, the value of P_b^p would vary between one to one-half the value for an impermeable rock given by Eq. (2). Haimson also presents a calculation for P_b^p for a horizontal fracture as

$$P_b^p = \frac{S_V + T_o^V - P_o}{1 - a(\frac{1-2\nu}{1-\nu})} \tag{5}$$

where T_o^V is the tensile strength of the rock in the vertical direction.

Comparing Eqs. (5) and (3), it is seen that the initiation of horizontal fractures would be much more likely to occur when fluid penetration occurs if there exists a mechanism for stress concentration such as at the bottom of the borehole or at an intersecting horizontal joint.

Essentially, the above equations state that the fluid pressure acts to reduce both the stress concentration and the effective stresses at the well face. As such, the breakdown pressure P_b cannot be less than the minimum earth stress value S_h of the formation. However, researchers have reported that fluid penetration does reduce the tensile strength T_o (Forman and Secor, 1974) and increases dynamic Poisson's ratio measured by acoustic techniques (Palen, 1978). An explanation for the decrease in the breakdown pressure with increased saturation could also be due to these effects.

Experimental results in sandstones and shales have shown that the difference between the tensile strength T_o as observed during diametrical loading tests and the T_o calculated by Eq. (2), differs only by the amount of the transient pore pressure P_o (Dunn, et al., 1978). This

would suggest that if the pore pressure distribution was known in the near wellbore region, its value could simply be subtracted from P_b to get an estimate of P_b^p. It also suggests that as the rate of pressurization increases that P_b^p would increase due to the smaller pressure transient in the formation. This has been partially verified by Haimson and Fairhurst (1969) who attribute the increase in the permeable breakdown pressure, P_b^p, with pressurization rate to an elastic strain phenomenon. Using permeable hydrostone samples with a centrally located borehole the initiation or breakdown pressure P_b was measured for permeable (open hole) and impermeable (rubber-lined borehole) conditions. While P_b^p increased with pressurization rate the agreement between Eqs. (4) and (5) and experimental results was not conclusive. The values calculated for P_b^p with Eqs. (4) and (5) were only lower bounds for the experimental results.

Medline and Masse (1979) investigated the response of fracture initiation pressure to fluid penetration involving uniform radial and variable axial (direction parallel to the wellbore) stresses. Using Biot's (1956) equations they derived identical expressions to Eqs. (4) and (5). However, when plots of P_b^p vs. the applied hydrostatic pressure were analyzed, it was found that while fluid penetration reduced the breakdown pressure it did not change the slope of the curves. This would be predicted applying Biot's poroelastic theory in deriving Eqs. (4) and (5). At best then, all that can be conclusively stated is that the effect of fluid permeation at the wellbore face acts to lower the fracture initiation or breakdown pressure P_b due to a variety of possible effects.

Estimating Breakdown Pressures: Fracture Gradients

The pressure required to fracture a formation, P_b, is dependent on the magnitude of the horizontal stresses S_h and S_H and on the ratio of these stresses. In general, the observed fracture breakdown pressure, P_b, increases with depth. Based on simple theory a "fracture gradient" can be calculated. Fracture gradient may be defined as the ratio of breakdown pressure to depth. In some of these calculations it is assumed that the material obeys Biot's (1956) relations, i.e., linear porous-elastic behavior, and that the horizontal stress in the formation is related to the overburden stress by the dynamic Poisson's ratio which should be used in transient stress problems. Felsenthal and Ferrel (1971) present a fracturing gradient equation that is independent of Biot's laws as:

$$\frac{P_b}{D} = \left(\frac{S_V}{D} - \frac{P_e}{D}\right)\left(\frac{\nu}{1-\nu}\right) + \frac{P_e}{D} \qquad (6)$$

where S_V is the overburden pressure,

D is the formation depth,

P_e is the shut in formation pressure,

and other terms are as defined above. This value calculated in Eq. (6) multiplied by the expected depth predicts the expected breakdown pressures used in design considerations. A slightly different form was derived by Anderson, et al. (1973) which took into account the effect of rock compressibility and porosity,

$$\frac{P_b}{D} = \frac{2\nu}{(1-\nu)}\,\frac{S_V}{D} + \frac{(1-3\nu)}{1-\nu}\,\frac{aP_p}{D} \qquad (7)$$

where P_p is the pore pressure and a is as defined in Eq. (4), usually given the value of 1.

Two facts are readily apparent from Eqs. (6) and (7). The first is that P_b does increase with depth if ν is relatively constant and if the formation fluid pressure P_e or P_p increases with depth due to hydrostatic head. The second is that, for cases where the formation fluid pressure is much less than the overburden stress S_V, Eq. (7) predicts a fracture pressure twice as high as Eq. (6) in the limit where $P_e = P_p = 0$. Equation (7) could predict for a sufficiently elastic rock (i.e., $\nu > 0.33$) a situation where the fracture gradient would actually exceed the lithostatic gradient pressure in a low fluid pressure reservoir. One would take care in applying Eq. (7) in this case.

One way to cause preferential fracture in a specific formation would be to draw down the fluid pressure in the formation. Equation (6) can be solved for the change in P_b vs. P_e as

$$\frac{\partial P_b}{\partial P_e} = \frac{-\nu}{1 - \nu} + 1 = \frac{1 - 2\nu}{1 - \nu} \tag{8}$$

For the upper bound limit on ν of 0.5 the fracture breakdown pressure increases with respect to reservoir fluid pressure at a fixed depth. Pressuring adjacent formations or drawing down the pressure in the one of interest, may help prevent rupture in unwanted formations. This often happens in large waste disposal wells. Typical fracture gradients are observed to fall within a range of (0.5 - 1.0) psi/ft (Howard and Fast, 1970) in which the latter value represents the lithostatic gradient. In using either Eqs. (6) or (7) care must be taken to avoid large density contrasts in the overburden where S_V must be calculated by an integration

of the density vs depth curve. Significant errors have been found when applying Eqs. (6) or (7) to offshore fracture stimulations where the observed breakdown pressures are less than those calculated, due to the density difference of the rock and of the ocean (Christman, 1973).

Fracture Orientation

Many researchers have reported laboratory and field experiments designed to determine the initial orientation of the fracture at the wellbore, its subsequent direction of propagation, and the final fracture orientation with respect to known or suspected orientation of the earth stresses.

Hubbert and Willis (1957) originally proposed that the fracture would initiate at angles θ and $(\theta + \pi)$ where the direction of the principal stress S_H would intercept the wellbore at an angle θ as seen in Fig. 3. The plane orientated at angle θ is also perpendicular to the minimum stress in the formation. In their laboratory experiments with gelatin molds, it was easy to create both horizontal and vertical fractures by physically distorting a cylindrical specimen by either squeezing it (causing vertical fractures) or stretching it axially (causing horizontal fractures). Later researchers using more competent media were successful in creating laboratory fractures from smooth hollow cylinders made of hydrostone (Haimson and Fairhurst, 1969). The reported values for breakdown pressure as calculated from Eqs. (2) and (3) indicated higher tensile strengths in the vertical direction, i.e., $T_0^V > T_0$, possibly due to a plastic skin zone that forms in the borehole and resists formation of horizontal fractures. Medline and Masse (1979) duplicated the hollow-cylinder experiments of Haimson and Fairhurst and also recorded the breakdown pressures in a spherical cavity, using reservoir rocks. By controlling the magnitude of the applied stresses they generated both

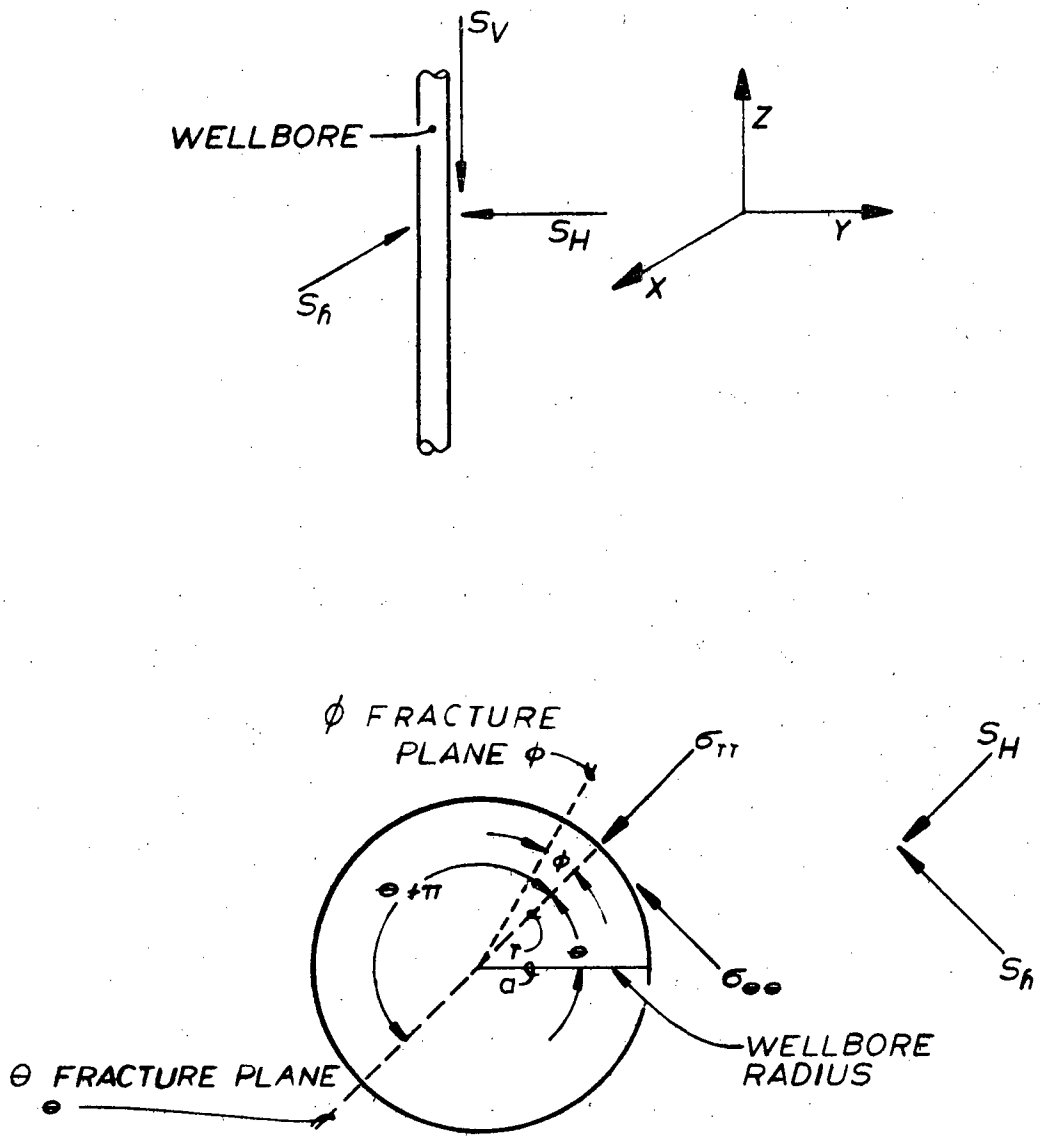

Figure 3 Stress Orientations in the Formation and at the Wellbore

horizontal and vertical fractures. However, they noted that it was very difficult to initiate horizontal fractures in the hollow cylinder tests and even when they did, the orientation of the fracture at the wellbore was not the same as the final fracture orientation (which was perpendicular to the minimum stress). Also noted was the fact that in cased wells where fractures are initiated through perforations the only plausible way to generate horizontal fractures was to use a thin ring of perforations that simulates the spherical pressure source they used in their experiments. The rock specimens behaved similarly even when notched along the cavity at angles different from θ. This observation that the fracture would ignore an artificial fracture path was borne out by experiments performed on cased holes using perforations (Daneshy, 1973a). In cases where the perforations did not lie on the $(\theta, \theta + \pi)$ plane, fractures initiated on the θ plane but did not contact the perforations. This could explain anomalously higher pressures observed in perforated vs open hole hydraulic fracture treatments in adjacent wells with similar formation properties.

The possibility that the fracture orientation at the wellbore may not be the same as that of the propagation direction θ, due to a non-aligned borehole-stressfield condition was investigated by (Daneshy, 1973b). Inherent in all previous discussions was the fact that the in-situ stress directions of S_V, S_h, and S_H were assumed to be oriented with respect to the wellbore in the σ_{ZZ}, σ_{RR}, $\sigma_{\theta\theta}$ directions. However, if the stress field S_h, S_H, S_V is not coincident with the stresses at the wellbore, it is possible that a stress state will exist that results in inclined fractures. Daneshy cured blocks of hydrostone then drilled into them at angles ϕ and β with respect to the horizontal plane. The fractures initiated along the wellbore axis then reoriented themselves in a direction

perpendicular to the minimum stress. The breakdown pressure also increased with pressurization rate as was indicated by the aligned stress field tests of Haimson and Fairhurst (1969). Field experiments in competent granite (i.e., large tensile strength, T_0) were carried out in mines with test boreholes. Von Schonfeldt and Fairhurst (1972) reported fracture orientations were horizontal near the top of the test boreholes where stress concentration was not uniform but became vertical at some distance down the borehole. This would seem to verify the fact that the propagation direction will be perpendicular to the least compressive stress.

Cleary (1979) attempts to explain the fact that even with axially oriented stress fields, elastic non-linearities may affect the stress field around the well. In this case α_1 and α_2 in Eq. (1) will not take the elastic values of 3 and 1, respectively. The borehole then distorts into an ellipse with a major axis oriented at an angle ϕ with respect to θ. Cleary's calculations indicate that the initiation path follows the ϕ plane for a distance equal to a only few times the wellbore radius before the fracture orients itself with the θ plane. Thus televiewer scans of the wellbore or packer impressions may not give correct fracture orientations when the rock is anisotropic or non-elastic.

Zoback et al., (1980) report that by careful analysis of pressure data observed during repeated mini-frac operations, fractures may initiate as vertical at the wellbore but "rollover" into horizontal fractures as predicted by Daneshy (1973b). Thus the fracture can initiate from the wellbore in any one of at least five ways: 1) an initial vertical fracture extends as a vertical fracture along the plane oriented normal to S_h, 2) a vertical fracture orients itself along the θ plane from an initial θ-ϕ plane at the wellbore, 3) a horizontal fracture extends in a

plane perpendicular to the overburden stress, 4) a vertical fracture initiates from a smooth wellbore with no stress concentration due to the packers but extends horizontally, 5) a fracture initiates horizontally at the borehole bottom then propagates vertically (rolls over). Normal field calculations assume types 1) and 3) behavior although 1) will prevail in the absence of significant stress-complicating factors such as rigid packers (Kehle, 1964).

Field Observations of Fracture Extension

For fields with cased holes the orientation of the fracture is important in deciding the preferred directions for maximum sweep efficiency in water flood operations. That is, the most efficient sweep directions are perpendicular to the fracture face. However, most cased hole orientation techniques depend on very long fractures to insure adequate detection of electrical or seismic discontinuities. Therefore the best results have been reported in MHF studies (Smith, et al., 1978; Power, et al., 1976). The methods of investigation used by these authors included analysis of electrical potential measurements at the surface and seismic surveys. The field results indicate that the azimuth of the fracture changes and thus the maximum stress direction may change considerably over the length of the field. Further analysis also indicated that the wing lengths may be unequal. This could be due to a change in the stresses at one end of the fracture or anisotropic properties causing fracture blunting. In essence, while the fractures may propagate parallel to the S_H stress orientation, this direction may change over the fracture length producing a slight fracture curvature. The effect of this curvature on design considerations is presently untreated and is not important if the curvature is small.

Fracturing in Cased Wells

Mentioned above was the fact that the process of hydraulic fracturing is complicated if the formation to be fractured is located in a cased area of the well or when only specific formations are to be fractured concurently. The perforations used in oil wells are usually created by explosive charges in the wellbore with "bullets" from this explosion penetrating the cemented casing and creating communication from the formation into the wellbore. The effect of stress concentration due to the perforations complicates the rupture pressure analysis as presented above. Most of the work done on perforation has been experimental and of a qualitative nature (Daneshy, 1973c). Blocks of hydrostone formed around hollow steel cylinders and placed in triaxial loading cells were used to represent cased boreholes. Different perforation orientations (linear along zz axis, helical along the zz axis, and circumferential along the $r\theta$ plane as referenced to Fig. 3) were tested along with open hole comparisons. Fracture pressures were found to be twice as high using perforations compared to open hole breakdown pressures with the magnitude increasing as the angle ϕ between the perforation plane and the θ plane increased (reaching a maximum at $\phi - \theta = 90^{o}$). Since orientation of the fracture cannot be absolutely determined by field data the helical arrangement was found to be the most logical since the fracture plane could possibly intersect one or more perforations. Unfortunately, in the use of field tests to determine in-situ stresses, there would be at least 3 additional effects to consider when using Eqs. (1) and (2). There is an added stress factor due to the casing in the wells, added pressure drop through the perforation, and an additional complication if the perforations did not lie on the θ plane. Daneshy was able to extend horizontal fractures from the cased holes, incidentally, but these were

initiated as vertical fractures from the well previously discussed as type 4 behavior.

Fracturing Fluids

Other variables in hydraulic fracture design include the type of fluid used during the wellbore pressurization and the type of fluid used to extend the fracture into the formation. Originally fluids based on petroleum and petroleum products were used in hydraulic fracturing. These included lease crudes, refined oils, and even Napalm derivatives (Howard and Fast, 1970). In the late sixties and early seventies more attention was concentrated on the properties of fluids due to their various effects on fracture extension, fracture width, proppant transport, leak off, and clean-up. Many types of fracturing fluids have been used with the intent of optimizing any or all of these phenomena. Viscous Newtonian oils have also been used as fracturing fluids in hydraulic fracturing. These fluids offer excellent sand transport properties (i.e., the sand will stay in suspension longer) and will also create large fracture pressures (due to the large shear forces acting on the fracture faces) with a minimum of fluid volume. Unfortunately, such fluids require very high pumping pressures and high horsepower and also create large pressure drops along the fluid injection tubing. However, if the fluid is mixed with a surfactant and injected down the tubing concurrently with an outer annular ring of water it is found that tubing pressure losses are less than that of water alone (Sinclair, 1970). This is due to slippage between the two fluids in a water and oil emulsion layer caused by the surfactant. These "Super Frac" fluids with viscosities of 500 to 100,000 cp would be delivered to the fracture face with minimal tubing pressure drop. An added benefit of these fluids is that with such a high viscosity, penetration into the fracture walls (leakoff)

is very low (Kiel, 1970). However, in gas well stimulation the formation may not have sufficient pressure, or transmissivity, to displace the viscous oil based fluids back out of the fracture and into the wellbore during fluid cleanup. Viscous, water-based non-Newtonian fluids have been used for these types of formations. These fluids offer lower viscosities (<500 cp) than "Super Frac" fluids but with much better temperaature stability, improved cleanup, and are logistically much easier to use.

Polymer emulsions have been used increasingly in hydraulic fracture stimulations (Sinclair, et al., 1974). In these systems a polymer and a surfactant mixture creates an emulsion with about 50-80% oil phase by volume. This emulsion is temporarily stable with viscosities in the 100 cp range during the injection and extension phase of the process. However, the polymer degrades with time and temperature and the fluid breaks down to lower viscosity oil and water phases, which facilitate fracture cleanup. These systems also are usually cheaper than the high viscosity fluid systems described above, depending on the cost of the polymer and surfactant. These polymers have typically been guar gels. However, if the guar polymer breaks down incompletely it will leave a residue in the system on the fracture face (Cooke, 1975) and creates fracture formation damage (or fracture skin). Gas fields are much more susceptible to such damage due to their inherent low permeability and other polymers with lower residue, and higher costs, have been used. These polymers include cellulose and polyacrylamide, which is a synthetic polymer. Liquid carbon dioxide is added to some treatments as a precursor fluid (often called a pad). The carbon dioxide pad easily permeates the formation ahead of the high viscosity fluid. During cleanup, the solution gas from the CO_2 aids in "cleansing" the pores at the rock

face (the skin zone) helping minimize this damage (Jennings and Sprawls, 1977) although it does increase the pressure drop in the tubing (Mathias, 1971). While these fluids using guar based polymers are cheaper and easier to mix than the other fluids, their apparent viscosities are much lower. A recent refinement is the addition of a cross-linking agent to the guar and guar residue based polymers. This created crosslinking between the guar molecules raise the viscosity of the emulsions by up to an order of magnitude and occurs as the fluid is pumped down the wellbore (Free, et al., 1978). This allows a high viscosity fluid to be injected into the formation (with its characteristic better sand transport and higher pressure drops), even though the apparent injection viscosity is much lower.

Temperature Effects on Fracture Extension

In most wells there is a significant change in temperature between the surface and subsurface formations due to the natural geothermal gradient of the earth. Design calculations are usually based on the assumed viscosity of the fluid at the reservoir temperature. This is at best an equilibrium assumption and is not likely to happen especially at moderate to high pumping rates. The fluid penetration in the reservoir will also affect the heat transfer at the face due to the thermal skin effects or blockage (Sinclair, 1971). A pad fluid is sometimes used in high-temperature wells ahead of a more viscous fracturing fluid. The relatively cooler pad fluid penetrates the formation and increases the local heat capacity of the rock, reducing the conductive heat transfer from the reservoir to the fracture face. If this "precooling" is not included in the design it is possible that a conservative estimate of the fracture properties may result (Whitsitt and Dysart, 1970). These

properties are dependent on the pressure drop in the fracture which is dependent on the apparent viscosity of the extension fluid.

Fracture Closure

One of the parameters in hydraulic fracture design is the fracture width, w, or the width of the fracture after a pressure drawdown is reestablished and the well returned to production. While the fracture is extending, its faces are being held open by a fluid extension pressure, P_{ext}, which is greater than the minimum earth stress S_h. After the fluid pressure is released, the fracture faces will return to their normal (closed) position if the formation behaves as an elastic medium. Some agent must be introduced during the extension phase that will keep the fracture faces from closing. These agents have commonly been acid washes and sand proppants (Krueger, 1973, Howard and Fast, 1970). The use of acid is restricted to formations that will dissolve in the acid phase (limestone and carbonaceous shales). The use of acid when possible is desirable due to the lower viscosity and pressure losses of the acid solvents and the ease of application (i.e., not having to prepare the fluid-proppant mixture). The amount of rock that is chemically eroded is a function of the strength of the acid when it contacts the fracture face. The strength of the acid in the fracture is a function of not only the injection rate but also fracture geometry, temperature, and rock type (Williams and Nierode, 1972). It is reasonable to assume then that the width of the fracture during production would also be a function of these parameters. This would result in a fracture geometry which strongly affects the local permeability of the fracture. Before consideration of the fracture geometry, however, and its relationship to the viscosity and pumping rates, the topic of fracture proppants will be introduced.

Fracture Proppants

The variation in proppant placement and types significantly affects the permeability of the fracture. Due to the increasing sophistication of laboratory techniques, the behavior of the fluid-proppant-fracture system can be duplicated under controlled conditions (Iwai, 1976). There are two basic types of proppants: deformable (e.g., crushed walnut shells); and "rigid" e.g., sand or glass beads. The deformable proppants would be used when the formations are made of very weak rock that would imbed a stiffer sand grain into the fracture face. Since the permeability of a propped fracture is many times larger than the formation permeability but lower than an acidized fracture (of the same width) industry trends have been towards injecting large volumes of proppants with the intent of keeping a large area of the fracture propped open (Coulter and Wells, 1972). While the dimensions of the fracture plane as depicted in Fig. 2 are h and x_f, the producing or effective fracture dimensions h_e, x_{fe} may be considerably lower. A problem occurs when the proppant concentrations are so high or the viscous transport so low that several layers of proppants build up. An ideal design would be a proppant monolayer but the density contrast of the particles with the fluids is still so large that even with highly viscous fluids a sand bed can be formed. When the fluid pressure is released and the formation begins to close the proppant particles may be crushed, reducing the proppant permeability by as much as two orders of magnitude (Seidel and Stahl, 1972).

This crushing effect may be reduced by mixing smaller and larger grain sizes, with the maximum grain size being one-third to one-fourth of the maximum fracture width (Williams, et al., 1973). The crushing effect will reduce the average size of the proppant particles and create very

small fines that may flow towards the wellbore. In sufficient concentrations, these fines may act with the smaller proppant particles to form an inverted filter and severely reduce or choke flow near the wellbore by reducing the local fracture permeability.

Fracture Design

Many assumptions are made in the calculation of the fracture dimensions (van Domselaar and Visser, 1974). These include: 1) the fracture growth is vertically confined and thus extends primarily in the horizontal direction as a vertically oriented planar fracture; 2) the fracture extends symmetrically about the well; 3) fracture dimensions are governed by ideal elastic theory; 4) fracturing fluids and proppants move with the same velocity with piston like displacement with no settling of the proppant; 5) leak off in the formation is proportional to $1/\sqrt{\text{time}}$. On this basis the calculation of fracture growth is based on a material balance

$$\int_0^t Q\,dt = h\int_0^{x_f} w_f\,dx_f + 2h\int q.\tilde{n}\,dx_f \qquad (9)$$

where x_f is the fracture length at time t,

Q is the surface volumetric injection rate,

h is the fracture height,

w_f is the fracture width as a function of x_f,

q_1 is the leak off at time t as a function of x_f and,

$\tilde{n}$ is the unit vector normal to fracture surface.

This equation simply states that cumulative fluid input is equal to the volume of the fracture plus the volume of fluid that leaks off into the formation. In this balance it is also implicitly assumed that the fracture will extend at a pressure $P_{ext} > S_h$ and that leakoff in the

wellbore is negligible. While many of the calculations by various authors all use a variation of the material balance equation, differences appear due to the relationship between the width of the fracture, w_f, and the fracture length, x_f.

Perhaps the earliest such calculations were presented by Howard and Fast (1957) who assumed a constant fracture width and constant pumping rate, Q_1. The relationship between the area A of the fracture (= hx_f) and the time was given as

$$A = \frac{Q_1 w}{4\pi C^2} * \left(e^{\beta^2} \operatorname{erfc}(\beta) + \frac{(2\beta - 1)}{\sqrt{\pi}} \right) \qquad (10)$$

where $\beta = 2C\sqrt{\pi t/w}$,

t is the time,

C is the fluid loss coefficient and the complementary error function is defined as

$$\operatorname{erfc}(\beta) = \frac{2}{\sqrt{\pi}} \int_{\beta}^{\infty} e^{-\gamma^2} d\gamma \ .$$

While this equation is somewhat unwieldy simpler forms were later derived where the fluid loss coefficient is only considered to affect the fracture dimensions at large times.

Fluid Loss Coefficient

The fluid loss coefficient is evaluated from laboratory tests using the fluids and cores from the field. The flow coefficient, C, is defined as the relationship between the leakoff from the fracture, q, and the reciprocal of the square root of time. This relationship is developed in

Appendix A as

$$q = \frac{C}{\sqrt{t}} \tag{11}$$

C is usually treated as a combination of two constants, C_{11} and C_{22}. The first, C_{11}, is defined when time = 0 and is described as the spurt loss coefficient and the second, C_{22}, is a constant property value for $t > 0$ (Williams, 1970). As seen from Eqs. (9) and (10) as the fluid loss coefficient increases the fracture volume must correspondingly decrease. When low viscosity fluids and/or high permeability formations are present fluid loss additives are sometimes used to build up a filter cake on the formation face and restrict fluid loss.

Fracture Geometry Parameters

The concept of variable fracture width, w_f, is often treated by relating the shape of the growing fracture to the shape of an equilibrium flat cavity in an elastic material. Assuming a uniform pressure, the cross section of the fracture in the x-y plane (Fig. 4a) is assumed to be elliptical (Sneddon, 1951). Using the elastic properties of the formation, relationships between the width, w, and the fracture length can be derived. Geerstma and de Klerk (1969) solved for w and found a dependence of the maximum fracture width, w_{max} (at the wellbore) with the fourth root of length as

$$w_{max} = 2.1 \left(\frac{\mu Q_1 L}{Gh}\right)^{1/4} \tag{12a}$$

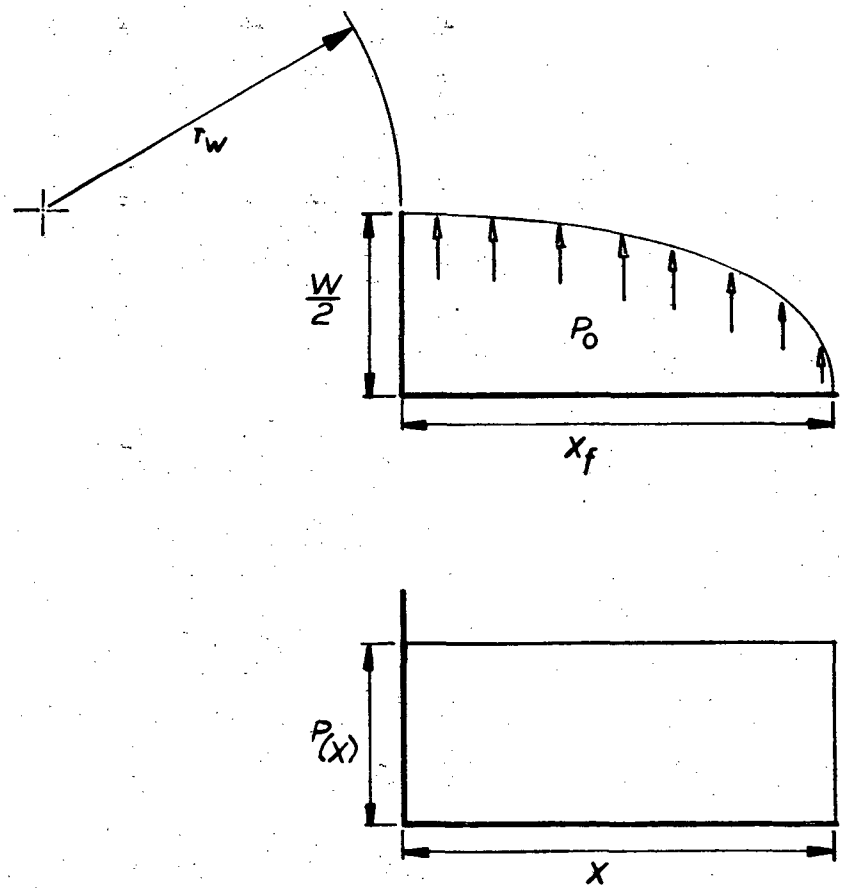

Figure 4a Elliptical Cross Section and Uniform Pressure Distribution

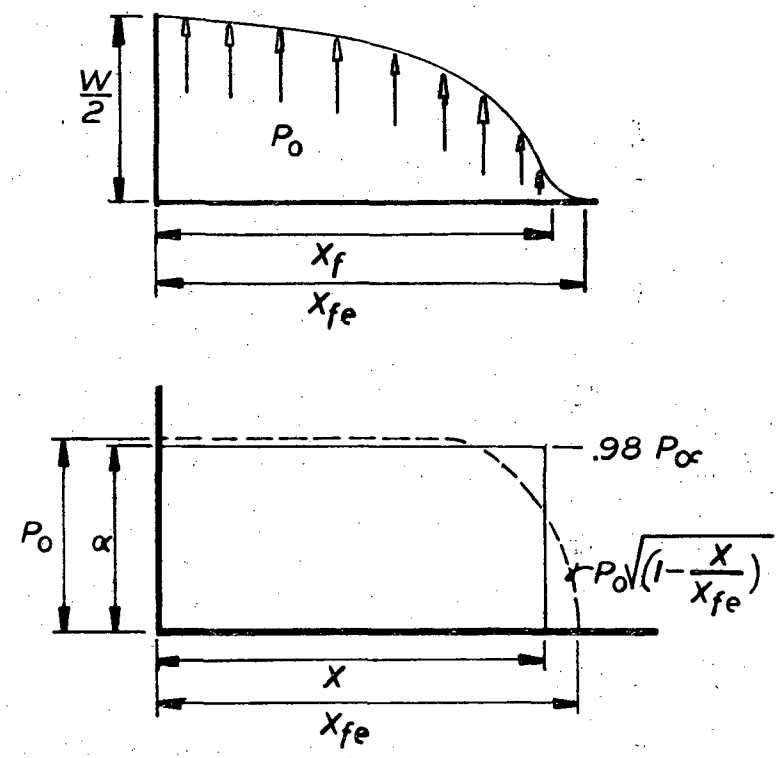

Figure 4b Corrected Cross Section and Polynomial Pressure Distribution

where μ is the fluid viscosity,

G is the formation shear modulus,

L is the instantaneous fracture length and

all other terms as defined above.

For a horizontal fracture the dependence is

$$w_{max} = 2\left(\frac{\mu Q_1 R}{G}\right)^{1/4} \qquad (12b$$

where R is the maximum fracture radius.

For a very large fracture it was found that a simple relationship between time and the length of the fracture was given by

$$L \simeq \frac{1}{2\pi}\frac{Q_1\sqrt{t}}{hC} \qquad \text{vertical case} \qquad (13a)$$

$$R = \frac{1}{\pi}\left(\frac{Q^2\ t}{C^2}\right)^{1/4} \qquad \text{horizontal (radial) case} \qquad (13b)$$

Kiel (1970) presents equations for fracture width based on an equilibrium shape distribution for constant pressure acting along the fracture but corrects for the stress concentration at the fracture tip as seen in Fig. 4b. Kiel's results show that the width of the fracture is proportional to the length and the average pressure in the fracture and that the length, L, depends on the square root of the ratio of the pumping volume divided by the fracture pressure. Kiel's equations are included in Appendix B.

Another form of Eq. (9), Eq. (14), was presented and solved numerically by Nordgren (1972) using a finite difference technique

$$\frac{\partial q}{\partial x} + q_1 + \frac{\partial A}{\partial t} = 0 \tag{14}$$

where $q = q(x,t)$ is the volumetric rate of flow across the constant x plane,

$q_1 = q_1(x,t)$ is the loss to formation per unit length at x and

$A = A(x,t)$ is the cross sectional area at x.

Nordgren's results presented in graphical form show a linear relationship between the log of a dimensionless length, L_D, and the log of dimensionless time, t_D, and a similar logarithmic relationship between a dimensionless width, w_D, and t_D (L_D, t_D, w_D are defined in Appendix C). At large time these solutions are expressed as

$$w_{max} = 4 \left(\frac{2(1-\nu)\mu\, Q_1^2}{\pi^3\, GCh} \right)^{1/4} t^{1/8} \tag{15a}$$

$$L = \frac{Q_1\, t^{1/2}}{Ch} \tag{15b}$$

where all terms are as defined previously. Note that Eqs. (15b) and (13a) differ by a factor of two.

To compare Eqs. (15a) and (12a) insert the expression for L in Eq. (13d) into Eq. (12a) to obtain

$$w_{max} = 2.1 \sqrt{\left(\frac{\mu Q_1^2}{2\pi G h^2 C}\right)} t^{1/4} \tag{16}$$

Thus w_{max} calculated by Nordgren is proportional to the square root of w_{max} as calculated by Geertsma and de Klerk. This difference is probably due to the fact that Nordgren assumes an elliptical cross section for A(x,t) while Geertsma and de Klerk assume a constant cross section over the fracture height. Nordgren's approximations for small time L (or no fluid loss) are

$$\max = 2.5 \left(\frac{(1-\nu) \quad Q_1^2}{Gh}\right)^{1/5} t^{1/5} \tag{17a}$$

$$L = 0.68 \left(\frac{G\ Q_1^3}{(1-\nu)\mu h^4}\right) t^{1/5} \tag{17b}$$

Daneshy (1973d) later modified Kiel's work by assuming a polynomial pressure distribution in the fracture and also assuming that the fracture tip always moves ahead of the fracturing fluid. This assumes that the fracture is only pressurized over an effective fracture length x_{f_e} such that $x_{f_e} < L$ (L = max fracture length). Calculating an equivalent pressure acting over x_{f_e} by integrating the polynomial distribution over L, a numerical iterative method was used to estimate w_f and x_f. The results presented tended to agree with calculation of Geertsma and de Klerk but were independent of the Poisson's ratio and of the stress, S_h. Daneshy correctly points out that the accuracy of these calculations depends on the validity of the constant height restrictions assumed by all the above authors.

Extension Pressure

Implicitly assumed by the authors in the above section is the fact that during extension the pressure in the fracture exceeds the value of the earth stress, S_h, and is the only requirement for extension. Thus, as long as $P_{ext} > S_h$ the fracture extension will proceed. It is accepted that the minimum extension pressure is S_h (Hubbert and Willis, 1957).

Geertsma and de Klerk (1969) derived an expression for the pressure at the wellbore needed for extension as

$$P_{ext} = S_h + \frac{2Gw_{max}}{3L} \tag{18}$$

As the length of the fracture increases the fracture pressure (assumed uniform) decreases to S_h for very large L. This is evidenced by many field (Howard and Fast, 1970) and laboratory observations where the value of P_{ext} is greater than or equal to $P_b/2$ (Medlin and Masse, 1979). However, for weak or extremely permeable rock the pressure may build up to S_h. This is evidenced by successive stimulation cycles when the initial fracture is repeatedly pumped and then bled-off (Zoback, et al., 1977) or when the fracturing process extends along preexisting natural paths. In operations where large fluid viscosity and constant pumping rates are used the observed pressure will build up to a value larger than S_h due to the pressure drop along the fracture. Thus, very viscous fluids are not appropriate for in-situ stress determination of S_h unless a correction factor can be added to Eqs. (1 to 4).

Analysis of Constant Geometry Systems

While a large part of this review has concentrated on the techniques and fracture processes involved during hydraulic fracturing, a similar treatment will be made for analyzing flow in a stabilized

fracture system. After the well has been stimulated and returned to production it is often tested to determine the fixed or "constant geometry" dimensions the fracture will assume after the fractures begin to close. In this instant the fracture permeability is determined by the proppant bed. After the system stabilizes the fracture geometry is fixed and attention is focused on the effect of the fracture properties on well production. This is usually expressed in terms of increased production ratio i.e., the ratio of the well's production from the fractured reservoir system to the production recorded during pre-stimulation conditions. Other analyses have led to generation of pressure buildup data (type curves etc.) that are used to analyze pressure transients at the wellbore in order to estimate the fracture geometry, permeability, and damage. The information in terms of production ratio is always field related and is quantitative in nature while the use of pressure drawdown data is qualitative (or analytical).

The value of using the production ratio of the well to express fracture behavior may be somewhat limited. The basic reason is that if the production measurements are taken right after stimulation, the effects of cleanup, skin damage, choking, etc. may still be affecting the flow capacity of a well, depending on the magnitude of the effective permeability of the formation (Morse and von Gonten, 1972). This effect is most noticeable in gas wells. In MHF applications the true well performance might not be realized for many years. Morse's estimated minimum value of formation permeability that would permit the successful use of the production ratio is 10 md, which is well above the range of formation permeabilities encountered in MHF operations. Thus a great many of the hydraulic fracture systems should rely on the qualitative method for post-stimulation analysis.

The qualitative or analytical investigations for the problem of a well intercepting a vertical fracture are based on a similar physical model. This consists of a well of radius r_w that fully penetrates a formation of height h and intercepts a rectangular vertical fracture that fully penetrates the formation. The fracture is symmetric with a half-length of x_f and permeability, k_f. The propped width, w, of the fracture is assumed uniform. The fracture is centered in a reservoir of radius, r_e, with a constant boundary pressure, P_e (the radius r_e may be infinite). The model is depicted in Fig. 5. The rock permeability, k, is also assumed constant. The term "fracture conductivity" is used to describe the relative ability of the fracture to produce fluid compared to an ideal infinite capacity fracture in which no pressure gradient exists. This term is often defined by use of the fracture conductivity, wk_f, in a dimensionless fracture conductivity parameter in the form of $(wk_f/kx_f)B$, where B is some constant. The parameter of dimensionless fracture conductivity used in this work will be defined in Eq. (19) to be consistent with current authors

$$C_r = \frac{w\ k_f}{kx_f\pi} \tag{19}$$

where C_r is the dimensionless fracture conductivity,

w is the fracture width,

k_f,k are the fracture, formation permeabilities and

x_f is the propped fracture half-length.

Infinite Fracture Conductivity

Prats (1961) solved the problem of steady state flow to a fractured well using conformal mapping to break up the flow field into an elliptic region near the wellbore to represent the fracture and an outer region to

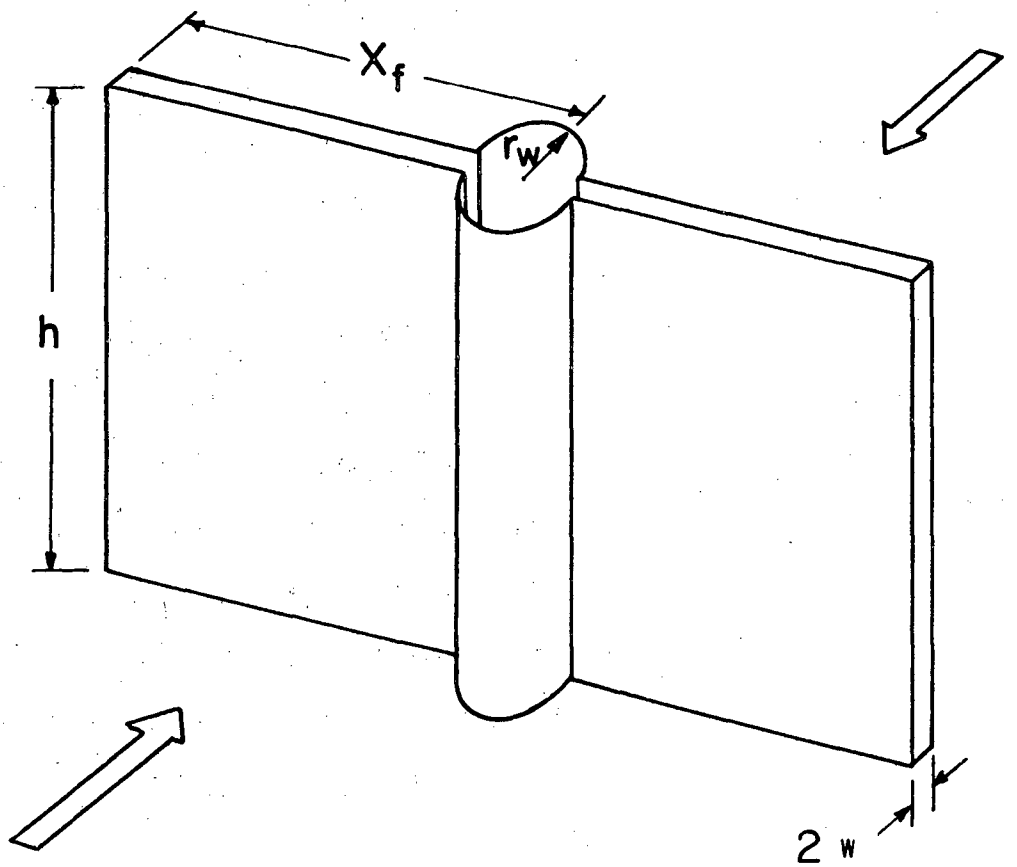

XBL 792-5743

Figure 5 Representation of a Well Intersepting a Single Vertical Fracture

represent the reservoir. For an incompressible fluid Prats found that the flow to the infinite conductivity well-fracture system could be treated as flow to a radial system with an effective wellbore radius, r_{we}, of one-fourth x_f. The effect of skin damage was not significant if the damage was restricted to a zone of one inch or less. The effect of using a compressible fluid was investigated by later researchers (Prats, et al., 1962) for the case of an infinite conductivity fracture. The compressible case introduces the effects of time on the system and the results indicate the production rate dropoff could be calculated if the fracture penetration, x_f/r_e, was less than 1/2. Conversely the production rates could be used to calculate the degree of penetration if data before and after fracturing is known. At large times it was again found that the fractured well behavior was the same as a radial system with r_{we} equal to one-quarter of the fracture half-length, x_f.

Steady State Fracture Flow Behavior

Analysis of pressure behavior in wells should indicate approximate radial flow behavior after long times (pseudo-steady state behavior). The form of this large time relationship between the observed pressure drawdown for a fractured well vs time was estimated by van Everdingen and Meyer (1971) using an elliptic flow model as Eq. (20a).

$$P_{e,T_{Df}} = 1/4 \ln (T_{Df}) + .800 \qquad (20a)$$

where $P_{e,T_{Df}}$ is the pressure drop in the well, and

T_{Df} is the dimensionless time = $kt/\phi\mu c x_f^2$.

The corresponding expression for the unfractured well would be

$$P_{a,T_D} = 1/2 \ln(T_D) + 0.809 \tag{20b}$$

where P_{a,T_D} is the pressure drop in the well.

Thus the pseudo-steady state behavior of a "fractured" well would differ markedly from the behavior of an unfractured well during a pressure drawdown test. However, much larger times are required for the fractured well to assume this pseudo-steady state behavior. Van Everdingen derived these equations by treating the fracture region as an elliptic flow region, hence the subscript e in Eq. (20a). If the external boundary pressure, P_e, is known or can be found, then type curve analysis may be used to evaluate pressure drawdown tests when the wellbore pressures are monitored under conditions of steady volumetric fluid withdrawal.

Type Curve Analysis

The advantage of type curve analysis is that there is no requirement that the time should be very large before the solutions become applicable. Type curves are plotted as the logarithm of dimensionless pressure, P_D, vs the logarithm of dimensionless time, T_{Df}. A similar plot of field data will match the appropriate shape of the correct type curve with only a translation of the values of the axes. The amount of translation in the axes indicates the geometric parameters of interest by comparing the values of real time and pressure vs their dimensionless counterparts. The initial solutions for type curve analysis for fracture applications were for the case of an infinite conductivity fracture, i.e., no pressure drop in the fracture, and for a uniform flux fracture (Gringarten, et al., 1974). Uniform flux describes a situation when a constant flux per unit area is entering the fracture face from the formation. The external boundary dimensions for the system are either an

infinite r_e or a fixed square drainage dimension, x_e, so that x_f/x_e is a variable parameter. Gringarten solved the above problems using an analytical technique employing source and Green's functions. The solution for the respective cases appears in Appendix D. For values of dimensionless time $T_{Df} > 3$, the infinite conductivity solution for a closed boundary takes the form of Eq. (21)

$$P_{wD}(T_{Df}) = 1/2 \ln(T_{Df}) + 1.100 \tag{21}$$

which is twice the slope found by van Everdingen for elliptical fracture flow, Eq. (20a). For smaller times the solution takes the form

$$P_{wD}(T_{Df}) = \sqrt{\pi T_{Df}} \tag{22}$$

which has a slope of one-half on a log-log plot. This is called the linear flow period when flow initially is governed by linear flow at the fracture face. The corresponding large time solution ($T_{Df} > 2$) for the uniform flux solution is

$$P_{wD}(T_{Df}) = 1/2 \ (\ln(T_{Df}) + 2.80907) \tag{23}$$

Here a radial flow period is evidenced in agreement with Prat's earlier work.

Gringarten and Ramey (1974) presented a similar treatment for horizontal fracture. They found that in addition to a "linear" and "radial" type flow period there was a definite transitional period in between. Gringarten, et al., (1975) conclude that the uniform flux solution will match the pressure drawdown data of a natural fracture system better than the infinite conductivity solution (which fits hydraulically fractured wells better). The reason for this is the permeability contrast of a

hydraulically fractured well is more likely to lead to high C_r values ($C_r \propto k_f/k$). Most hydraulic fractures, when propped, would show a much larger permeability contrast with the natural formation than would a native fracture. Later authors commented on the use of the Gringarten type curves for analysis of field data (Raghavan, 1976). The effects of wellbore storage would modify the very early time data giving the type curves another characteristic slope of unity. This unit slope can easily be seen from the fact that if the initial volume of the wellbore is $V = \pi r_w^2 h$ then the change in pressure in the wellbore for early time (when there is minimal flow to the well from the formation) is related to the change in the fluid volume by

$$P_{ws} - P_{wf}(t) = \frac{V - Q_1 t}{\pi h r_w^2} \tag{24}$$

where

Q_1 is the constant pumping rate,

P_{ws}, $P_{wf}(t)$ are the static, flowing wellbore pressures and

V is the volume of the fluid in the wellbore.

From Eq. (24) it is seen that the graph of the log of quantity $h(P_{ws} - P_{wf})/Q_t$ vs the log of $t/\pi r_w^2$ will be linear with a unit slope. Using the conventional definitions for $P_{wD} = 2\pi kh(P_{ws} - P_{wf})/q\mu$, and $T_D = kt/\phi\mu c r^2$, then log P_{wD} = log T_D plus a constant. If T_D is replaced with $T_{Df} = kt/\phi\mu c x_f^2$, then log P_{wD} = log T_{Df} plus another constant. This early unit slope could dominate the early time data if the initial fluid volume, V, is large enough.

The Effect of Fracture Skin on an Infinite Conductivity Fracture

The importance of the concept of fracture damage or "skin" was recognized relatively early in analyzing post production data. Van Poolen (1957) used electrical analogy models to study the effect of fracture skin damage on flow rate. Most field skin damage is located within one inch of the fracture plane and the resultant permeability of this zone is reduced up to 95% of the undamaged formation. This one-inch skin damage had a small effect on the steady state flow capacity, a fact that Prats (1961) later calculated. However, the relative amount of flow restriction was important if skin damage was greater farther from the well. Over 40% of the total flow entered the infinite conductivity fracture in its last 10% of length which made the system potentially susceptible to reduced production if the skin thickness increased with the fracture half-length, x_f. Fortunately, the skin thickness is proportional to the exposure time of the fracturing fluid to the fracture walls which causes the skin thickness to decrease with fracture length in field applications.

In gas formations that are much more sensitive to fracture fluid invasion, attempts have been made to correlate skin damage with turbulent flow in fracture (Tannich, 1973). This was explained by Raghavan (1976) by his conclusion that skin could be treated as mathematically equivalent to reducing the fracture conductivity. However, since fluid turbulence can also be effectively treated as reducing the fracture conductivity, the effects of skin and turbulence are hard to distinguish.

The effect of fracture length in gas formations is important since if the field pressure is low and the fracture length long, then fluid cleanup may never be complete near the fracture ends (Holditch, 1979). Here the effective fracture length, x_{fe}, is much lower than x_f. However,

while long fractures in high pressure gas reservoirs may take a long time to clean up, they suffer no permanent production damage but rather just a delayed response.

Finite Conductivity Fractures

The concept of infinite fracture conductivity must be considered in terms of a more realistic assumption. A fracture propped over its height with fine mesh sand may exhibit a fracture flow conductivity, wk_f, that only exceeds the formation conductivity, kh, by a few orders of magnitude. Thus C_r may have a value on the order of 1.0 especially for long thin fractures. Cinco-Ley, et al. (1978) presented a solution for an infinite reservoir finite capacity fracture based on analyzing the flow in the fracture and the flow in the formation separately, again using Green's functions. The two solutions were numerically matched using the common flux boundary condition and by discretizing the fracture plane into a finite number of fracture elements. The solution was numerically iterated until it agreed both on the boundary condition and also did not change as the number of elements increased. The solution depends on two variables A and B defined as

$$A = \frac{w\phi_f \; c_{ft}}{\pi L_f \; \phi c_t} \qquad \text{and} \qquad B = \frac{k_f \; \phi c_t}{k\phi_f \; c_{ft}}$$

Cinco-Ley, et al. conclude that in the absence of fracture storage, A and B could be combined to define the dimensionless parameter C_r, as defined above, i.e., $C_r = AB$. For values of $C_r > 500$, Cinco-Ley found excellent agreement between his work and that of Prats for large values of dimensionless time and Gringarten's solutions for large x_f/x_e (that is the finite radius boundary effect is not noticed). Cinco-Ley, et al. concluded that the amount of flux into the latter fracture half decreased

as the fracture conductivity decreased. Thus a small fracture would yield the same production as that of a longer fracture for low values of the dimensionless conductivity ratio C_r. Cinco-Ley and Samaniego (1977) added the effects of wellbore storage and skin damage to their finite conductivity solution.

Quantitative treatments for finite conductivity fractures resulting from acid treatment (Novotny, 1977) and two-phase flow (Raghavan, 1977a) have been presented in the literature. Finite fracture conductivity solutions involving a fully numerical method using finite difference (Agarwal, et al., 1979) with no wellbore storage and integral finite difference techniques (Narasimhan and Palen, 1979) including wellbore storage have recently appeared.

Calculation of Fracture Orientation

The use of analytical solutions to predict fracture orientation was suggested by Komar, et al. (1973) by using pressure tests in observation wells to correlate the fracture orientation with surface phenomena. Using the increased transmissivity of the fracture, Pierce, et al. (1975) investigated the difference in the time lag between a pulsed well and observation wells before fracturing and the time lag after fracturing the source well. This allowed a computation of the fracture length x_f as

$$\left(\frac{T_{LA}}{T_{LB}}\right)^{1/2} = \frac{x_f}{r}\sqrt{\frac{k}{k_f(0.005)} - 1} + 1 \qquad (25)$$

where T_{LA}, T_{LB} are the time lags after and before fracture and

r is the distance between source and observation wells.

The constant 0.005 in the argument of Eq. (25) was the experimental value relating the fracture permeability k_f with the effective fracture permeability, $F_f k_f$ (i.e., $F_f = 0.005$).

Uraiet, et al. (1977) used Gringarten's (1974a) solution for flow in an infinite system (i.e., $x_e = r_e = \infty$) to find the dimensionless pressure drop for an observation point removed from the wellbore a distance r_D and at an angle τ from the fracture plane. Here $r_D = (1/x_f)\sqrt{x^2 + y^2}$, where x and y are measured from the wellbore. Cinco-Ley and Samaniego (1977b) extended Uraiet's work by incorporation of finite fracture conductivity. The effect of finite fracture conductivity was very pronounced on the results as it delays the pressure pulse in the fracture. Interpretation of field data assuming the wrong conductivity could lead to serious errors in estimating the orientation angle τ. The above analyses ignore the effect of wellbore storage which also could have a corresponding effect of delaying arrival of the pressure transients to the observation wells.

Pressure Dependent Permeability

The effect of the fracture closure on the permeability of the fractures has so far been ignored in the type curve literature, even though studies have been made on the effects of fracture closure stress on fracture proppant permeabilities (Cooke, 1973) and on the quantitative effects on gas turbulence in flowing fractured gas wells (Holdich and Morse, 1976).

The effect of stress sensitive gas formations has been described in analyzing pressure buildup data (Vairogs and Rhoades, 1973; Evers and Soeiinah, 1977). However, there has been little reported on the effects of stress sensitive formation on drawdown behavior and on type curve analysis. Further treatment of the subject of pressure analysis for fractures is thoroughly summarized by Raghavan (1977b).

Summary

This chapter has dealt with some of the previous work conducted in the fields of hydraulic fracture design, operations, and post stimulation analysis. The intent of this review was to provide an overall understanding of the complex processes relevant to hydraulic fracturing and identify some key issues needing further resolution. The purpose of the present work is to investigate some of these issues. The investigation will be carried out through the use of a mathematical model.

The development of the model is presented in the next chapter. The model is designed for use in numerical simulations. Parametric studies included with the model included the following analyses: the effects of fluid viscosity, pumping rate, and variable formation properties on the growth of hydraulic fractures; possible control of the initial fracture growth to prevent undesirable vertical extension; and the usefulness of the parameter C_r in analysing well tests conducted in systems with non-linear properties.

III. MODEL DEVELOPMENT

This chapter will present the development of a model designed to assist in the analysis of pressure transients observed in wells intercepting either a fixed length fracture or a growing hydraulic fracture. Ideally, a method (either analytic or numerical) should be found that could incorporate variations in boundary conditions (including flexible geometry), three-dimensional fluid flow, and pressure dependent material property variations. That is, the model should be able to reflect, conceptually, the physics of the problem and have a minimum of restrictive assumptions. Recent trends toward this conceptual understanding have become possible with the advancement of both numerical techniques and high speed digital computers (Narasimhan and Witherspoon, 1977).

In the present work a numerical approach will be taken. Hopefully, material in this chapter will not only illustrate the flexibility of the particular method but will also help quantify the effects that the analytical assumptions may have on the results. Material covered in this chapter will include: limitations of the analytic models; considerations involved in a numerical approach; meshes used in the simulation of fixed length and growing hydraulic fractures; and development of the criteria used to control the fracture growth in the simulations presented in the next chapter.

A. LIMITATIONS OF THE ANALYTICAL MODELS

Fixed Length Fractures

The analytical solutions for systems with fixed fracture geometry have been presented for two-dimensional systems (Gringarten, et al.,1974, Cinco-Ley,et al., 1978). Although a solution for the three-dimensional

is certainly possible (Gringarten and Ramey, 1973) it has not appeared yet. In the present form, the solutions of Cinco-Ley can handle wellbore storage, fracture skin, and finite fracture conductivity although the analysis does not deal with the problems associated with variable fracture permeability and stress sensitive formations. Another assumption in the available fixed geometry solutions is that the influence of flow from the wellbore face is ignored. The analytic solution treats the fracture-formation system as being isolated, ignoring the contribution of independent flow from the formation and the wellbore itself. In cased wells this may be a good assumption but in many wells perforations will open the wellbore face directly to the formation unless all the perforations lie on the (fracture) plane. The use of the type curve solutions depend on determining a single value of the dimensionless fracture conductivity parameter, C_r,which may not be unique.

Growing Fractures

Calculation of the geometric properties,such as the aperture and wing length, of a growing hydraulic fracture as it extends from a wellbore has been done by analytical and numerical techniques, each with some limiting assumptions. For a fracture growing with time the methods used to estimate the fracture geometry were based on the assumption of a constant pumping rate, constant leak-off coefficient C, constant fracture extension pressure, P_{ext}, and ideal elastic behavior. In practice a constant pumping rate has become standard procedure but is not always practically achieved. The compressibility of the fluid in the subsurface tubing is ignored even though it may affect the pumping pressure and speed of fracture initiation. The constant leak-off coefficient is a reasonable approximation only when fluid loss additives are used and the fluid pressure is relatively constant over the fracture length. The fact that

the wellbore pressures are often higher than the calculated P_{ext} (with use of highly viscous fracturing fluids) indicates that a pressure gradient will exist along the fracture. Thus, while the fracture tip may be extending at some minimum P_{ext} the rest of the fracture will be at higher pressures, the pressure monotonically increasing towards the wellbore. The ideal elastic assumption of uniform or near uniform pressure in the fracture as it extends may not be valid for these cases. Some researchers have incorporated viscous effects in their impermeable rock models (Zoback and Pollard, 1978) including variation of fracture permeability with length. Yet, there has so far been no anlytical work that combines the fracture extension mechanics with fracture-reservoir flow. While an anlytical solution to the problem of a growing fracture coupled with the fluid flow between well, fracture, and reservoir may yet be found, the complexity of properly formulating the problem in analytic terms may be prohibitivly difficult.

B. NUMERICAL APPROACH

There are, generally speaking, three numerical techniques commonly used to solve problems involving fluid flow in porous media. One is the finite difference method (FDM) which directly discretizes the differential equation at each nodal point of the flow region. Another is the finite element method (FEM). This method uses an integral approach to solve for fluid flow in the volume surrounding a point in the flow region by summing a weighted average of the flow in the volume near the point and using a set of non-collinear points for evaluating spatial gradients of potential. The third approach is the integral finite differene method (IFDM). This is also an integral technique that relates the change in pressure in an explicitly defined volume element with the normal flux of fluid over the volume surface and uses the finite difference approximation

for measuring spatial gradients of potential (Narasimhan and Witherspoon, 1977).

Each of the above methods has some inherent advantages and disadvantages. Finite difference is conceptually the easiest to implement and has been used extensively by mechanical and petroleum engineers to solve problems in potential theory. However, finite difference techniques can become very un-wieldy when non-trivial geometry is used. Finite element has found increasing use in solving structural problems and was first introduced in the civil engineering discipline. It has since been applied to potential theory problems with a marked degree of success (Pinder and Frind, 1972, Neuman and Narasimhan, 1975). However, while the finite difference method can be solved explicitly for small time steps, the finite element method is often implicitly formulated and procedurely cumbersome in three-dimensions. The integral finite difference method, also called the finite volume method (Thomas and Lombard, 1979), combines the advantage of explicit formulation with arbritrary geometry. It can easily be applied to heterogeneous flow. However, it uses finite difference (linear) gradients between grid points (nodes) and can approximate steep gradients in pressure potential only with small grid spacing. The method does (as does FEM) permit the use of more flexible geometry than FDM but handles boundaries of dissimilar materials in a more realistic fashion than does FEM. For the present work the IFDM was found to be especially well suited and was chosen as the principal method of solution.

Aspects of IFDM Formulation

For an arbritray volume 1, the equation of mass conservation for the IFDM formulation, developed in Appendix E, can be expressed as

$$S_l V_l + \sum_{i=1}^{n} \frac{k_i(P_i - P_l + \rho g(z_i - z_l))A_{i,l}}{\mu_i D_{i,l}} = \frac{(\phi c)_l V_l (P_{l_{t+\Delta t}} - P_{l_t})}{\Delta t} \qquad (26)$$

where k_i is the permeability of node i,

P_i, P_l are the pressures at nodes i, l,

$A_{i,l}$ is the interfacial area between elements i and l,

$D_{i,l}$ is the perpendicular distance between $A_{i,l}$ and node i,

$(\phi c)_l$ is the storage coefficient of the material of element l,

Δt is the time increment between time steps in the calcuation,

ρ is the fluid density,

g is the acceleration of gravity,

S_l is a fluid source or term in node l,

μ is the fluid viscosity,

z_i is the elevation of node i, and

n is the number of adjacent nodal elements to element l.

A sketch of the geometric terms defined above for an arbtritrary three-dimensional nodal element is shown in Figure 6. In areas of relatively steep pressure gradients, e.g., near the face of the fracture, the volume elements will have to be made very small to maintain accuracy of the gradient approximation. The meaning of a volume element in Eq. (29) is completely general. Thus, surface pumps, wellbore tubing, and packer cavities can be treated as volume elements. In array notation Eq. (26) can be rearranged to appear as

$$\overline{A_{l,m}} (\tilde{P}_m - \tilde{P}_l) - MC_l \frac{\Delta \tilde{P}}{\Delta t} = \tilde{S}_l \qquad (27)$$

where $\overline{A_{l,m}}$ is a matrix of conductance elements $a_{l,m}$ where $a_{l,m} = \frac{k}{\mu} \frac{A_{l,m}}{D_{l,m}}$

MC_l is a mass capacity matrix of the ϕc terms,

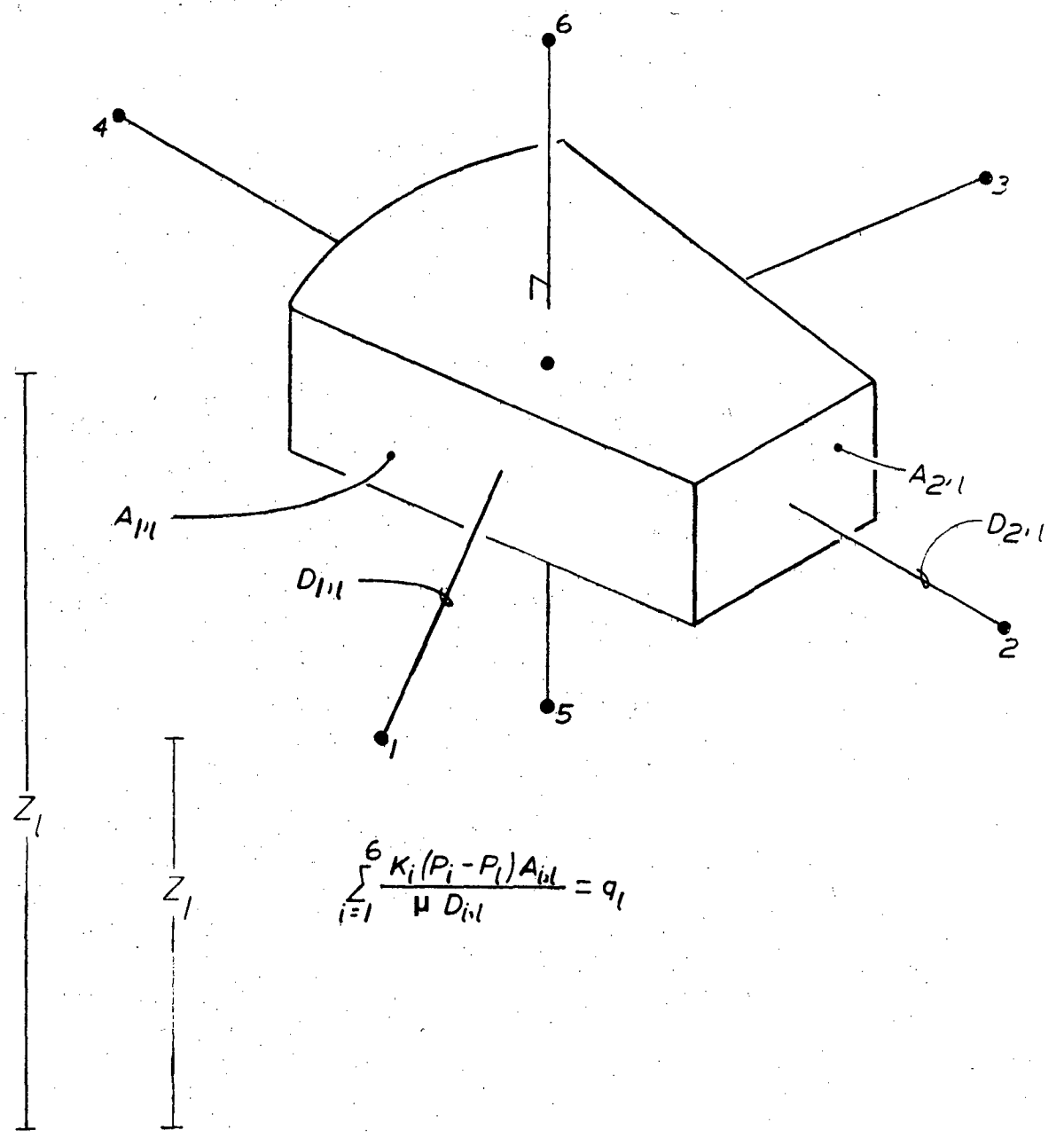

Figure 6 Volume Element Representation Used in IFDM Formulation

$\tilde{S}_l$ is a source term vector, and

$\Delta\tilde{P}_l = \tilde{P}_{l_{t_o + \Delta t}} - \tilde{P}_{l_{t_o}}$ is the vector of pressure and elevation changes in the nodes over a time Δt.

The size of the largest stable time step depends on the volume of the node and is equal to (Narasimhan, et al., 1977)

$$\Delta t_{l_{stable}} = \frac{\overline{MC_l}}{\overline{A_{l,m}}} = \frac{(\phi c)_l V_l}{\sum_n \frac{k_m A_{m,l}}{\mu D_{l,m}}} \tag{28}$$

However, in the present work the time steps allowed by Eq. (28) were prohibitively low so an implicit formulation of Eq. (26) was used.

Previous Computer Codes

Edwards (1969) developed an IFDM code TRUMP for use in the field of fluid flow in porous media. Narasimhan (1975) adapted this program to handle the flow of fluids in partially saturated deformable porous media in his program TRUST. He later generated a fully saturated version of TRUST as the program TERZAGI.

The present work utilizes program HYDFR which resulted from further modifications in program TERZAGI. HYDFR has provisions for solving the implicit set of equations either by using a mixed implicit-explicit iterative scheme originally formulated in TERZAGI or by a direct solution technique (Duff, 1977).

Solution Techniques

The use of iterative methods to solve Eq. (27) is efficient as long as there are no large permeability contrasts in the flow region, when highly permeable volume elements adjoin volume elements with very low permeability. Such contrasts will occur during modeling of hydraulic

fracture systems. Experience gained during this work showed that while the iterative method was adequate for solving the equations involved in the study of a fixed length geometry fracture, the method could not be efficiently used to assist in the treatment of the growing hydraulic fracture. The direct solution technique employing Duff's direct solver in programs DIRTER and CCC (Bodvarsson, et al., 1979) is also used in program HYDFR. In retrospect, direct solution techniques should be used in such computationally difficult problems as the growing hydraulic fracture if the solutions are to be tractable within a reasonable machine computation limit. This conclusion has been reached by other authors (Pierce, et al., 1975; Holditch and Morse, 1976).

C. MESHES USED IN THE FIXED FRACTURE LENGTH SIMULATIONS

General Considerations

The speed and accuracy of the IFDM calculations may be enhanced by exercising care in the design of the meshes used in the simulation. The design of the meshes must take into account both the shapes of the elements and the placement of the nodal points within the elements. The nodal point placements within the elements is critical in determining the conductance between nodal points since the conductance is inversely proportional to nodal point separation. For example the conductance element in $\overline{A_{1,m}}$ expressing flow between elements 2 and 3 can be expressed as

$$a_{2,3} = \frac{k_{2,3}A_{2,3}}{\mu(D_{2,3} + D_{3,2})} \tag{29}$$

where $A_{2,3}$ is the surface area common to nodes 2 and 3 and

$k_{2,3}$ is the harmonic mean permeability.

The harmonic mean permeability is especially useful when there is a

permeability contrast at the interface. The harmonic mean permeability is defined as

$$k_{2,3} = \frac{k_2 \, k_3 \, (D_{2,3} + D_{3,2})}{k_2 \, D_{3,2} + k_3 \, D_{2,3}} \tag{30}$$

where $D_{2,3}$ is the perpendicular distance between the node location of element 2 and the interface between elements 2 and 3.

From Eq.(29) is is apparent that different values of $a_{1,m}$ in the conductance term matrix $\overline{A_{1,m}}$ will arise from changing the position of the nodal points within the elements and thereby the $D_{1,m}$. The optimum location of the nodal elements within the elements is governed by the gradient of expected flow at local steady state conditions. The gradient is expressed as a linear relationship in IFDM. Thus, for IFDM elements used in cylindrical systems the nodal points are located at the logarithmic means of the nodal volume to determine the optimum values of the $D_{1,m}$. The logarithmic spacing is explained by the fact that in steady state flow in a radial reservoir, the pressure gradient is linear in ln(r). Similarly, for rectilinear elements designed for linear flow regions the optimum position of the nodal points would be the linear mean or centroid.

Since the fracture technically has no solid volume (other than proppants), the location of the nodal points within the elements used to represent the fracture is relatively important. For fully developed laminar flow between parallel plates the pressure gradient is linear (White, 1974). Therefore, the nodal point positions will be centrally located with respect to the x (fracture flow) direction, with nodal spacing decreasing near the wellbore. The nodal point location with respect to the y direction (normal to the fracture plane) is at the face

of the fracture elements and thus the value $D_{l,m}$ between the fracture element and the first formation element was zero.The nodal point location is placed at the fracture face since there is no pressure gradient across the width of the fracture and no contribution from the fracture elements in calculating the conductance terms $a_{l,m}$ in Eq. (29). The product of the conductance terms with the factor $\rho^2 g$ is called TRAN in the programs used in this study. TRAN represents a fluid conductance, i.e., the amount of fluid flux per unit change in fluid potential. TRAN will be used in this work to refer to the fluid conductance value for each individual element connection. The TRAN value for flow into the fracture face must be independent of the fracture conductivity as the fracture conductivity is only defined in terms of flow within the plane of the fracture.

Deformable ("Breathing") Fracture

A fracture which has an aperture that varies with the difference in pressure between the fracture and the formation, i.e. a stress dependent formation, is called a "breathing" fracture and is treated in a very general manner. The computer codes have the capability of storing non-linear pressure dependent permabilities. Thus the values cited in the literature of pressure dependent proppant permeabilities could easily be assigned to the fracture elements. The conductance and TRAN values for the elements would be calculated by Eq. (29). However, an alternate method was used that represents the permeability of the fracture as a function of the square of the fracture width. This assumes sufficient mobility of the proppant to prevent bridging when the fracture walls "breathe". Iwai (1976) showed that the Darcy permeability defined for laminar flow in a natural fracture obeyed the cubic law, Eq. (31)

$$Q = - C^* \frac{w^3}{12\mu} \frac{dP}{ds} \tag{31}$$

where Q is the volumetric flow rate,

w is the fracture aperture or width,

C^* is a constant, and

dP/ds is the pressure gradient in the direction of s.

If this relationship is applied to the fracture the TRAN values for flow in the fracture elements can be calculated by considering the fracture geometry as the wedge depicted in Figure 7. Figure 7 shows representations of both the fixed aperture fracture and breathing fracture cross-sections. The value of the fracture permeability, k_f, used in the TRAN values for the connections between the fracture elements is $w_{1,2}^2/12$ where $w_{1,2}$ is the harmonic mean width as defined in Fig. 7. For the case when $d_{1,2} = d_{2,1}$, i.e. evenly spaced fracture elements, $k_f = ((w_{1,2} + w_{2,1})/2)^2/12$.

It is convenient to make use of a substitution to handle the variation of w with the pressure in the fracture. Program TERZAGI uses a simple one-dimensional theory of consolidation that calculates the change in the void ratio, e, with the change in effective stress, which is equal to the overburden weight minus the fluid pore pressure. If e is defined as the ratio of the void volume to that of the solids volume, the fracture can be treated as an equivalent rock mass with a solids volume of unity and a porosity approximately equal to the aperture of the fracture, which would be equal to e. A change of pressure in the fracture will then change the void ratio and the width. That is at a fixed overburden stress and at any x_f, a change in the fracture void volume (wx_fh) affects the fracture width and hence the permeability, directly. A similar treatment has been

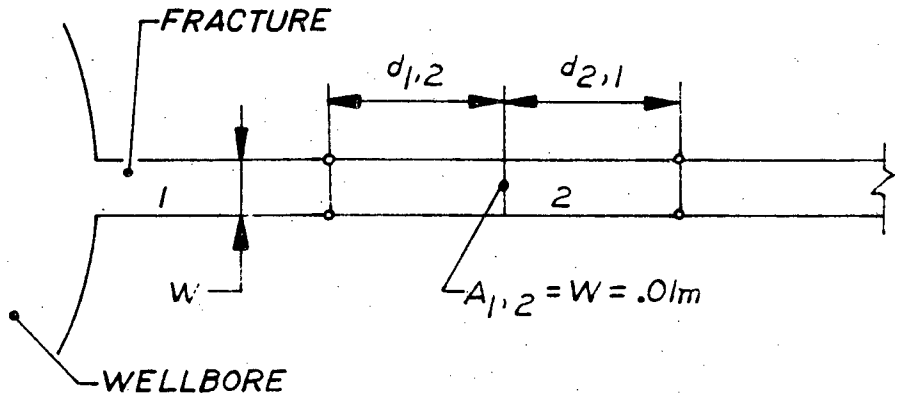

$$q_{1,2} = \frac{k_{1,2} A_{1,2}}{\mu (d_{1,2} + d_{2,1})}$$

FIXED FRACTURE REPRESENTATION

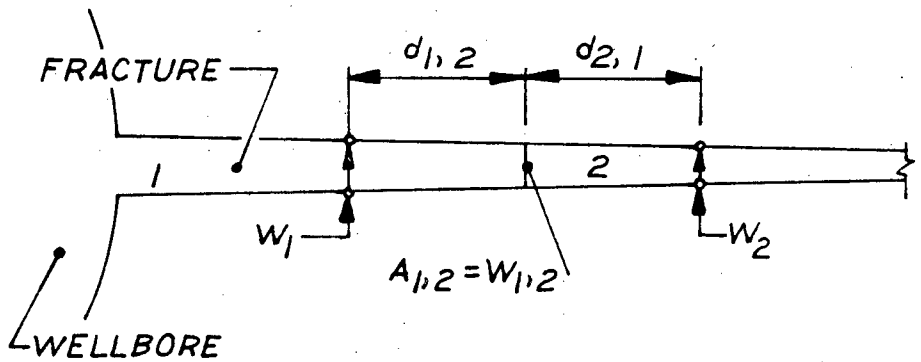

$$q_{1,2} = \frac{(W_{1,2})^3}{12\mu} \qquad W_{1,2} = \frac{W_2 d_{1,2} + d_{2,1} W_1}{d_{1,2} + d_{2,1}}$$

DEFORMABLE FRACTURE REPRESENTATION

Figure 7 Fracture Element Representations

used to study the effects of pore pressure on the storage capacity, ϕc, of reservoir rocks (Jones, 1975). The TRAN value for the connection between the well and the fracture elements is governed solely by the conductance of the first fracture element for both the fixed aperture and deformable fracture meshes.

Fractures with Fixed Geometry

The model for the fixed geometry fracture (i.e. fixed wing length) assumes: a completely penetrating vertical rectangular fracture; homogeneous formation properties ϕ, c, k; constant fluid properties μ, β; constant fracture width w (with the exception of the deformable fracture) and half-length x_f; symmetry with respect to the fracture plane and the wellbore; and fluid flow according to Darcy's law. Fluid flow is permitted between the formation and the wellbore through the wellbore face and flow may enter the fracture tip from the formation. The mesh for the fixed fracture length system appears in Fig. 8. The view of the mesh is along the axis of the wellbore in the xy plane. Presented in the upper diagram in Fig. 8 is a large scale representation of the mesh. The outer boundary (not shown) is at a distance of 80 meters from the edge of the fracture in the x direction and 80 meters from the formation face in the y direction. This large scale mesh is designed in accordance to the radial flow behavior expected at large times and the elements are curvilinear at $r > 20$ m. The elements for the near fracture region are aligned normal to the plane of the fracture as seen in the middle diagram of Fig. 8. This is designed to best fit the expected linear flow regime near the fracture face. The elements are spaced much closer together near the fracture plane to account for the sharp pressure gradient expected at the formation-fracture interface.

The lower diagram in Fig. 8 shows the near wellbore mesh used in the

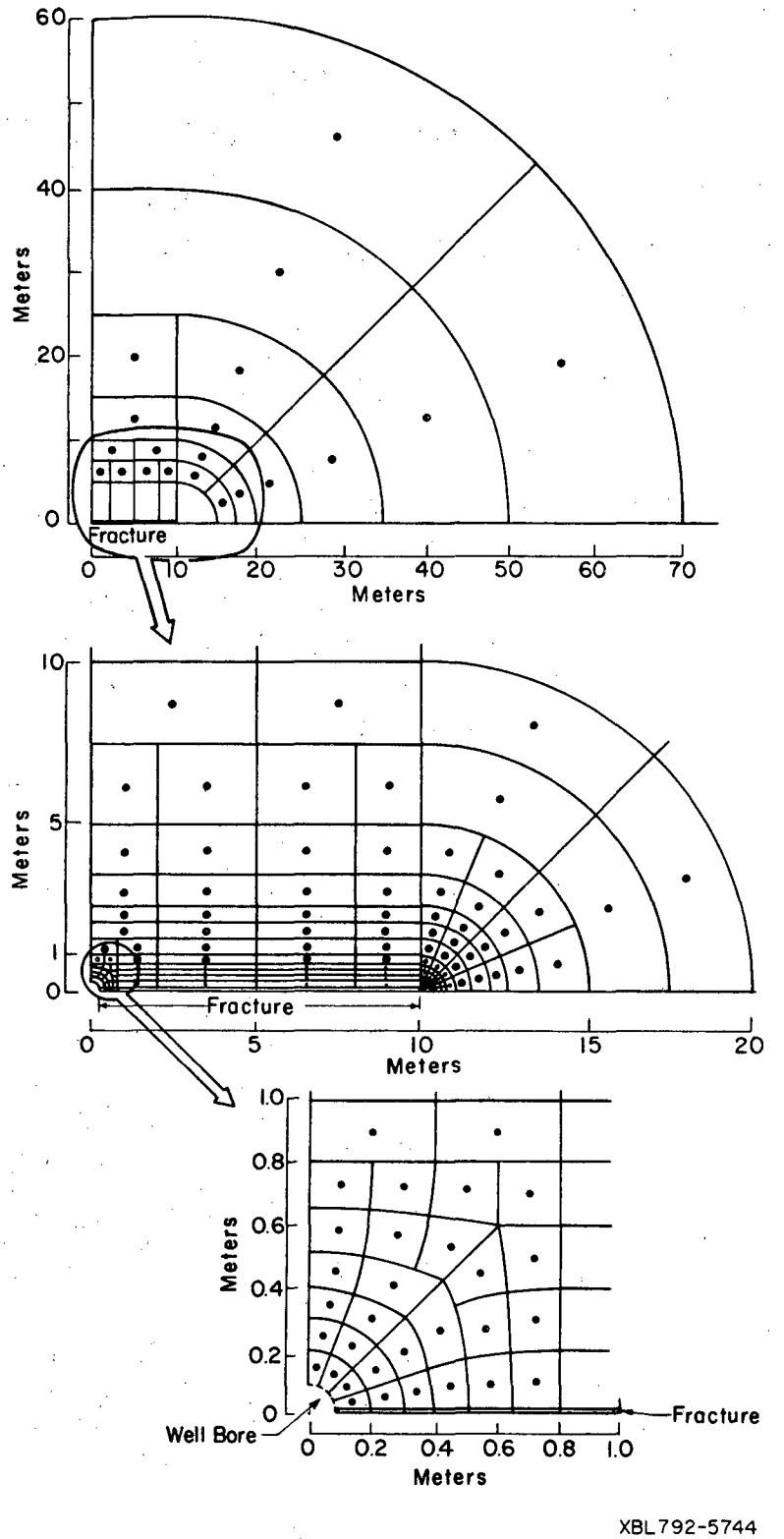

Figure 8 Mesh Used in Fixed Fracture Length Simulations

fixed fracture geometry simulations. At the wellbore the mesh is similar to the mesh from the 10-20 m region at the fracture tip, as seen on the preceding sketch. Both of there areas are simulated by a curvilinear mesh. This implies that flow from the wellbore to the formation is expected to be radial as is flow from the region at the fracture tip into the formation.

The fracture itself was modeled as a number of finite thickness (w = .001 m) elements with individual lengths and total number of elements that depend on the fracture conductivity. For an infinite conductivity fracture only one fracture element is needed since there there is no pressure gradient in the fracture. For the fixed geometry system, as C_r decreases the fracture conductivity also decreases, if the formation properties are constant. As the fracture conductivity decreases the pressure gradient becomes steeper and more elements are needed to simulate the pressure drop.

From the general shape of the mesh in Fig. 8 it is apparent that the fractures considered are symmetric and the flow can be accurately described by consideration of one-fourth of the total flow area. This mesh can also easily be used to study the effects of fracture damage by assigning lower permeability values to the elements adjacent to the wellbore and to the elements composing the fracture face. Fracture "choking" as defined above, can be treated by lowering the permeability of the first fracture element to represent the effects of undesirable sand placement or of flow restricting turbulence. The wellbore is also modeled as having one-fourth the true wellbore volume. The source or sink terms providing the constant flow rate associated with type curve analysis are located in the wellbore node.

D. MESHES USED IN THE GROWING FRACTURE SIMULATIONS

General Considerations

The physical concept used in simulating a growing fracture is based on modeling the fracture extension process and formation-fracture flow by a succession of equilibrium states. The criteria for changing between successive equilibrium steps will be developed in the next section and is related to the elastic-plastic behavior of the formation rocks. Therefore, a consecutive series of reservoir meshes was used to model the growing fracture problem, each mesh representing an equilibrium extension of the fracture.

The configurations of the growing fracture models are based on the meshes used for the fixed geometry fractures. Two different meshes were used representing, (i) a circular (penny-shaped) vertical fracture and, (ii) a rectangular shaped vertical fracture. The speed of the extension process is assumed to be greater than the speed of the fluid migration in the reservoir so that the mesh boundary is only slightly larger than the fracture half-length x_f. That is, fluid from the well is assumed to move faster in the fracture plane than outwards into the reservoir. When the fracture growth is stable, i.e., where the wellbore pressure increases or is constant with fracture growth, this may not be strictly true depending on the magnitude of the transmissivity, $k/\phi\mu c$, of the formation.

The boundary condition for the rectangular fracture in the vertical directions assumes that there is no growth. Thus the elements in the fracture and reservoir are bounded by a hypothetical barrier that will allow movement of the fracture faces normal to each other but not fluid or fracture penetration. This is typically explained by the assumption that the fracture toughness of these boundary layers is so large that penetration is prohibited. However, the fracture edges are allowed to

grow parallel to the barrier surface or are allowed to "slip" against the inhomogeneity. The "slip" barrier assumption will be critiqued in the last section. The fracture elements themselves are handled mathematically like the breathing fracture elements discussed previously with the exception of the leading (last) element. The width of the last fracture element used in the TRAN calculation is no greater that one-half the maximum fracture width calculated at the fluid pressure of the element. This is based on the continuity requirement of a sharp edged fracture. The leading fracture element is the end of a triangular wedge and must have no cross-sectional area at the tip. Thus the effective width can be no greater than half the maximum width of the element (at the point where it contacts the next to last fracture element). This representation also means that there cannot be flow in the plane of the fracture from the leading element since there is no interfacial area at the fracture tip.

Computational Aspects of Fracture Extension

The problems associated with the series of fracture element meshes used to represent the growing fracture could be efficiently handled by either of two methods. The first technique would be to input an entire mesh similar to that of the fixed geometry fracture. The fracture elements would all be given conductance values of zero until the extension criteria are met. Then the first element adjacent to the wellbore element could be "opened" depending on the initial conditions of the problem. This "opening" would simply involve using a finite value of the TRAN term for the first fracture element. Analogously, all the other fracture elements could be "opened" when appropriate conditions are met. This method has two serious drawbacks. The first is choosing an adequate mesh size such that the final fracture length, x_f, will not exceed

the estimated length. This presents difficulties modeling systems with arbitrary formation properties where the fracture lengths cannot be accurately estimated beforehand. The second drawback is the extra computational effort needed to handle the superfluous nodal elements. In general the amount of time needed to solve the n x n matrix $\overline{A_{l,m}}$ used in the numerical solution is proportional to n^2. While the direct solver used in HYDFR will handle larger time steps than the iterative solver previously used, it requires many times the storage space. Effectively that means there is a smaller number of elements the program can handle before the additional storage requirements of the direct solver become prohibitive. Hence, to optimize a given amount of computational time and storage space, the nodal elements and mesh are generated within the program as needed. This was done by adding a subroutine EXTEND in the program that generates the additional fracture elements and associated reservoir elements. EXTEND also calculates the volumes and other matrix coefficients appearing in Eq. (29). The treatment of the growing fracture models through the use of the self-generating mesh subroutine in combination with the direct solver were, perhaps, the most important factors in the success of the present numerical modeling effort.

Rectangular Mesh Entension Factor

During extension the length, Δx_f, of each successive fracture element is increased in the rectangular mesh. A mesh extension coefficient ε was used to expand each successive element by an amount $(1 + \varepsilon)$ with the exception of the second element. This element had a constant fracture length of 0.5 m. For example, the 10th fracture element would have an effective length of $x_f = 0.5\ (1 + \varepsilon)^8$. This stretching coefficient was varied to allow either a very closely spaced fracture mesh ($\varepsilon = 0$) when extremely large fracture pressure gradients were expected, or a larger

spacing for smaller pressure gradients. This is a direct result of work done with the fixed geometry mesh that proved the necessity of increasing the number of fracture elements only when large pressure gradients (i.e., lower C_r values) were being modeled. The length of the elements was increased at greater distances from the well due to the consideration that the fracture pressure gradient is steeper nearer the wellbore where the mass flow rate is greatest. That is, the flow rate will decrease in the fracture as more of the fluid leaks off into the formation when very permeable rocks are modeled. The use of the ε factor was also necessary due to the small size of the initial elements. To model a fracture of only 10 m in length would take 20 fracture elements and 120 associated reservoir elements for a constant $\Delta x_f = 0.5$. However, with an extension factor of only 10% ($\varepsilon = 0.1$) the total fracture half-length x_f will be 26 m with 20 elements and, for $\varepsilon = 0.2$, x_f will be 78m. To be able to compare the model results with those in the literature, the length of the fracture must be much greater than the height, h. The ε factor allows a long rectangular fracture to be generated and the numerical computations to be solved within reasonable computational time limits. The ε factor was not used in the radial meshes.

Growing Fracture : Mechanical Connections

In addition to the formation-fracture mesh, volume elements are used to represent the surface piping and pumps, the wellbore tubing, and the packed-off section of the wellbore. The configuration assumed appears in Fig. 9. The surface piping pressure is measured upstream of the wellbore section. There will be a viscous pressure drop through surface equipment and the wellbore tubing that must be corrected in order to compare the pressure in the fracture with that recorded at the surface. There will also be a pressure increase measured at the surface due to the head

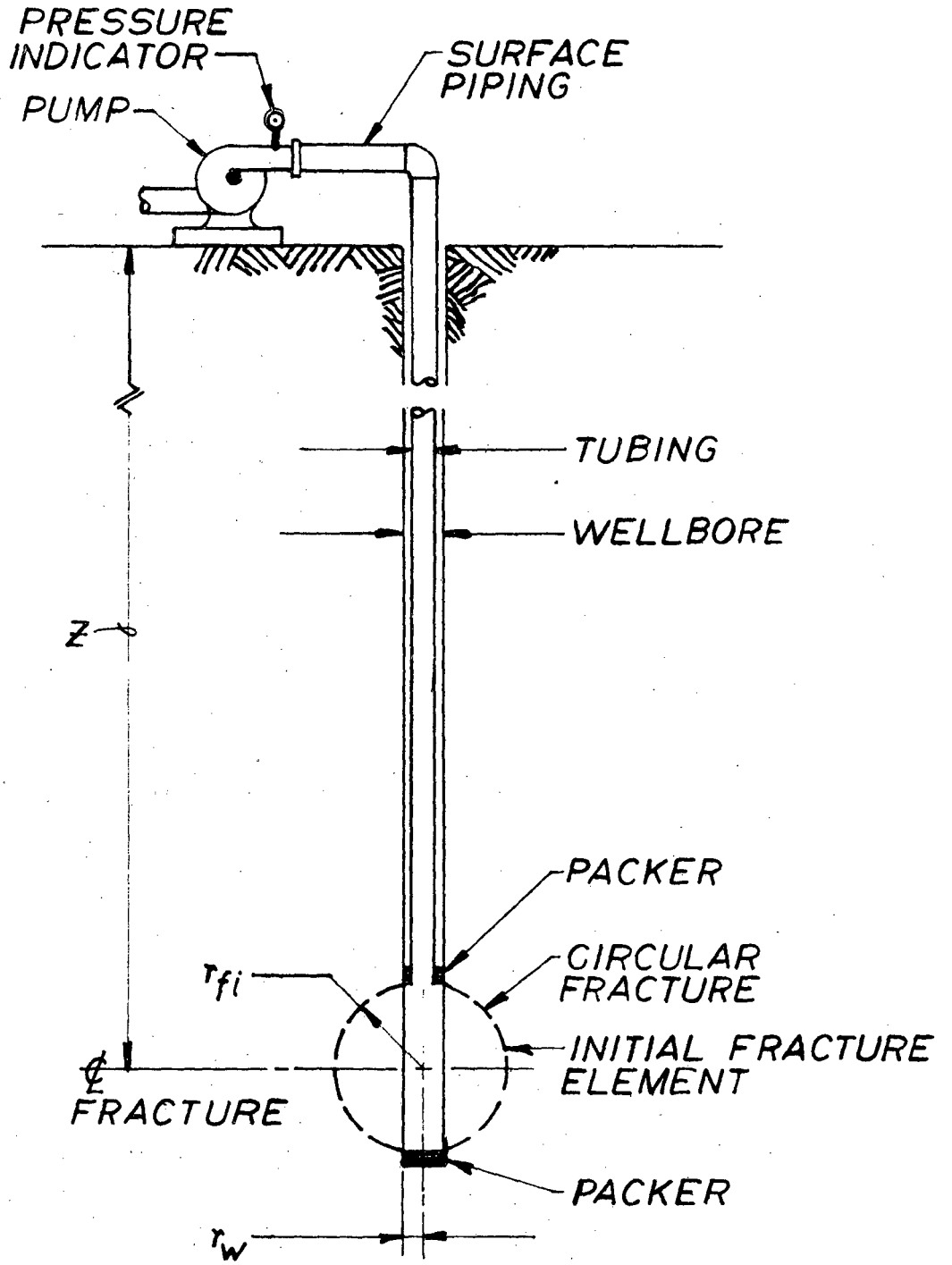

Figure 9 Growing Fracture Tubing Element Representation

difference between the surface and the formation. This head term is a function of the fluid density and compressibility. The incorporation of elevation in the modeling process makes the overall problem three-dimensional. However, flow in the fracture-formation system will be two-dimensional in that only one layer of elements will be used for the fracture and reservoir mesh, restricting vertical flow.

The growing fracture is connected at the wellbore with nodes that represent the surface piping, pumps, and the wellbore tubing. These nodes are modeled as long cylindrical elements with length of 30 m for the surface piping and either 300 or 1000 m for the tubing. The 30 piping length was the value used for the experimental simulation runs with Monticello data, to be discussed in a later section. The wellbore tubing length of 300 m is the average depth used for simulation of the Monticello experiments which uses a circular fracture mesh. The 1000 m length was only used with the rectangular fracture mesh used in simulating larger, deeper fractures. Three elements were used to model the latter subsurface tubing, each 333 m in length. The nodal locations were at the midpoints of each element to correspond with the linear pressure drop down the tubing. The volume of each of the tubing elements was one-fourth of the true volume as the model simulates one-fourth of the assumed symmetric flow field.

The permeability used to calculate the TRAN values for the pipe elements was taken from the laminar flow equation relating the pressure drop along the pipe radius (White, 1974).

$$q = -\frac{r^2}{8\mu}\frac{dP}{dx} \tag{32}$$

where q is the flow rate,

r is the pipe radius,

μ is the fluid viscosity, and the equivalent pipe permeability

$k_{pipe} = r^2/8$.

A permeability value was calculated for the packer-wellbore element but was not used since the wellbore dimensions, r_w = 0.0762 m (3") and h = 3 m, are small enough so that no pressure gradient is assumed to exist. The wellbore dimensions were taken from field data and are considered to be representative.

Fracture Element Mesh

Once the fracture breakdown pressure, P_b, is reached, flow is allowed into the initial fracture element. When the extension criteria are met, the fracture can propagate in one of two modes: radial (circular penny-shaped) or linear (rectangular).

The fracture meshes representing the extension phase are shown in Figs. 10a and 10b for the circular and rectangular extensions, respectively. The views are in the planes of the fracture.

The circular mesh used a constant wellbore element height of 3 m and an initial fracture (element 100) radius r_f of 1.5 m. The first element was assumed to be circular in shape. This has been observed by Zoback (personal communication, 1979) using transparent plexiglass samples. After the initial fracture node is opened, the fracture extends in a purely radial mode. For this mesh the extension increment was constant at a Δr = 0.5 m. The surface area of successive elements increased during extension as r_f increased. The central plane of the formation (z = 0) contained the axis of the nodal point locations. While this assumes a priori that the effect of gravity within the fracture is negligible, for sufficiently large fractures more fracture elements would

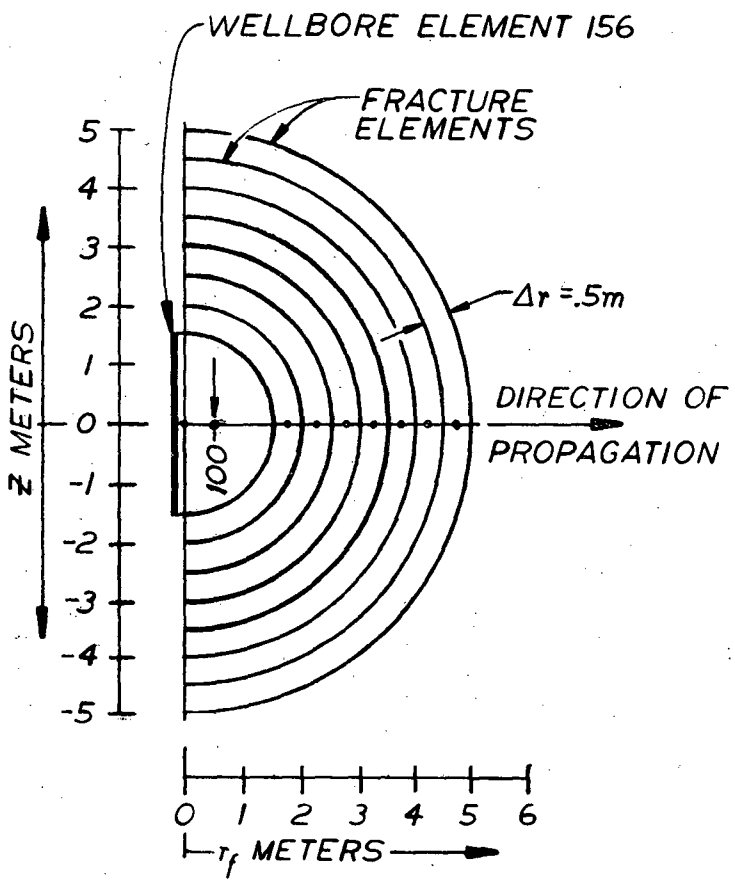

Figure 10a Circular Fracture Mesh

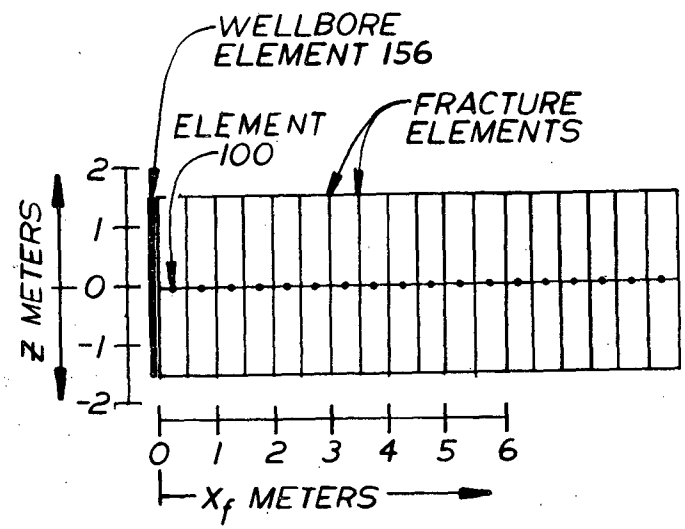

Figure 10b Rectangular Fracture Mesh

have to be used. These elements would incorporate changes in elevation by having nodal centerlines at angles different from the horizontal ($z = 0$) centerline.

The rectangular extension mesh shown in Figure 10b uses a rectangular first element (element 100) of height equal to 3 m with an initial x_f of .424 m. The shape of all additional fracture elements created during propagation are also rectangular although the individual lengths, Δx_f, of the fracture elements will increase if $\varepsilon \neq 0$.

Circular Fracture Reservoir Mesh

The reservoir mesh for the growing circular fracture is shown in Fig. 11a,b. The reservoir elements are generated along with each adjacent fracture element and take the shape of the radial fracture elements rotated through angles of 15°, 30°, or 45°. The reservoir elements are shaped like slices of a thick walled hollow sphere, e.g., similar to a peach slice. A view of one of the reservoir elements is shown in Fig. 11a. Figure 11b shows the $r\theta$ (or xy) plane cross-section of the reservoir mesh. The mesh was designed to represent flow in systems where fluid leakoff is very small, e.g., in-situ stress measurement experiments or the "hot-dry-rock" system both of which operate in very low permeability granite. The mesh could conceivably be used for select interval (perforation) fracturing of a thick, low permeability gas zone. However, interaction of the fracturing fluid with the gas phase present in the formation would introduce relative permeability effects into Eq. (29). The current HYDFR program does not treat the case of partial liquid saturation.

For low formation pressures and high gas compressibilities the fluid penetration is assumed to be piston-like in the reservoir, totally

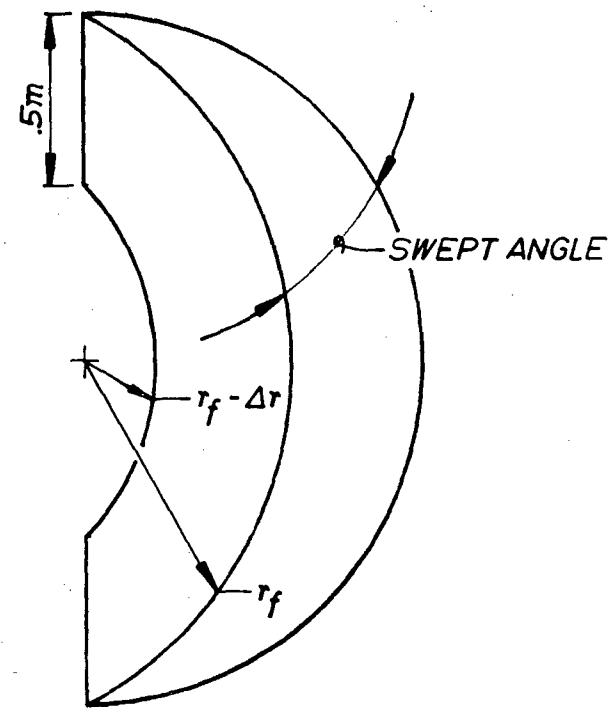

Figure 11a Circular Reservoir Mesh Element

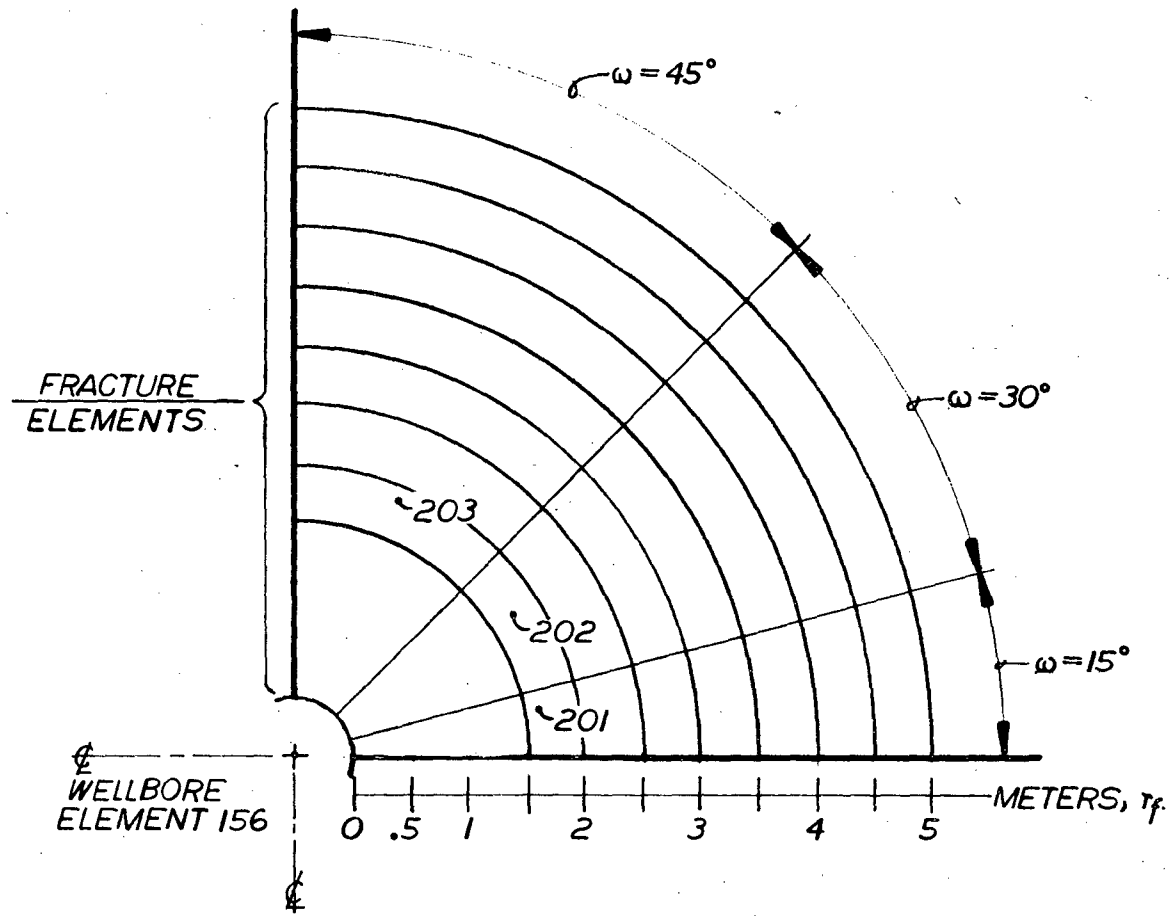

Figure 11b Circular Reservoir Mesh Plane View

displacing the gas phase due to extremely low mobility ratios of the fracturing fluid compared to the formation fluid. For high fluid viscosities and low formation permeabilities there is little fluid penetration for HDR systems modeled by use of the circular fracture mesh and the coarse nature of the mesh is somewhat justified. While the mesh used for circular growing fracture is coarse compared to the constant geometry fracture mesh in Fig. 8, the larger element sizing is necessary to help compensate for the increased computational time the constant fracture spacing requires. A concession is made for handling the neglible formation flow by decreasing the size of the elements closer to the fracture face, i.e., the 15° elements are adjacent to the fracture elements.

The rock permeability is assumed to be so small that there is no penetration of the fracturing fluid in the formation ahead of the fracture tip during fracture growth. This is treated in the model by creating the fracture and reservoir elements simultaneously in radial sweeps, when the extension criteria are met.

Rectangular Fracture Reservoir Mesh

The rectangular growing fracture mesh is shown in Figs. 12 a,b for $\varepsilon = 0$. Figure 12 a shows an overview of the reservoir mesh as seen in the $r\theta$ ($z = 0$) plane. The mesh is patterned directly after the mesh used for the constant geometry fracture. There is a region representing radial flow some distance away from the wellbore and a rectilinear mesh near the fracture face is used to handle resevoir-fracture flow. Figure 12b shows the detail of the mesh near the wellbore which is again curvalinear in design. The first wellbore surface elements and the first formation surface elements have thicknesses of 0.024 m and 0.03 m, respectively. These elements were designed to aid in the modeling of skin effects when using fluid loss coefficients and are on the order of 2.5 cm

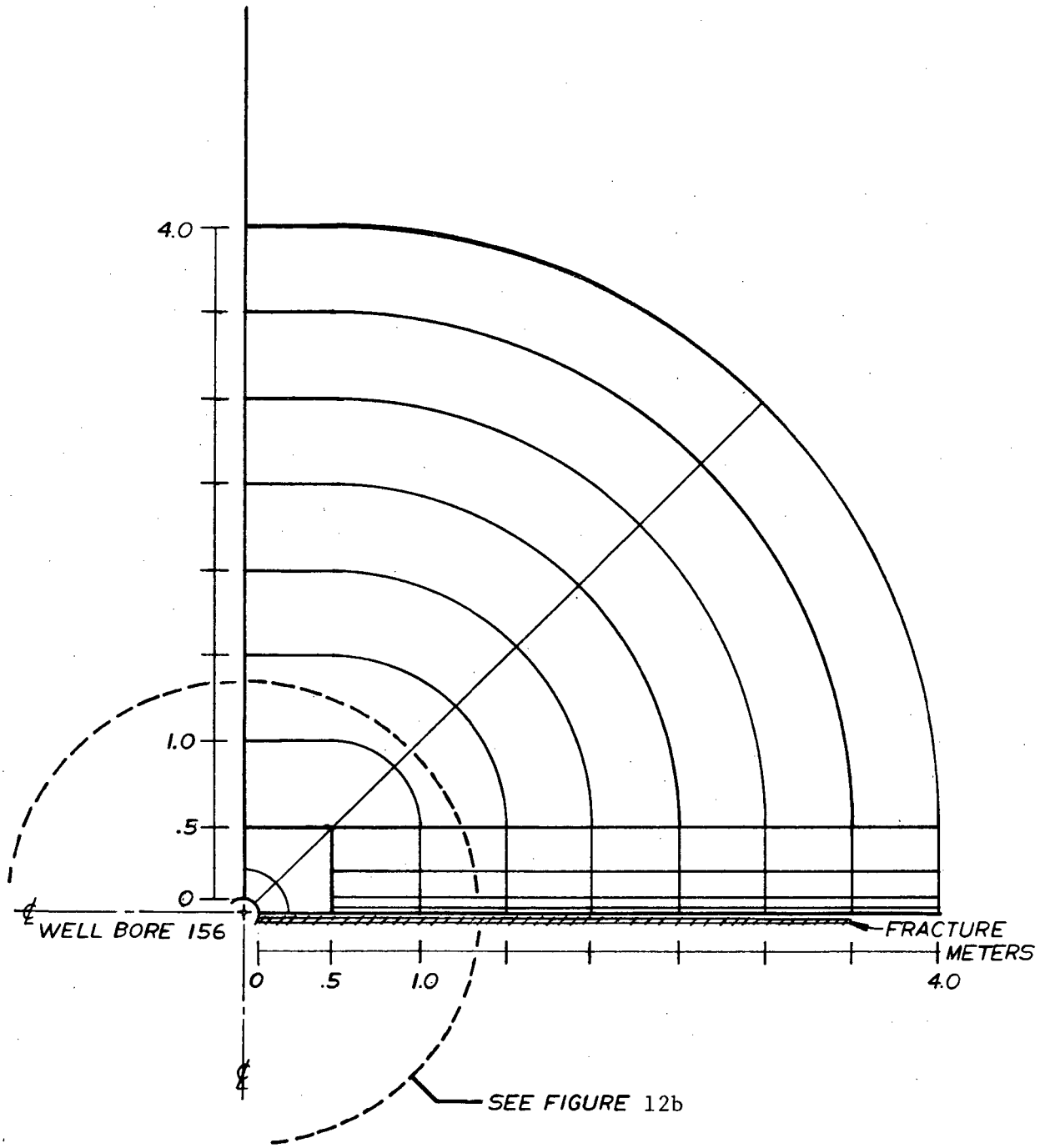

Figure 12a Rectangular Reservoir Mesh Overview

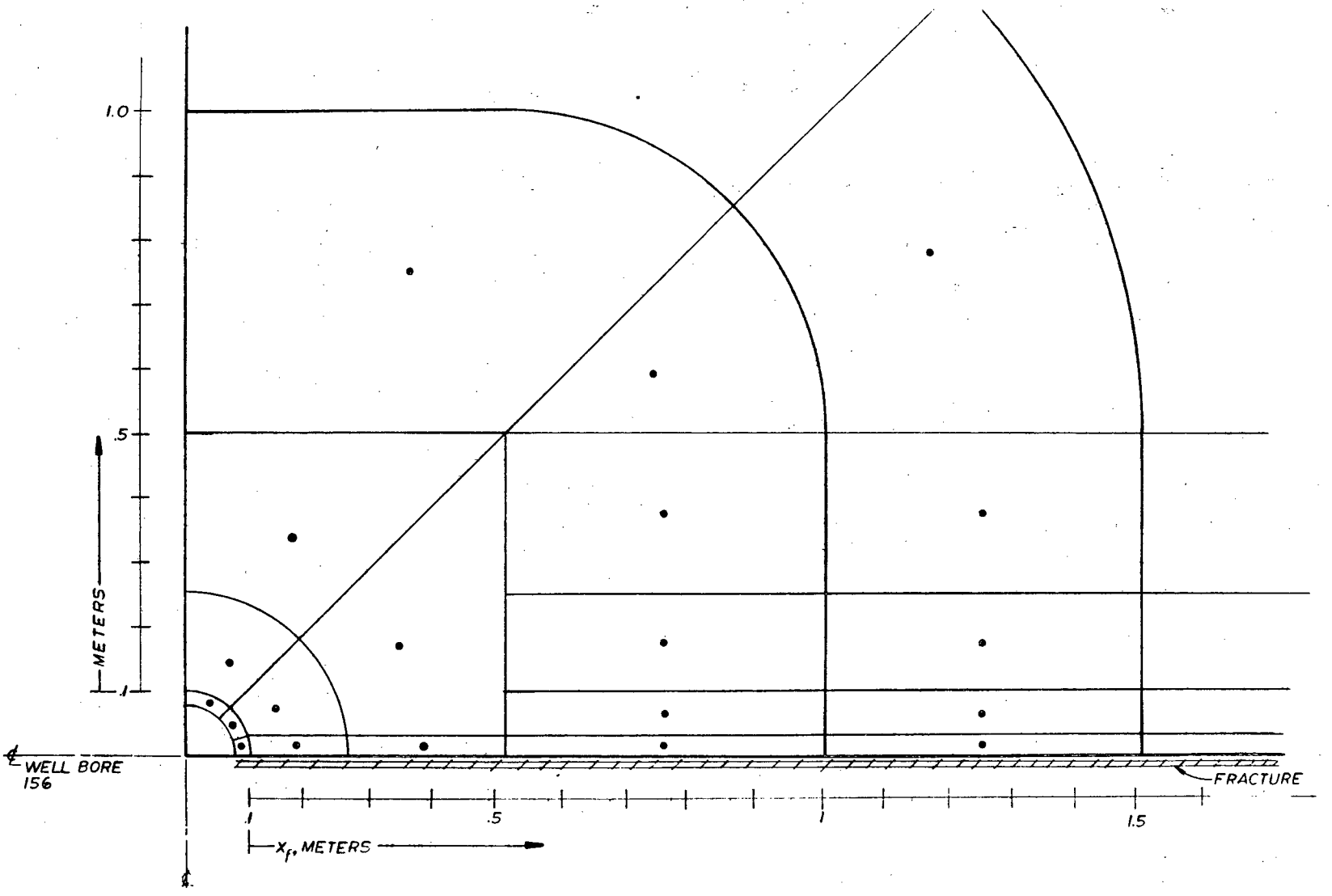

Figure 12b Rectangular Reservoir Mesh - Expanded View

in width as suggested by van Poolen (1957). For each fracture element created, six reservoir elements were generated. However, during extension the reservoir elements are created one step ahead of the fracture elements.

The initial reservoir elements associated with the first fracture element (100) intercepting the wellbore are initialized in HYDFR by the input data thereby allowing changes in wellbore dimensions. Until the breakdown pressure p_b is reached element 100 is mathematically eliminated due to manipulation of the conductance terms mentioned above. The next set of reservoir elements are already generated when P_b is reached in the wellbore and element 100 "opened". The pressure builds in element 100 until the extension criteria are reached and then the next fracture element and reservoir elements are generated. The total fracture length will always trail the reservoir mesh radius, r_e, by a distance of $0.5\ (1 + \varepsilon)^{(n-2)}$, where n is the number of fracture elements. If, for example, fracture element 1800 was created, then so would leading elements 1901 - 1906, allowing fluid flow in the region ahead of the fracture tip. While the leading reservoir element generation may seem pointless, it is conceivable that during stable fracture growth or when modeling very permeable formations that fluid penetration in the formation ahead of the fracture tip may occur. The use of the leading elements would help correct the boundary effects that this penetration would have on the pressure calculations.

E. FRACTURE EXTENSION CRITERIA

Introduction

While there have been many criteria proposed for the extension of a crack or fracture in brittle elastic media, only two were investigated in the development of the present model. These methods involve the use of stress intensity factors and Griffith's criterion for crack propagation.

A crack propagates in one of three ways, generally referred to as Modes I, II, and III (Corten, 1972). For an incipient crack in a two-dimensional solid, when motion of the surfaces is normal to each other (away from the plane of the crack), the displacement is called Mode I behavior. If the motion of the crack faces relative to each other is in opposite directions but parallel to the plane of the crack and in the direction of crack propagation the displacement is called Mode II behavior. Mode III behavior occurs when the faces move parallel to the plane of the crack but in directions normal to the direction of propagation.

The extension process used for this model assumes that the formation will be rigid in the direction of propagation and is also bounded by the "slip" barrier making translation in the z direction impossible. This restricts the modeled fracture growth to Mode I behavior, although in unconsolidated shallow sands it is thought possible that Mode I and II behavior may occur simultaneously during the extension process (Dusseault, 1979).

The extension of a crack in an infinite solid is governed by the stresses involved at the tip of the crack. A parameter that describes the material's resistance to fracture is called the fracture toughness constant, K_c.

Stress Intensity Factors

The concept of stress intensity factors has been used to determine the conditions necessary for propagation of a crack in a solid. The stress intensity factor is defined in terms of the magnitude of the stress in the area of the crack tip as the radius of curvature of a circle inscribed at the crack tip, ρ, approaches zero. Tetelman and McEvily (1967) define the stress intensity factor for Mode I displacement as

$$K_I = \lim_{\rho \to 0} \frac{\sigma_{max}}{2} \sqrt{\pi\rho} \tag{33}$$

where K_I is the stress intensity factor for Mode I displacement,

ρ is the radius of curvature of the crack tip, e.g., $\rho = d^2/b$ for an ellipse of semi-minor axis length d and semi-major axis length b, and

σ_{max} is the maximum tensile stress acting on the crack surface.

For an infinitely sharp fracture

$$K_I = 1.12\ \sigma \sqrt{a\pi} \tag{34}$$

where σ is the applied tensile stress and

a is the crack length.

Thus for a sharp crack in semi-infinite elastic solid the stress intensity factor increases with length and is independent of the material composition.

When the stress intensity factor K_I is greater than the fracture toughness K_c of the material, the fracture will propagate in an unstable fashion; that is no increase in pressure is required for fracture

extension. Conversely for a fixed pressure or tensile stress the value of the stress intensity factor causing instability will depend on a given length, or critical length as observerd by Zoback (1978). For any fracture length, a, greater than the critical length the fracture will extend if the tensile stress, σ ,remains constant. However, the values Zoback obtains for fracture toughness for rocks by assuming a fixed critical length do not consistently agree with other values in the literature. This may reflect on the difficulty of applying elastic media theory in analyzing rock fracture behavior by assuming an invariant critical length.

Griffith's Fracture Criterion

An alternate and earlier method used in the study of fracture behavior was developed by Griffith (Corten, 1972). His method is based on the concept that energy is required to separate the material at the fracture tip. This work term is expressed using an energy per unit area term, γ . Thus if the fracture extends by an amount dx_f the energy required to create the new fracture surface is

$$dW_e = h\gamma dx_f \tag{35}$$

where dW_e is the incremental work required to extend the fracture by dx_f,

γ is the value of specific surface energy,

dx_f is the incremental fracture extension, and

h is the fracture height.

The forces acting on the fracture contribute to the total net energy of the system, W_s. Here W_s will refer to the total strain energy

stored in compressing the fluid in the fracture minus the work stored as potential energy in deforming the fracture walls. The Griffith energy criterion (Sneddon, 1951) states that the fracture will extend only when

$$\frac{dW_s}{dx_f} \geq \frac{dW_e}{dx_f} \tag{36}$$

Sneddon defined the internal work, or potential energy, done on a uniformly pressurized circular crack of radius r, with an elliptical cross-section located in a semi-infinite elastic medium as

$$\text{potential energy} = \frac{2\, P_o^2\, w_{max}}{6(1 - \nu^2)} \tag{37}$$

where ν is the Poisson's ratio,

w_{max} is the maximum fracture width, and

P_o is the constant internal pressure.

Equation (36) is a mathematical statement of an energy related criterion. Physically, this means that the fracture will extend if the total energy of the system is greater than the energy required to create a new fracture surface.

Despite the apparent differences in approach the stress intensity factor and Griffith's energy criterion can be shown to be mathematically equivalent (Tetelman and McEvily, 1967; Corten, 1972). The two methods can be related in Mode I behavior by their respective constants K_c and γ by $K_c = E\gamma$ where E is the Young's modulus. For an ideal elastic system the extension process can be explained by either of the elastic concepts.

Extension Criteria and Model Considerations

A Griffith's crack energy approach will be utilized in the extension

criteria used in the present work. The choice, while not arbritrary, is weighted by the general acceptance of the Griffith's energy method for use in geophysics research (Peng and Ortiz, 1973; Sandhu and Huang, 1975; Cornet, 1979).

Sandhu (1975) combined a finite element method with a modified Griffith's energy approach to predict micro-fracture growth and orientation in rocks. Sandhu also raised the possibility that the fracture direction could reverse itself or that the fracture could blunt out. Blunted fracture growth would indicate that the stored potential energy of the system has become greater or equal to the work done on the fracture system by the fluid pressurization. Then dW_e/dx_f would be negative and Eq. (36) cannot be satisfied. Actually the form of Eq. (36) would indicate the possibility of fracture healing if $dW_s < 0$. This blunting behavior was found to occur in the growing fracture simulations as will be discussed in the next chapter.

Another factor involved in the choice of the Griffith's method was the size of the meshes used in the simulations. It is physically impossible to derive detailed stress information at the fracture tip with an element 0.5 m in length. That is, the stress intensity factor could not be numerically evaluated using Eq. (33) with the mesh size required for simulating the large fractures modeled in this study.

If the assumption by Kiel (1970) that the fracturing fluid does not actually reach the fracture tip during the growth process is correct, the simple application of stress intensity factors and a critical length theory may be inaccurate. The physics of the real system require that the fracturing fluid only reach the tip of the fracture during blunting or stable fracture growth. Abé, et al., (1979) argue that the fracture toughness criterion for a circular fracture or a rectangular

fracture is only valid at small distances r_f or x_f or at very low pumping rates. As the fracture grows, the rate of fluid propagation will always lag the fracture growth and there will always be an energy requirement for fracture extension due to the fracture toughness of the material, even at distances past the critical length. This means that fracture growth is likely to be unstable at small fracture lengths and will be stable or may blunt out at larger lengths. In the discrete system used for the model the fracture growth always precedes the fluid flow. If the elements were chosen so that the discrete system behaved as the continuous system (i.e. Δx_f approaches zero) then the correction in the stress intensity factor calculation proposed by Abé could be used. The use of the large element sizes in the discrete approach and the one-dimensional deformation used in the program were the main reasons a modified energy approach is used to determine the extension criteria.

A Modified Griffth Energy Concept : System Boundary

Direct integration of Eq. (40) yields

$$W_s + C > W_e \tag{38}$$

where W_s is the net work done on the system minus the potential energy stored in the system,

W_e is the total surface energy required to create the fracture surface, and

C is the constant of integration.

If the total system boundary is defined to include the surface pumps, piping, and wellbore tubing, the constant C simply becomes the pressure-volume (PV) work done on the fluid in the pipe if there is no energy lost across the system boundary. This realistically requires that the system boundary be isothermal and adiabatic. If the system is defined only in

terms of the area immediately surrounding the fracture then C must necessarily be zero. Either approach should work regardless of where the system boundary is chosen. Early comparisons in duplicating field data showed that both definitions gave essentially the same results. However, the system boundary will be defined in this work to exclude the surface piping and wellbore tubing. This choice is necessary due to the fact that energy would be lost if there is viscous dissipation in the tubing when super-viscous fracturing fluids are used. The use of the Darcy pipe flow law in Eq. (32) would nesessitate an artificially high tubing permeability to model the minimal pressure drops during "Super Frac" type operations. This artificially high permeability would affect the calculation of the PV work in the tubing. To eliminate this source of error, the system boundary will be defined such that C = 0.

Minimum Extension Pressure

Another condition that is important to the development of the extension criteria is the fracture pressure during extension, P_{ext}. The minimum pressure that may exist in the fracture during extension is, of course, the pressure required to keep the fracture faces open. This pressure is equal to the minimum earth stress S_h or SHMIN as it is called in the program. Thus the first requirement for extension of the fracture is the minimum pressure condition

$$P_{n-1} > P_n > S_h \tag{39}$$

where P_n is the pressure of the last fracture element (i = n) and

S_h is the minimum earth stress in the horizontal direction.

The requirement that the pressure in the next to last element (i = n-1) be greater than P_n is designed to damp out numerical transients in the pressure calculations that occur when the fracture mesh is extended.

Application of the Energy Criteria

The fracture itself is divided into discrete elements. Evaluating Eq. (38) over the system boundary surrounding the fracture plane yields

$$\sum_{1}^{n} W_s \geq \sum_{1}^{n+1} \gamma \Delta A_{f_i} = \gamma \sum_{1}^{n+1} \Delta A_{f_i} \tag{40}$$

where n is the number of open fracture elements,

ΔA_{f_i} is the area of each fracture element,

γ is the specific surface energy requirement per unit area of fracture surface, and

W_s is the net available internal energy.

The fracture system boundary will be defined as the surface of the fracture including the wellbore surface. The surface energy criteria, Eq. (38), is not applied during the time that the first fracture element is "closed" since the initial fracture element is only opened when P_b is reached in the wellbore. The fracture may realistically propagate through the rock grains during the initial fracture growth instead of creating the intergranular type of separation associated with stable fracture growth (Tetleman and McEvily, 1967). Thus, the surface enery requirement would be much higher during the initial fracture extension and is not treated due the the difficulty of estimating a representative value of the surface energy coefficient, γ, for the initial element. The wellbore will be considered to be within the system boundary as it is technically part of the fracture plane and contributes to the total applied force on the fracture faces.

Development of the Internal Energy Terms

Consider an arbritrary volume with an adiabatic surface as depicted in Fig. 13. The first law of thermodynamics states that the change in

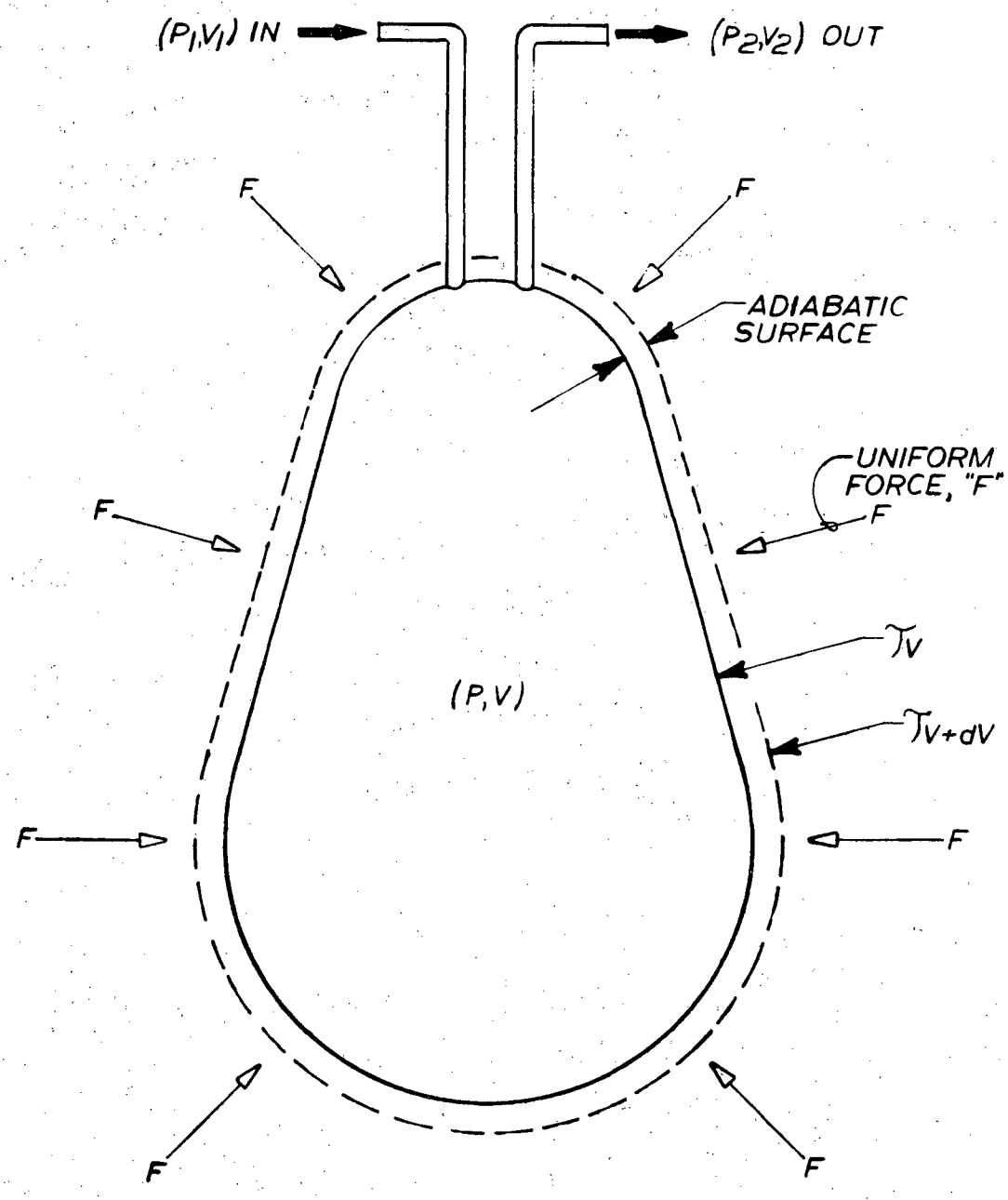

Figure 13 Representation of an Arbritrary Thermodynamic Volume

internal energy of an adiabatic system is due to the PV work carried by fluid entering or leaving the system. If the boundary of the volume is flexible, however, a certain part of the internal energy is lost in the volumetric expansion of the system. If the system does work in displacing a force acting uniformly over its surface, an amount of internal energy is also lost to the surroundings. For the fracture system, the sum of these three terms would be equal to the net internal strain energy available to extend the fracture. This term is called SURGY in the program and is defined by Eq. (41)

$$W_s = \iint_\tau PV - \iiint_V PdV - \iint_\tau Fd\tau \qquad (41)$$

where W_s is the excess strain energy of the system,

$\iint_\tau PV$ is the sum of all the PV work contained in fluids crossing the system boundary τ,

$\iiint_V PdV$ is the potential energy stored in the expansion of the volume V at pressure P, and

$\iint_\tau Fd\tau$ is the work done on the surroundings by displacing the force F on the surface.

Equation (41), while derived for an arbritrary volume, can be applied to the fracture system defined above. Application of this energy balance in the model will be seen by expanding each of the terms in Eq. (41). The end result is that W_s, or SURGY, is equal to the PV work done injecting the fluid into the fracture minus the energy stored in expanding the fracture and compressing the fluid in the wellbore volume. The use of Eq. (41) would also require that the fracture system considered be isothermal.

In the model, the first term on the right hand side of Eq. (41) is

equal to the area under the curve formed by graphing the volume vs the injection pressure of the fluid as it is pumped into the wellbore. Subtracted from this term is the energy lost by fluid permeating from the wellbore into the formation and the energy lost by the fluid permeating from the fracture faces. The integration is performed numerically by using the trapezoidal formula. A similar technique has been used successfully by Aamodt (1977) to estimate the surface energy of rocks involved in HDR experiments. The last two terms can be combined as long as F is not a function of volume or pressure. For the hydraulic fracture the external force acting on the fracture is simply equal to the minimum earth stress, S_h.

Use of Fracture Stiffness in the Energy Calculation

Consider the potential energy stored in an elastic spring in Fig 14a. As the force, F, displaces the spring a distance x, the potential energy of the spring system increases by an amount equal to $\int_0^x F \cdot dx$. For a linear spring the force is equal to the spring constant k times the change in position, $(x - x_0)$ where x_0 is some reference position, equal to zero for this example. The potential energy becomes

$$P.\ E. = \int_0^x F \cdot dx = \int_0^x (kx)dx = \frac{kx^2}{2} \qquad (42)$$

where k is the spring constant relating force to displacement.

Consider the fracture half element as depicted in Fig. 14b. In this example the movement of the fracture is restricted to Mode I displacement where the motion of the fracture walls is normal to the plane of the fracture. The rock displacement in the model is governed by a similar linear elastic behavior of force proportional to displacement. The applied force on the fracture face is just the pressure in the fracture

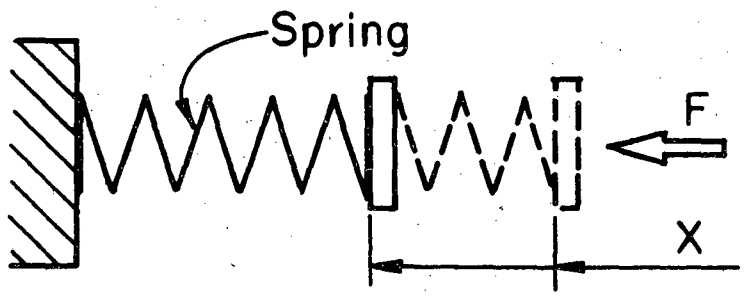

$$P.E. = \frac{1}{2}kx^2$$

Figure 14a Potential Energy Stored in an Elastic Spring

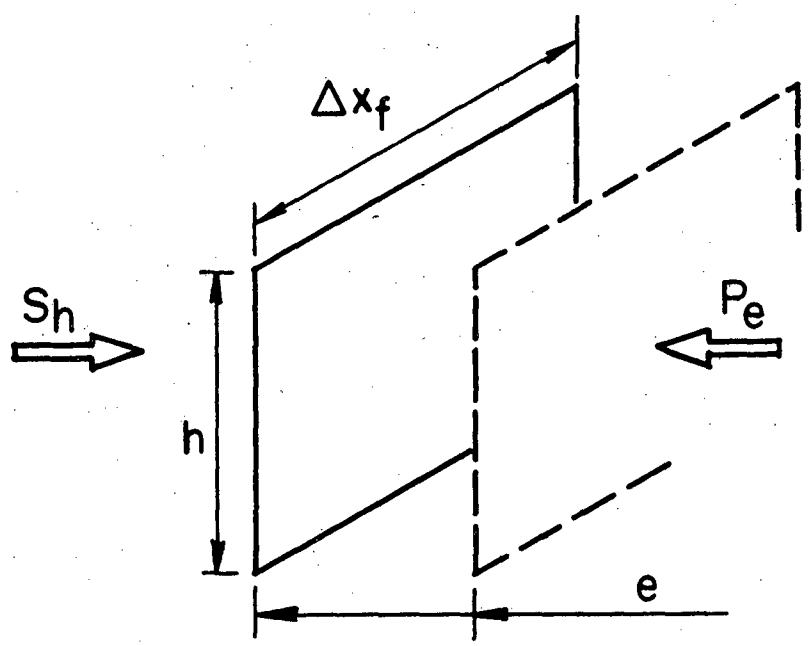

$$P.E. = \frac{h\Delta x_f (P - S_h)e}{2}$$

XBL807-3482

Figure 14b Potential Energy Stored in an Elastic Fracture

element multiplied by the element area $h\Delta x_f$. The stiffness of the fracture is defined by the constant a_v which relates the pressure to the void ratio, e, of the material by

$$e = e_o + (P_e - P_{e_o})\, a_v \tag{43}$$

where e is the void ratio at pressure P_e,

e_o is the void ratio at reference pressure P_{e_o}, and

a_v is the fracture stiffness coefficient.

Previous consideration of the deformable fracture led to the calculation of the fracture width, w, as w = e. If the half-fracture considered has a solids volume of unity, e = w/2, and e will hence be used to represent the fracture half-width in this section (since the model represents one-fourth of the flow region). A spring constant for the fracture can be defined as $k' = \text{area}/a_v$. Multiplying k' by the displacement Δe and substituting $\Delta e = \Delta P a_v$ from Eq. (43) results in $k'\Delta e = \Delta P \cdot (\text{area})$ which has the units of force, analagous to the spring constant defined above in Eq. (42). The potential energy stored in the fracture is given similar to Eq. (43) as

$$\begin{aligned} P.\ E. &= \int_o^e (k'e)\, de = 1/2\, k'e^2 \\ &= \frac{e^2(\text{area})}{2a_v} \end{aligned} \tag{44}$$

where the (area) is $\Delta x_f h$ and

h is the constant fracture height or formation thickness.

The substitution of Eq. (43) into Eq. (44) yields

$$P.\ E. = \frac{e(\text{area})}{2a_v}\left\{e_o + (P_e - P_{e_o})a_v\right\} \tag{45}$$

The minimum pressure restriction, Eq. (39), requires that the fracture elements be closed until the fracture pressure is greater than the magnitude of S_h. Thus $e_o = 0$ when $P_{e_o} \leq S_h$. The substitution of S_h into Eq. (45) results in

$$\begin{aligned} P.\ E. &= \frac{e(\text{area})}{2a_v}(P_e - S_h)a_v \\ &= \frac{e}{2}\,\text{area}\,(P - S_h) \end{aligned} \tag{46}$$

where P is the pressure in the fracture element,

and all other terms as defined above.

Equation (46) may be compared directly to Sneddon's internal energy term, Eq. (37). Sneddon's term was developed with no external boundary force so that S_h would be equal to zero. For a radial fracture the area term above is equal to πr^2. Equations (37) and (46) would then differ by the term $\pi/3(1 - \nu^2)$ which is always greater than unity. What this difference truly means is not readily apparent since the expressions were developed for cases with different boundary conditions.

The last term in Eq. (41), as applied to the model, would be equal to the work done in displacing the constant earth stress S_h acting normal to the fracture. The work term $\iint_\tau F d\tau$ becomes $S_h \iint_\tau d\tau$ which for the rectilinear fracture elements can be expressed as

$$\iint_\tau F d = S_h \Delta x_f h \int_o^e de = S_h(\text{area})e \tag{47}$$

Using Equations (41), (46), and (47), Eq. (40) and be written for the total n elements composing the fracture an any time (i = 0 is the wellbore element) as

$$PV_{i=0} - \sum_{i=1}^{n} PV_i - \sum_{i=1}^{n} e_i \frac{(P_i + S_h)}{2} \quad area_i \geq \frac{\gamma}{2} \sum_{i=1}^{n+1} area_i \tag{48}$$

where PV_i is the PV work done by fluid crossing the system boundary,

e_i is the fracture half-width of element i,

P_i is the pressure in fracture element i,

S_h is the minimum earth stress,

γ is the specific surface energy coefficient, and

$area_i$ is the area of each fracture element where

$$area_i = A_{f_i} = h\Delta x_{f_i} \text{ for the rectangular case}$$
$$= \pi((r_f + \Delta r)^2 - r_f^2) \text{ for the circular case.}$$

Equation (48) and the minimum pressure requirement, Eq. (39), are the criteria that must be satisfied for the discrete fracture growth of the next (n + 1) fracture element.

Chapter Summary

The IFDM formulation was chosen to model flow to a well intercepting a single vertical fracture, the results of which are shown in the next chapter. The success of modeling the fixed length fractures led to the concept of simulating a growing hydraulic fracture. This involves the use of successive reservoir meshes that represent the fracture growth as a series of discrete changes in fracture length. The deformable fracture representation permits the change in width of the fracture with internal pressure, which controls the fracture permeability and fluid storage capacity. This model uses a calculation of an energy term, SURGY, that is used to determine when the next jump in fracture length is allowed.

This calculation is directly related to the pore pressure in the fracture and the amount of fluid that is injected into the fracture or that permeates into the reservoir. The present study resulted in the program HYDFR which can be used to estimate the physical properties of the static and growing fractures by analyzing the pressure transients associated with the injection or withdrawal of fluids from the surface. The use of an expanding geometry mesh and an improved solution technique allows the calculations in a reasonable amount of computational time.

However, the model in its present form has some apparent limitations. The use of the model to determine the breakdown pressure, P_b, which is found by trial and error, cannot be used to calculate the parameters S_H and T_o in Eq. (2). This results from the length of the first fracture element of 0.5 m which is much greater than the few wellbore radii length that the equations of Hubbert and Willis (1957) or Cleary (1979) are limited to. While the first element treatment thus precludes detailed information about conditions at the wellbore during breakdown, it also circumvents the problems of fracture mis-orientation and initial grain rupture considerations in the energy calculation. In other words, the present model is too coarse in space and time to simulate fracture propagation in the region close to the wellbore.

Other limitations may arise in the discrete form of the energy calculation. Corten (1972) has suggested the use of a plastic zone correction factor in such energy calculations that requires a minute crushing zone ahead of the fracture tip, but which is orders of magnitude smaller that the minimum fracture element. This is perhaps more useful in a microscopic system. Krech and Chamberlin (1974), however, present calculations of the rock specific surface energy coefficient that includes the precrushing at the fracture tip. The use of the surface energy

coefficient in calculating the times of the discrete fracture jumps is valid since researchers have repeatedly observed that fracture growth does involve rapid macroscopic jumps or changes in fracture length during extension, (Perkins and Krech, 1966; Daneshy, 1973b).

The greatest weakness of the present model may lie in the IFDM formulation used in the program. While the formulation excels in solving diffusion problems, it is not designed to yield shear stress information. Without adequate shear stress information the fracture width calculation is only one-dimensional, that is the fracture aperture is strictly a function of the fluid pressure in each fracture element and independent of the deformation of adjacent elements. This could lead to conservative estimates of fracture width.

The model will allow examination of parameters that may effect the fracture behavior. These include variable pumping rate, effect of fluid compressibility in the wellbore tubing, variation of formation permeability and skin effects, fully two-dimensional flow in the reservoir, the effects of variable fracture stiffness, and the effect of the magnitude of the earth stress S_h. None of these has been fully treated in the literature.

While this model is admittedly a first order approximation it is sufficiently advanced to help understand the interrelationships between pore pressure and fluid flow in the analysis of fixed geometry fractures and in the hydraulic fracturing process.

IV. RESULTS AND DISCUSSION

This chapter presents the results of simulations conducted with the present model. The topics investigated include: type curve analysis of pressure transients arising from a well intercepting a single, fixed length vertical fracture; the simulation of field data conducted in mini-fracture experiments by the US Geological Survey in the Monticello field in South Carolina; and studies of the growth rate of large, rectangular vertical fractures created by hydraulic fracturing. A section on possible refinements of the model and recommendations for future work conclude the chapter.

A. FIXED GEOMETRY FRACTURE

The simulations run with the numerical model and fixed geometry meshes were compared with the previously described analytical solutions of Cinco-Ley and Samaniego (1978). Constant production rate was modeled by placing a sink term in the wellbore node. The mesh was extended to 90 meters to approximate the semi-infinite boundary condition assumed in Cinco-Ley's solution.

The fracture as modeled was of unit height with a half-length of 10 meters and an aperture of .01 m (.4 in). A total of over 220 mesh elements was used to simulate the reservoir with element volumes ranging between $2 \cdot 10^{-2}$ m^3 near the wellbore node to $2 \cdot 10^3$ m^3 at the reservoir edge. The number of fracture elements used in the simulation varied between 12 for the lowest fracture conductivity (C_r = .02) simulations to only 2 elements for the higher fracture conductivity cases (C_r > 100). The reason for this will be explained in a later section. The effects of wellbore storage were initially simulated by wellbore nodes with radii of .0762 m (3 in) and .005 m (.02 in) representing both

realistic and vanishingly small wellbores. However, to duplicate the exact results of the analytic solutions the wellbore volume could be set equal to zero. For a non-zero volume the wellbore storage was assumed to be free surface, that is, the water level in the well is always above the the fractured interval.

Simulation Parameters

The parameters varied in the validation studies were fracture permeability, k_f, formation storage coefficient, ϕc_t, and formation permeability, k. In addition, other studies were completed in this work that involved variation in the choked fracture permeability, k_{ch}, fracture skin permeability, k_s, and the fracture storage capacity, $(\phi c)_f$. The values used for the fixed geometry fracture simulations are presented in Table 1. The graphs of the computed results are presented in log-log type curve format for comparison with the analytical solution. The coordinate axes are the dimensionless time and dimensionless pressure. For convenience the dimensionless variables used in the type curve analysis are summarized as Equations (49).

dimensionless time	$T_{Df} = kt/\phi\mu c_t x_f^2$	(49a)
dimensionless pressure	$P_{wD} = 2\pi kh\Delta P/q\mu$	(49b)
dimensionless fracture conductivity	$C_r = wk_f/\pi kx_f$	(49c)
dimensionless wellbore storage	$\overline{C} = c/2\phi c_t x_f^2$	(49d)
dimensionless fracture skin	$S_{fs} = (\pi w_s/2x_f)(k/k_s - 1)$	(49e)

Table 1 Parameters Used in Fixed Fracture Simulations

Parameter	SI Units	Oilfield Units
k	$1.02 \cdot 10^{-13}$ m^2	103 md
$(\phi c)_t$	$1.02 \cdot 10^{-8}$ Pa^{-1}	$7.03 \cdot 10^{-5}$ psi^{-1}
x_f	10 m	30.5 ft
w	.01 m	$3.05 \cdot 10^{-3}$ ft
z	100 m	305 ft
h	1 m	3.05 ft
w_s	0.2 m	0.61 ft
k_s	$7.7 \cdot 10^{-14}$ m^2	78 md
q	$6.28 \cdot 10^{-3}$ m^3/sec	341 bbl/day
g	9.81 m/sec^2	32.2 ft/sec^2
ρ_f	1000 kg/m^3	1.0 gm/cc
ρ_r	2000 kg/m^3	2.0 gm/cc
μ	10^{-3} Pa-sec	1.0 cp

where k is the formation permeability,

k_f is the fracture permeability,

μ is the fluid viscosity,

ϕc_t is the formation storage capacity,

x_f is the fracture half-length,

q is the fluid withdrawal rate,

ΔP is the pressure drawdown,

w_s is the skin thickness,

k_s is the skin permeability, and

c is a wellbore storage coefficient.

The wellbore storage coefficient, c, in the above equations is defined as a mass storage term, i.e., the amount of fluid released per unit change in fluid potential. Since the model assumes free surface behavior, a change in one m-H_2O of pressure will release one volume (πr_w^2) of fluid per unit height of the wellbore. Thus the value of c used in this work will be equal to the wellbore volume per unit height.

Finite Conductivity Fractures

Figure 15 shows the results of the numerical simulation for a well intercepting a single finite conductivity vertical fracture. The parameter for the different curves is the dimensionless fracture conductivity C_r with four values ranging between $C_r = 0.2$ to $C_r = 100$. The formation properties are fixed so that the change in the dimensionless fracture conductivity is

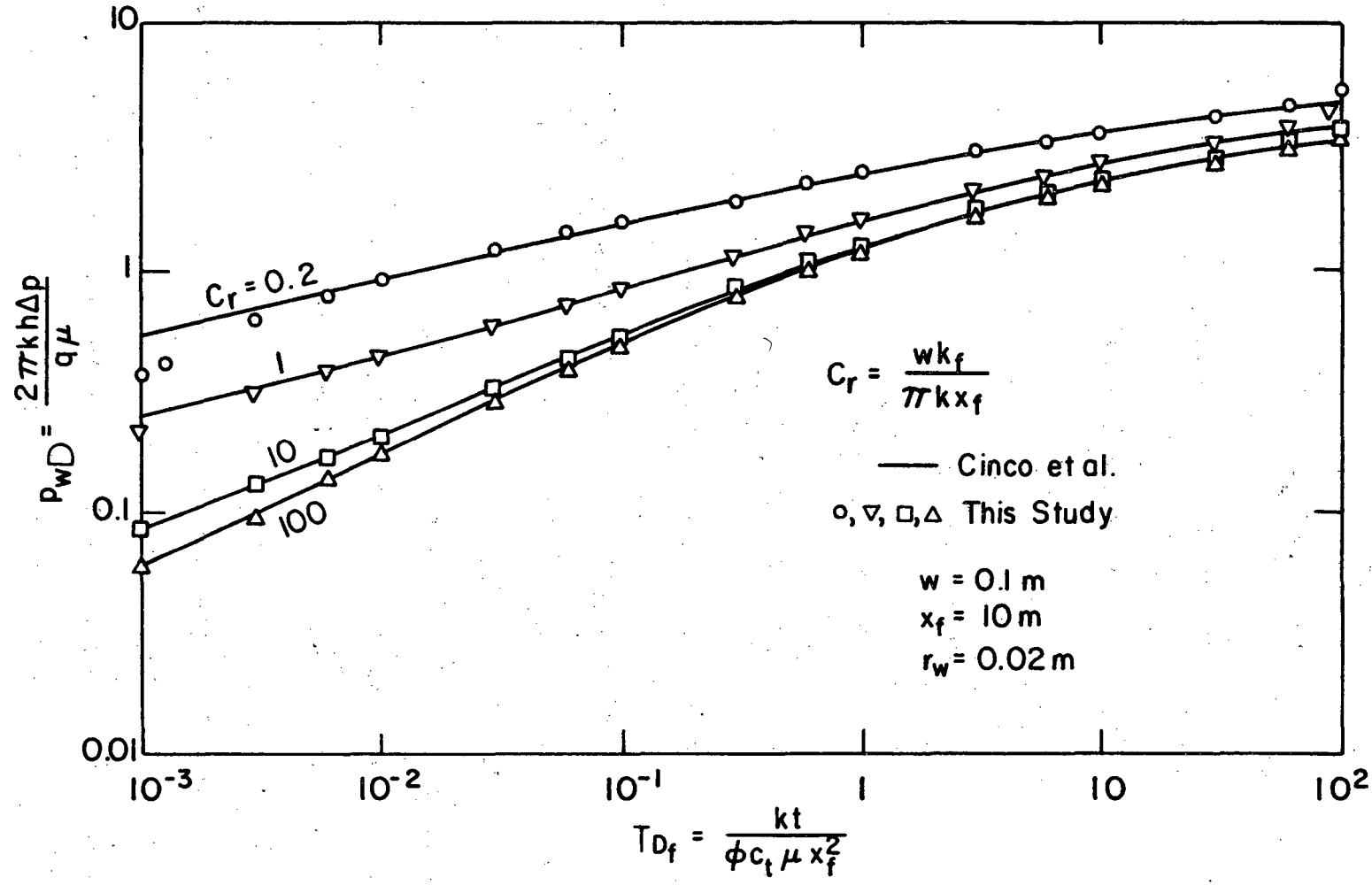

Figure 15 Log - Log Plot of P_{wD} vs T_{Df} for Various Values of C_r

XBL 792-5741

reflected only in a change in the propped fracture permeability, k_f.

Agreement with the analytical solution is excellent over the time ranges of T_{Df} from 10^{-2} to 70. Above the value of 70 the effects of the finite outer boundary of the mesh are felt. At this point the curves begin to follow the solution calculated by Gringarten, et al., (1974) for a closed reservoir system. At times below a T_{Df} of .01 the numerical solutions start to differ from the analytical solution due to the presence of the wellbore. This effect is very marked on the C_r = 0.2 curve and is also evident on the other curves for T_{Df} values below 10^{-3}. Changing the volume of the well to zero will cause the points to fall exactly on the analytical solution but again this would ignore the physical presence of the wellbore. Even with a .005 m wellbore the solution in the time range below a T_{Df} of 10^{-3} is dominated by wellbore storage and the characteristic unit slope will dominate the type curve.

The excellent agreement with the analytical solution serves to point out three interesting features. The first is that the assumption that flow from the formation to the wellbore is negligible is not necessarily wrong. All the simulations presented included wellbore communication with the reservoir. However, no effect of this is observed in the comparison with the analytical solution without wellbore flow. It would seem that the fracture truly dominates the flow to the well and that this analytic assumption is valid at least for normal values of wellbore radius. Another interesting point is that while the drawdown increases with a decrease in fracture conductivity, the change is not proportional to the change in C_r. That is, the separation in the curves for a change of C_r between 100 and 10 is not nearly as dramatic as the change from 10 to 1, even accounting for the compression effect of the logrithmic scale. This would make

the use of type-curve matching to distinguish the differences of two relatively short high permeability fractures very difficult if the magnitude of C_r is greater than 10. Finally all the curves do, at large times, fall on the infinite conductivity ($C_r > 100$) line as predicted by Prats, et al., (1962) and thus exhibit radial flow behavior. During this radial flow period the well test data cannot be effectively used to determine the fracture properties.

Due to the limited information one can obtain from drawdown data of fractured wells at very large and very small values of dimensionless time, the graphs will be limited to values of T_{Df} greater than 10^{-4} but less than 10. The upper limit is the value where pseudo-radial flow begins and the lower limit corresponds to the period below which wellbore storage dominates the slopes of the curves, and the parameter C_r cannot be used. C_r is defined using the fracture half-length x_f but at low fracture conductivities the pressure transient moves slow enough through the fracture mesh so that the effective fracture length may be less than x_f. In this instance the parameter C_r is not unique and it cannot be properly defined.

Wellbore Storage Effects

The effect of wellbore storage was investigated to evaluate its affect on the type curves for values of dimensionless time greater than 10^{-4}. The results for a C_r value of 100 and different values of dimensionless wellbore storage coefficient ranging between 0 and 0.5 are presented in Figure 16. In Figure 16 the solid lines represent the analytical solutions of Cinco-Ley and Samaniego (1977a). Again the agreement is excellent over the range of T_{Df} from 10^{-4} to 10. The value of dimensionless wellbore storage $\overline{C} = 1.25 \cdot 10^{-3}$ is nearly indistinguishable from the zero wellbore storage solution. At lower values of C_r, however, even a $\overline{C}$ of $1.25 \cdot 10^{-3}$ (corresponding to a .005 m wellbore radius) will depart markedly from the

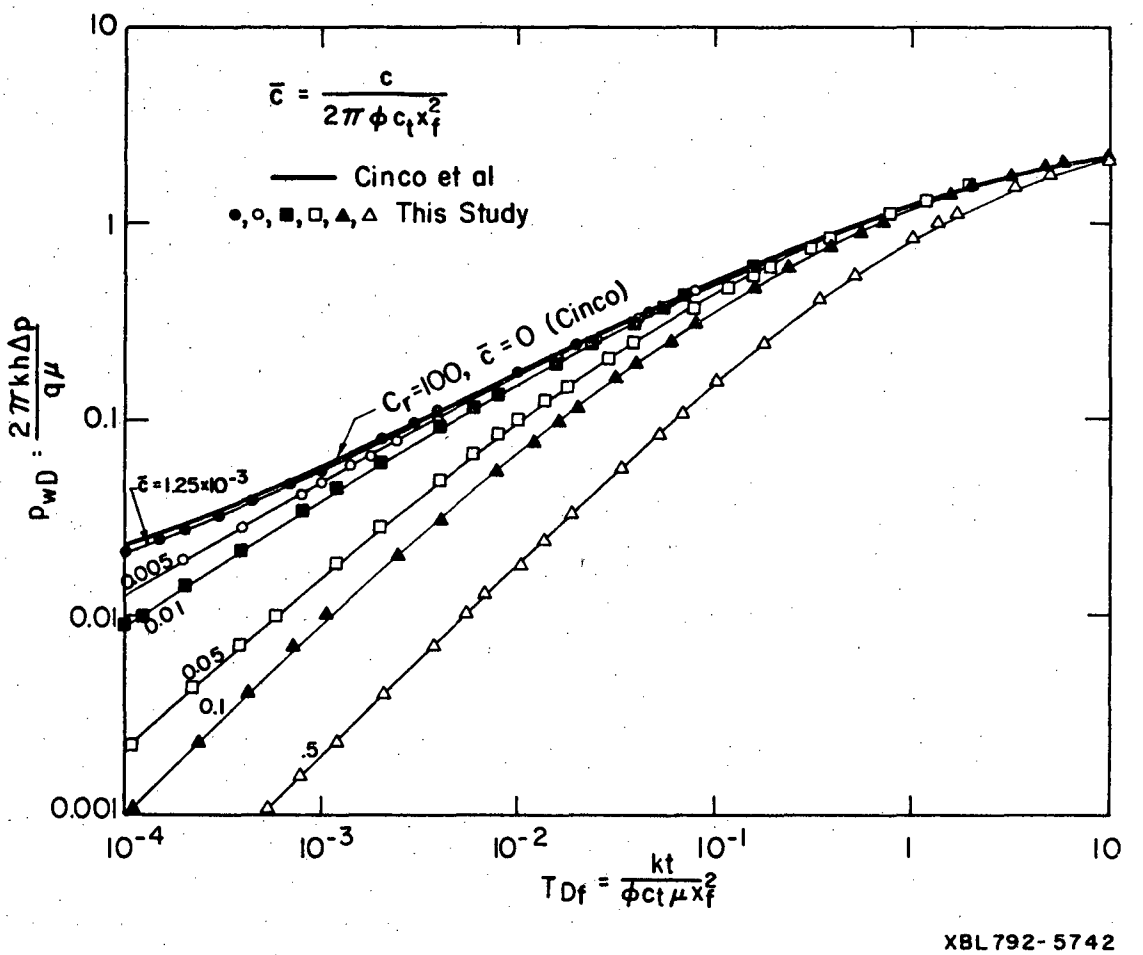

Figure 16 The Effect of Wellbore Storage

analytical solution as seen when comparing the C_r = 0.2 solutions in the previous figure. This is easily understood from the definition of the wellbore storage period. The duration of the storage effects is an indication of the transition between the two sources of the fluid produced from the system. The wellbore storage effect will dominate as long as most of the fluid produced from the well comes simply from reducing the volume of fluid initially in the wellbore. The transition period ends when fluid begins to be produced from the formation and hence becomes the dominant source of production. This naturally requires an increase in the pressure drawdown of the reservoir. As C_r declines, for a fixed geometry fracture, it takes longer for the transition to occur due to the lower fracture permeability restricting the release of formation fluids. The value of C_r = 100 represents a situation where the storage effects should be minimized since the fluid is produced from the fracture almost immediately, reducing the wellbore storage period. However, even at a C_r = 100 the wellbore storage period can persist throughout the duration of the test. A value of $\overline{C}$ = 0.5 creates a storage effect that lasts until T_{Df} = 10 as seen in Figure 16. The value of $\overline{C}$ = 0.5 corresponds to a wellbore radius of .1 m (4 in) with the time corresponding to T_{Df} = 10 being 10^5 seconds. Since these values are representative of actual field tests, it is quite possible that storage effects may completely eliminate the early usefulness of the type curves in relation to using the parameter C_r. Thus, it may be necessary to use double packers to reduce the influence of wellbore storage on the data used for the pressure transient analysis.

Effects of Fracture Skin

Fluid loss additives, such as guar residues from incomplete polymer degradation or fines produced by proppant crushing, may act to lower the permeability of the formation during the hydraulic fracturing process. This

could result in a permanent permeability reduction in which the damaged formation skin permeability, k_s, is easily two orders of magnitude lower than for the undamaged rock.

It is quite well-known that formation damage around a wellbore can be handled quantitatively with the use of a skin factor. So also one can define a similar skin concept for damage around a fracture. Thus Cinco-Ley and Samaniego (1977a) define a dimensionless fracture skin, S_{fs}, by the relation given in Eq. (49e). The effect of S_{fs} on the dimensionless pressure, P_{wD}, for $C_r = 100$ is demonstrated by the family of curves shown in Figure 17. The four upper curves and the Cinco-Ley solution in this figure pertain to $r_w = .005$ m while the two lower curves pertain to a $r_w = .076$ m (3 in). The mathematical representation of the finite-width skin is shown as an inset in Figure 17.

Three points of interest may be noticed in Figure 17. First the effects of wellbore storage become more pronounced as S_{fs} increases, since higher values of S_{fs} imply a general degradation of permeability around the well. Second, there is a slight drawdown increase between the analytical solution and the present study for $S_{fs} = .1$ and $T_{Df} < 10^{-2}$. This is consistent with Cinco-Ley and Samaniego's derivation which considered an infinitesimal skin. However, they do state in their paper that a skin of finite width should be expected to produce a slightly different well response at early times. In other words, for the same S_{fs}, different combinations of k_s and w_s will lead to a different P_{wD} versus T_{Df} relation for small values of time. To verify this a second simulation was carried out in which the width of the skin was increased by a factor of two over the value used for the results presented in Figure 17. A comparison of the two different finite-width skin solutions is given in Figure 18. It can be seen from Figure 18 that as the skin width is increased for a constant

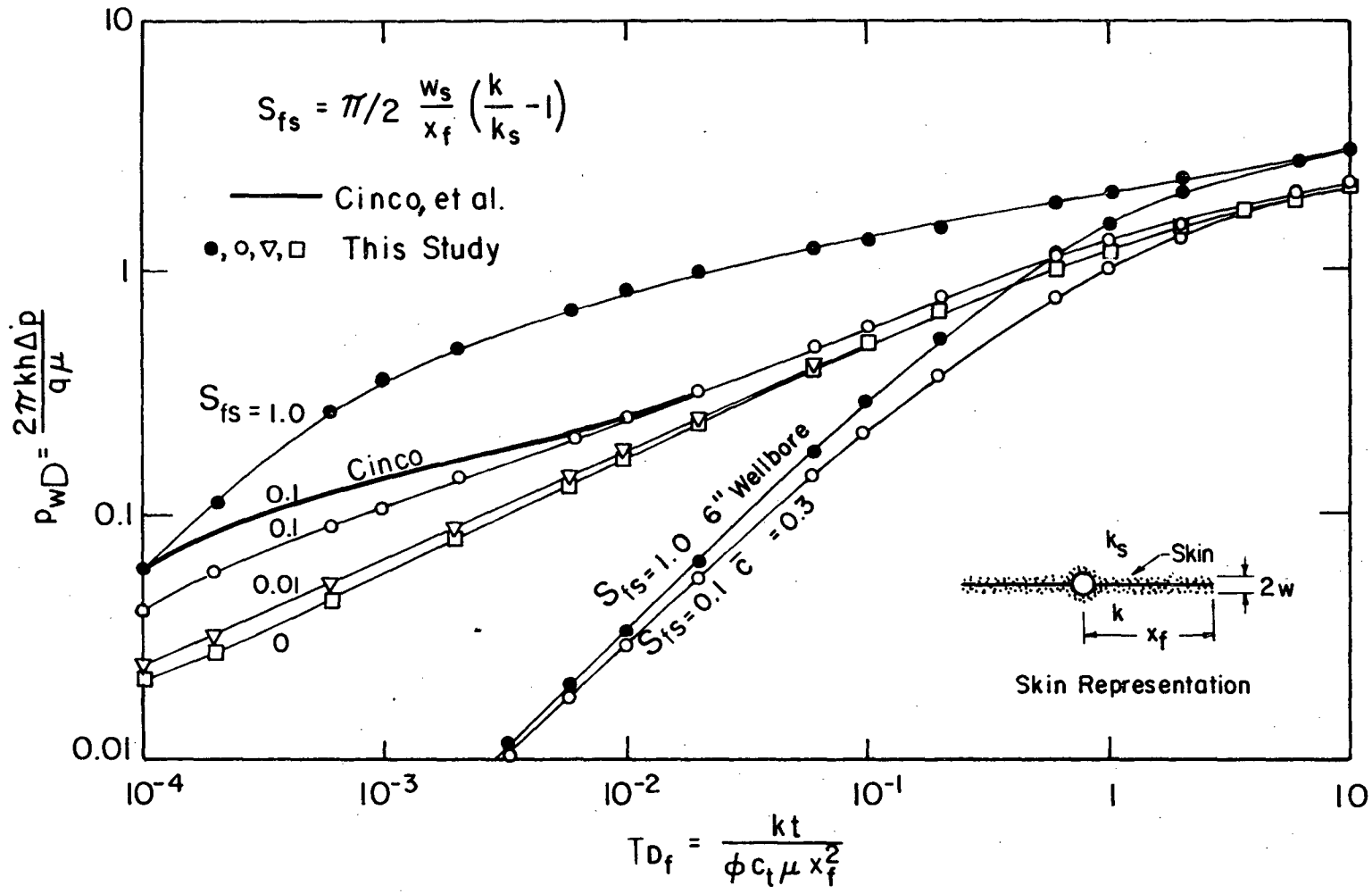

Figure 17 The Effect of Fracture Skin

XBL792-5740

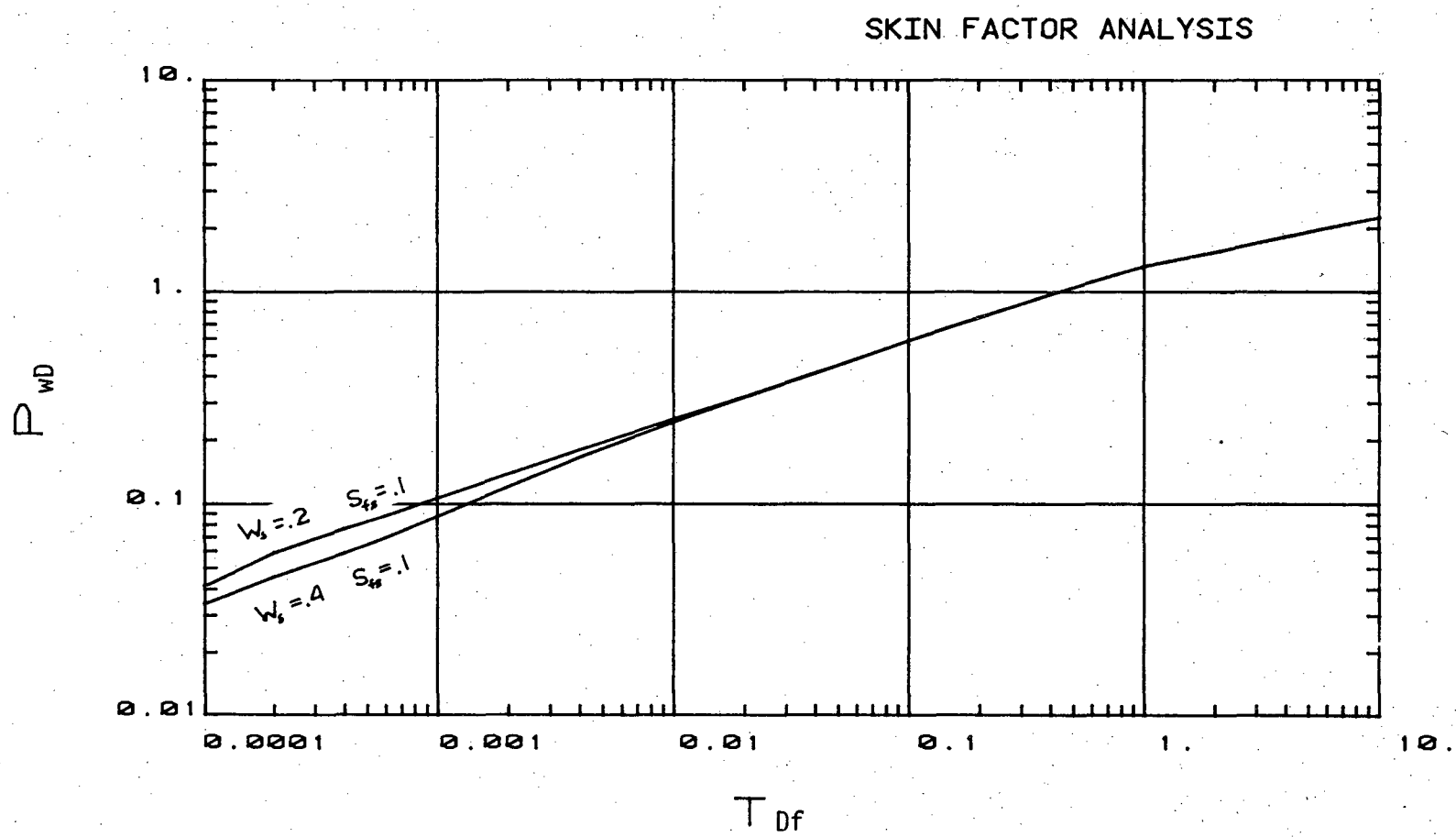

Figure 18 Skin Factor Analysis - Variation in Skin Thickness

XBL 792-8501

S_{fs}, the curves tend to move down on the log-log plot. The final feature worthy of note in Figure 17 is that as the wellbore radius is increased, in order to represent realistic field cases, the early time details are so completely masked that the utility of the S_{fs} parameter in type curve interpretation is curtailed.

Comments on the Validation Studies

The emphasis of the previous sections has been in the validation of the fixed geometry flow model by comparison with the analytical results of Cinco-Ley and Samaniego. While further simulations were performed to investigate some parameters not considered by these other authors, it is of interest here to make two observations regarding the use of the fracture meshes in the simulations. The first of these is the optimum number of fracture elements into which the fracture is discretized for purposes of simulation. It is obvious that the number of elements should be increased as the fracture conductivity decreases and the gradient of potential within the fracture becomes significant. Conversely, as the conductivity of the fracture becomes infinite, the entire fracture can be treated as a single element or even as an intrinsic part of the well. In the simulations, two fracture elements were used for C_r = 100 and 12 fracture elements were used for C_r = 0.2. The drawback in using a large number of elements for higher values of C_r is that the higher conductivity greatly decreases the stable time step for the fracture elements, resulting in greatly increased computational effort. On the other hand, reducing the number of elements for lower values of C_r leads to a loss of accuracy. The optimum number of elements depends on the fracture surface area, fracture storativity, and the contrast between k and k_f. Although in the present study the number of fracture elements was determined by trial and error, it should not be difficult to formulate a

rational criterion for deciding on the optimum number.

A second point of interest concerns the manner in which flow at the edge of the fracture is handled. In all the simulations the edge was assumed to be rectilinear with fluid entering the fracture through the narrow end. Examination of the computer simulations showed that of the total flux entering the fracture, only about one-percent was entering through the end. Although the flux may be negligible, the velocity of entry at the fracture end was always found to be very high due to the narrowness of the opening. Considering the fact that little is generally known about the fracture edge, this topic will not be considered further except to mention that the actual flux through the end depends very much on the geometry assumed.

The validation simulations led to the investigation of various parameters that could reasonably be expected to affect the nature of the solutions when presented in type curve format. The advantage of using type curves when analysing the drawdown data of fractured wells, lies in the ability to identify a unique value of C_r. As has been demonstrated above even with the conventional analytic assumptions, the use of C_r is relegated to ideal systems with infinitesimal wellbores. However, there are also many other factors that may influence the shape of the type curves in such a way that conventional analysis may prove to be very difficult or result in non-unique estimation of the parameter C_r.

Variation in Fracture Storage

In the previous validation studies the storage coefficient of the fracture $(\phi c)_f$ was taken to be the same as that of the formation $(\phi c)_t$ and equal to 10^{-8} Pa^{-1}. However, any number of factors may change the storage coefficient of the fracture. These include the effects of proppant placement, proppant size, and residual or immobile fracturing

fluids remaining in the fracture. To investigate the possible effects of the variation of the fracture storage coefficient the value was both increased and decreased by an order of magnitude relative to the value used for the previous simulations. The results are presented in Figure 19. In all three cases presented the wellbore radius was set equal to .005 m to minimize the wellbore storage effects and the fracture conductivity was fixed so that $C_r = 100$. From Figure 19 it is seen that while lowering the fracture storage coefficient to 10^{-9} Pa^{-1} makes little difference in the shape of the curve, raising the fracture storage to 10^{-7} Pa^{-1} has a significant effect. The fracture storage value of 10^{-7} Pa^{-1} is the same order of magnitude as the wellbore storage value and the shape of the curve indicates a storage effect analagous to wellbore storage. It is conceivable that in MHF stimulations the size if the fracture may be large enough so that fracture storage will persist past the wellbore storage period. This would also make conventional type curve analysis difficult.

Unequal Wing-Length

It is customarily assumed that hydraulic fracturing at depth creates an opening symmetrical about the wellbore. However, it is conceivable that the fracture is initiated in only one direction (single-wing; see inset Figure 20) or that it propagates only partially in one direction due to rock inhomogeneities. Investigation of the problem is summarized in Figures 20 abc. In as muchas an asymmetrical wing requires the simulation of one-half of the flow region, and since a symmetrical wing requires only one-quarter of the flow region, two different meshes were designed to handle the single-wing and one and one-half wing cases.

Figures 20 abc, show drawdown behavior for $C_r = 1$, 10, and 100 with one wing, one and one-half wing, and two wing simulations. In all cases,

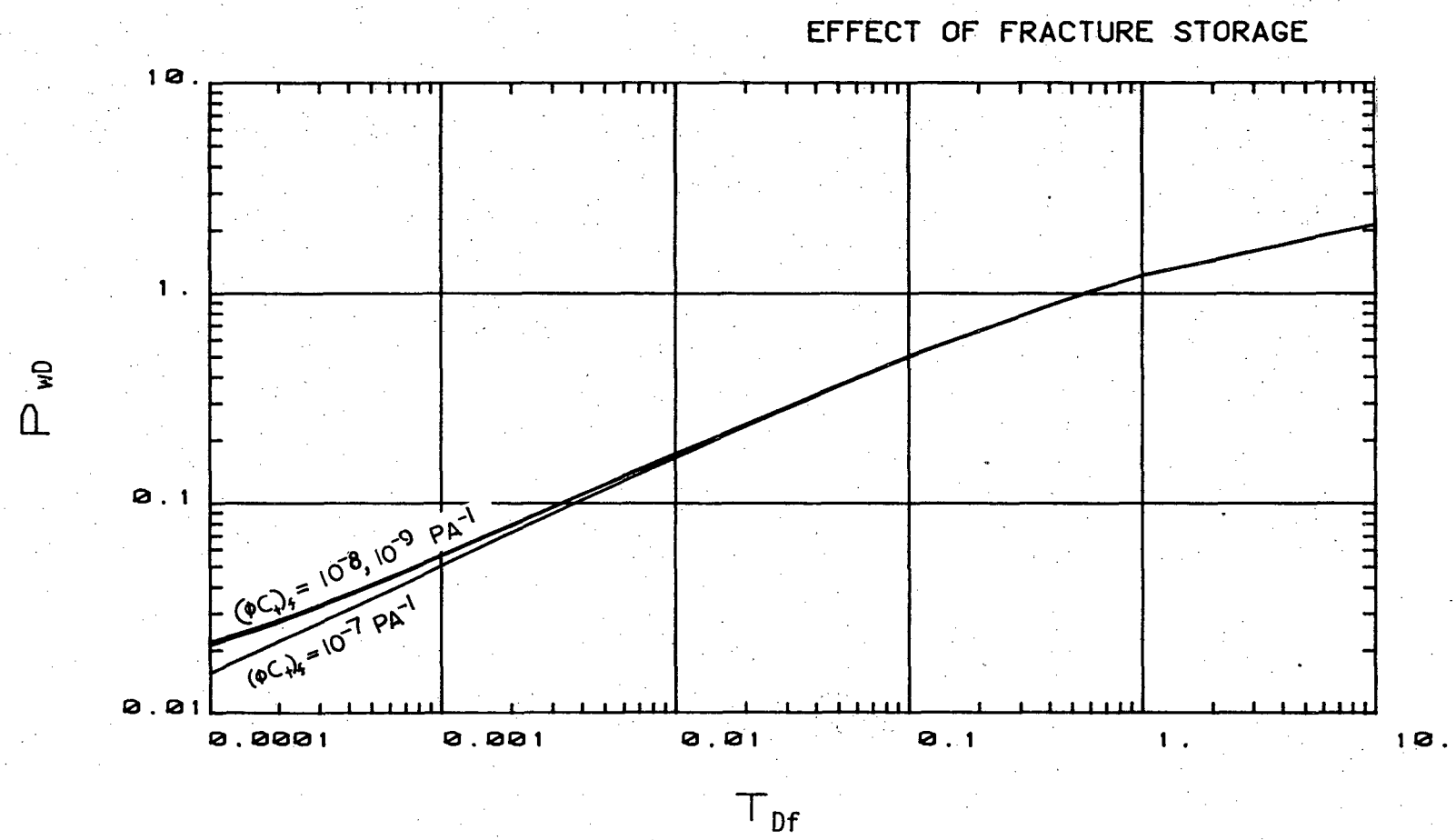

Figure 19 The Effect of Fracture Storage

XBL 792-8502

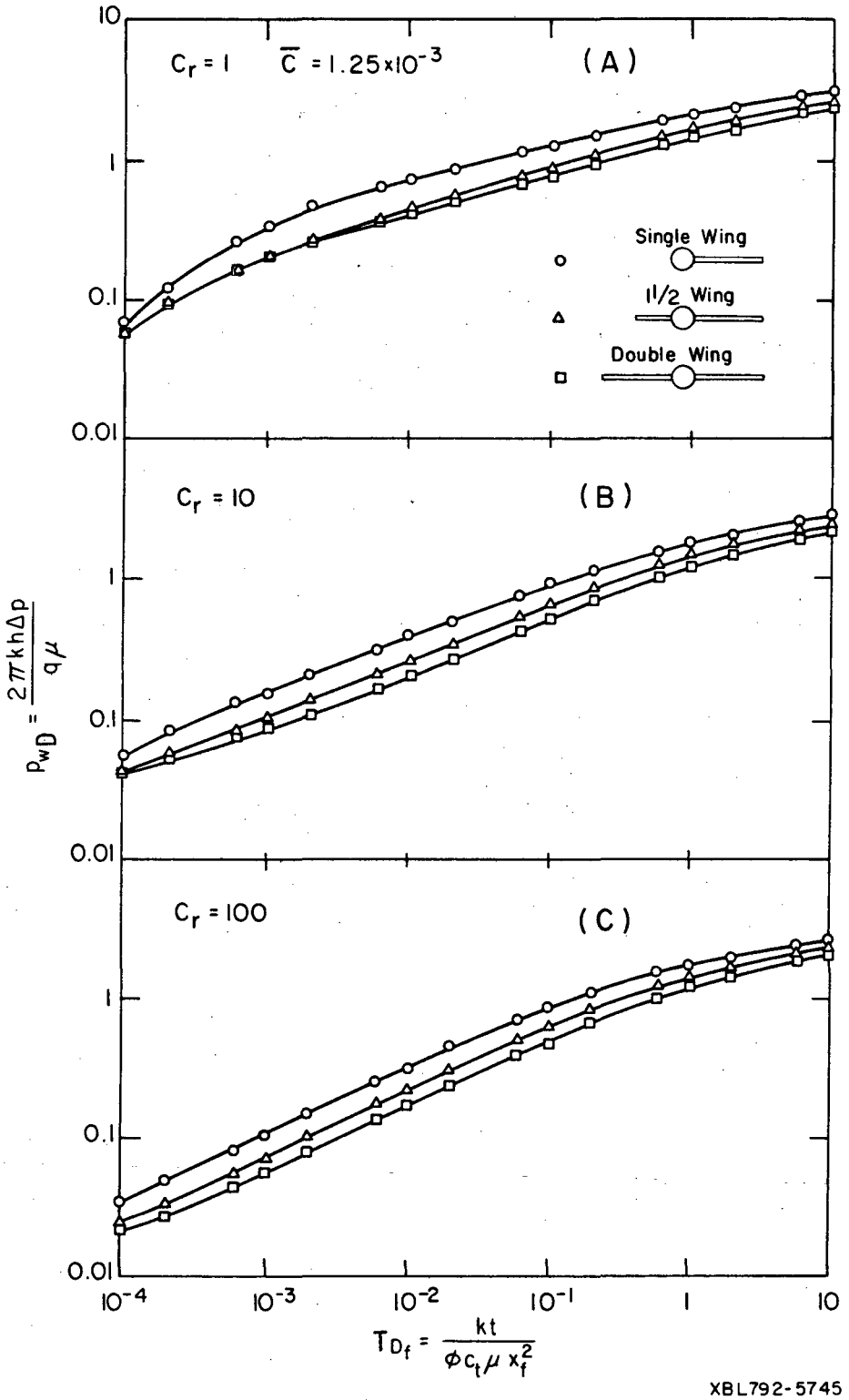

Figure 20 The Effect of Unequal Wing Length

the undamaged well had an r_w = .005 m, corresponding to a $\overline{C} = 1.25 \cdot 10^{-3}$. In all three cases, the drawdown for the single-wing condition is quite distinct from those of the one and one-half wing and two-wing conditions. This is due to the decrease in overall permeability on the unfractured side. While the difference between the one and one-half and two-wing case is distinct at C_r = 100, it is not so clear at low T_{Df} for C_r = 10 and disappears below $T_{Df} = 10^{-2}$ for the tight fracture case (C_r = 1). This is to be expected since, in tight fracture cases, flow is governed by the wellbore end of the fracture. Indeed, other results generated during the present study showed that for C_r = 0.2, reducing the permeability of the farther half of the fracture by an order of magnitude had little effect on the pressure-transient response of the well. Thus in tight gas sands the MHF treatments may not be as advantageous as thought to be due to the fact that in these very large fractures the influence of the ends of the fracture may never be seen on the resultant well production if the propped fracture permeability is low.

Choked Fractures

The process of actually creating a hydraulic fracture is mechanically complicated. After the well has been stimulated and before the well can be put back onto production, the subsurface tubing and packers must be removed. It is conceivable that if sufficient time is not allowed for the formation to compress the proppant pack, the removal of the equipment may act as a swab drawing some of the fluid and proppant from the wellbore end of the fracture (Goranson, personal communication 1980). This would create an area of fracture constriction near the wellbore that was defined earlier as a choked region. In general, the effects of any arbritrary permeability variation in the fracture is of interest especially since the proppant distribution is likely to be non-uniform (Cooke 1975).

However, for this work the permeability variation is restricted to the wellbore end of the fracture,whether due to choking or turbulenceeffects.

The choked fracture simulations are presented in Figure 21 for a C_r = 100. The four cases presented include values of choke permeability, k_{ch}, equal to k_f, 10^{-2} k_f, and 10^{-3} k_f. The upper four simulations were run with an .005 m radius wellbore. The length of the choked region, x_{ch}, was 0.8 m. From Figure 21 one immediately notices that the effect of reducing the choke permeability will show up as an increased pressure drop exactly like the skin effect presented in Figure 17. This has been predicted by Raghavan (1976). The choke value equal to 10^{-3} k_f creates a pressuredrop that persists throughout thetime ranges presented. Perhaps with this great a permeability reduction C_r should be calculated using the values of k_{ch} and x_{ch} which would give an effective value of C_r = 1.25. The curve for the C_r = 1 simulation presented earlier in Figure 15 is replotted on Figure 21. The C_r = 1 curve is similar to the upper curve in Figure 21 even though the conventional C_r value for the upper curve is two orders of magnitude larger. This again serves to show that the uniqueness of the parameter C_r is restricted to simpler systems than the choked fracture proposed here. The effect of wellbore storage dominates the choked fracture effects as seen in the lower two curves in Figure 21 for r_w = .0762 m. These latter curves are identical even though the choke permeability varied by a factor of 10.

Deformable Fractures

The deformable or 'breathing' fracture was treated as described in the previous chapter. The case presented in Figure 22 used a fracture-proppant stiffness coefficient, a_v = $1.3 \cdot 10^{-10}$ Pa^{-1}, with an initial fracture opening of 10^{-3} m. As the pressure is reduced in the fracture due to fluid withdrawal, the fracture closes in accordance with Equation (43).

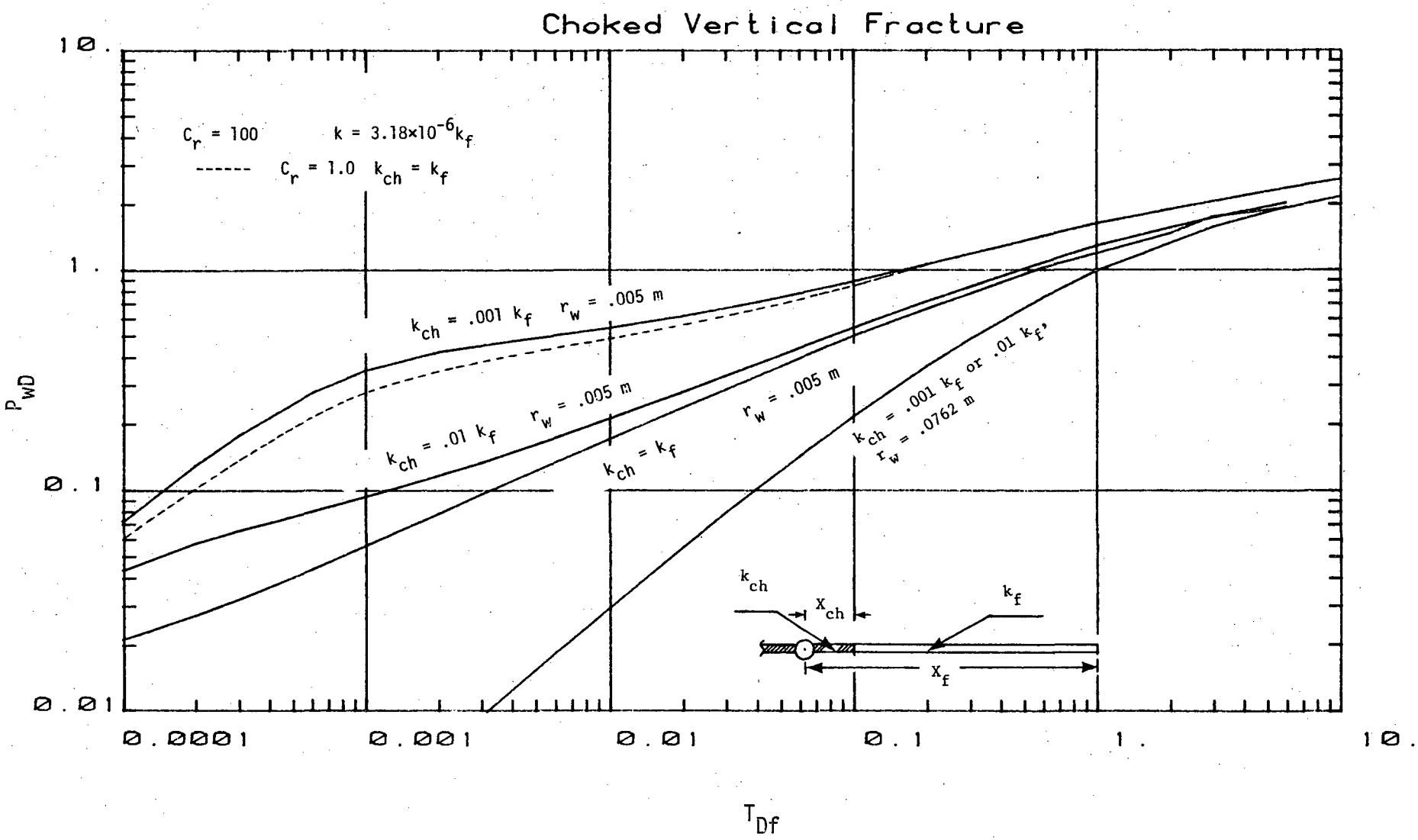

Figure 21 The Effect of a Choked Region on the Pressure Drawdown

XBL 792-7377

The pressure drop then increased further as the fracture permeability is reduced. The above parameters of stiffness and initial fracture opening have been arbitrarily chosen only to demonstrate an application of the model. Figure 22 shows the 'breathing' fracture drawdown curve along with two 'rigid' fracture curves with C_r values of 26.2 and 1.0. The former value corresponds to a fracture that had the initial width and permeability of the deformable fracture. The latter corresponds to a fracture with an equivalent conductivity of the deformable fracture at the time corresponding to $T_{Df} = 10$. The deformable fracture curve actually starts below the $C_r = 26.2$ curve at $T_{Df} = 10^{-4}$ and slowly rises to the $C_r = 1$ curve at $T_{Df} = 10$. Two general points to note that are not intuitively obvious are related to the behavior of the deformable fracture at large and small values of dimensionless time. At $T_{Df} < 10^{-2}$ the deformable fracture drawdown is actually less than the equivalent rigid fracture curve due to a storage effect. The storage capacity of a rigid fracture is due only to the compressibility of the fluid contained within it. The deformable fracture, however, includes an additional term in the fracture storage capacity due to the compressibility of the fracture itself. The second point of interest is that the curve for a deformable fracture solution would continue to rise at larger values of T_{Df} than shown, crossing all the C_r curves so far presented until it stops at the limiting value of $C_r = 0$. This latter curve is the Theis solution for drawdown of a well in a homogeneous medium.

Summary of the Fixed Geometry Fracture Solutions

The model has been validated against the known analytical solutions of Cinco-Ley and will give equivalent results if the analytical boundary restrictions are assumed. The parameter C_r, when used in type curve analysis, may be useful for determining fracture conductivity and fracture

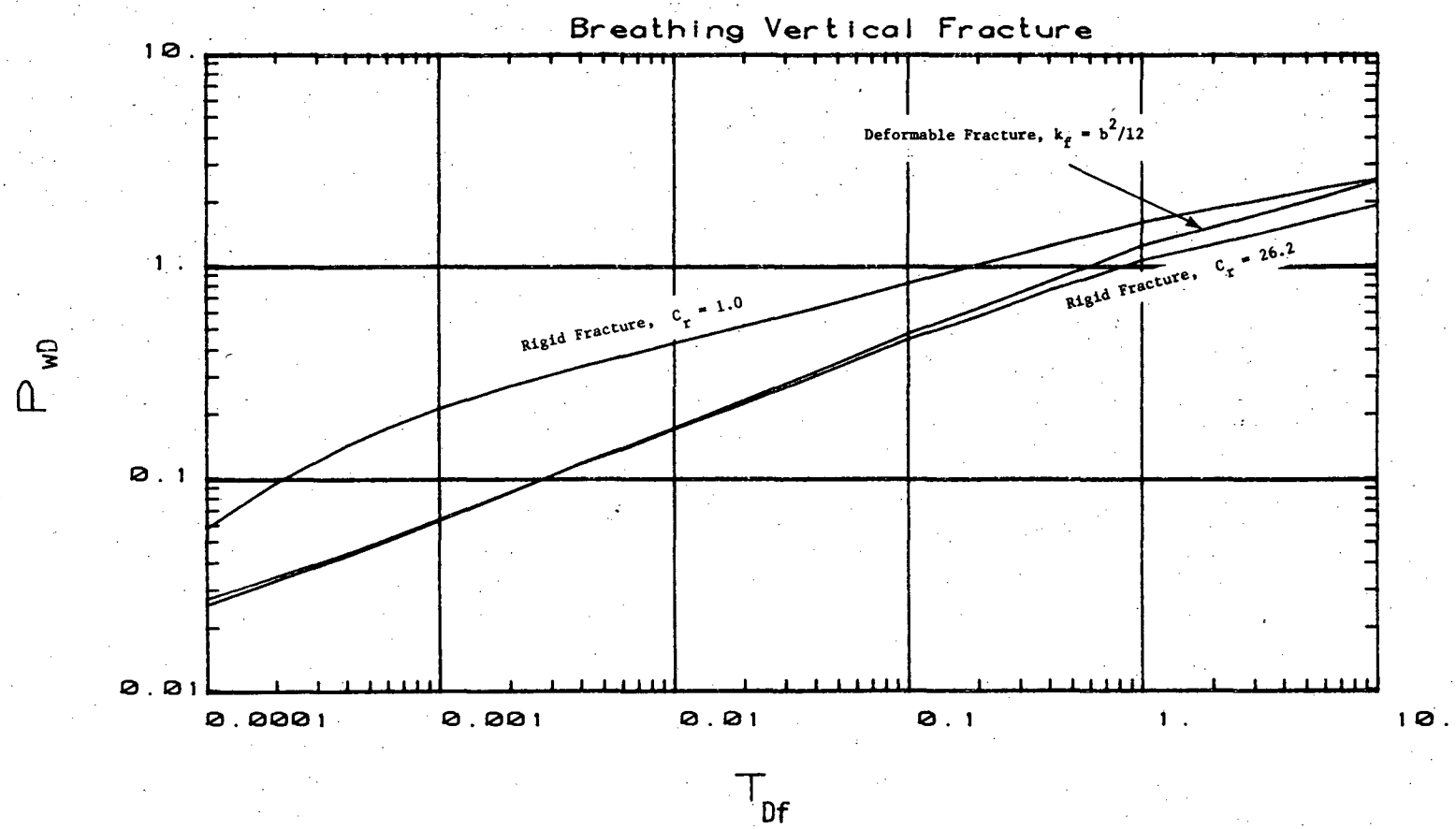

XBL 792-7378

Figure 22 The Effect of a Deformable 'Breathing' Fracture

length but only when used with simplifying assumptions. These latter assumptions include negligible wellbore or fracture storage, symmetrical fracture wings, uniform fracture permeability, and rigid fracture walls. Results from parametric studies using the model indicate that if any of these latter assumptions are invalid, the use of the parameter C_r in type curve analysis is suspect. The effects of formation damage and fracture damage cannot be distinguished without other information which could complicate the analysis of wells exhibiting low productivity. While it is true that such damage shows up basically in transient effects it is possible that the length of the transient phenomena may last years after the stimulation if long, thin fractures are created, which would have correspondingly low values of fracture conductivity.

The type curve matching process should be used with other techniques such as conventional semi-log plot analysis. This allows independent verification of the fracture conductivity, wk_f. The fracture orientation has not been discussed but conceivably could be found by the observation well techniques mentioned in the second chapter. Alternately, the solutions generated by the present model could be substituted for these same calculations when wellbore or fracture storage is significant. While the data has not been reduced for such uses, as yet, it would be a straightforward although laborious procedure. If the effective length of the fracture can be independently estimated along with the fracture conductivity the accuracy of the fracture geometry analysis would be greatly enhanced when using type curve analysis.

B. GROWING FRACTURE VALIDATION : THE MONTICELLO EXPERIMENT

The validation of the growing fracture model is much more difficult due to the lack of any available solutions for comparison. The solutions presented earlier relating the fracture geometry with time are really

approximations derived under the assumption of stable fracture growth and are not representative of the initial breakdown period. However, carefully controlled field experiments have been conducted in 'mini-frac' operations by Zoback (1979) and data were supplied for use in this work. These data were originally used for the determination of in-situ stresses in the investigation of induced seismicity of the Monticello Reservoir in South Carolina. The data includes measured well-head pressures as a function of time and a detailed record of the fluid injection rate with time. This was particularly suited to analysis by the HYDFR program since virtually any time dependent source terms can be modeled due to the flexibilty of the program. A typical injection vs. time and pressure vs. time record used for the Monticello simulations appears as Figure 23. The data had to be further reduced to correct for the head loss and friction loss in the surface piping.

Well Test System

The dimensions of the surface piping, wellbore tubing, and packer spacing used in the well tests by Zoback were presented earlier when discussing the mesh arrangement in the model development section. The fluid viscosity was determined from calibration tests in the surface piping and found to be approximately $2.35 \cdot 10^{-3}$ Pa-sec (2.35 cp). The flow in the surface piping was found to be turbulent due to the small cross-sectional area. Since the model is only designed to simulate flow obeying Darcy's law, which requires laminar flow, the wellbore pressure was calculated by subtracting a pipe pressure gradient factor provided by Zoback from the data in Figure 23. This has the effect of lowering the indicated pressure in the system although the maxima and minima can still be observed from either the surface or subsurface data. In other words the surface (well-head) data can be used to distinguish trends in the behavior of the

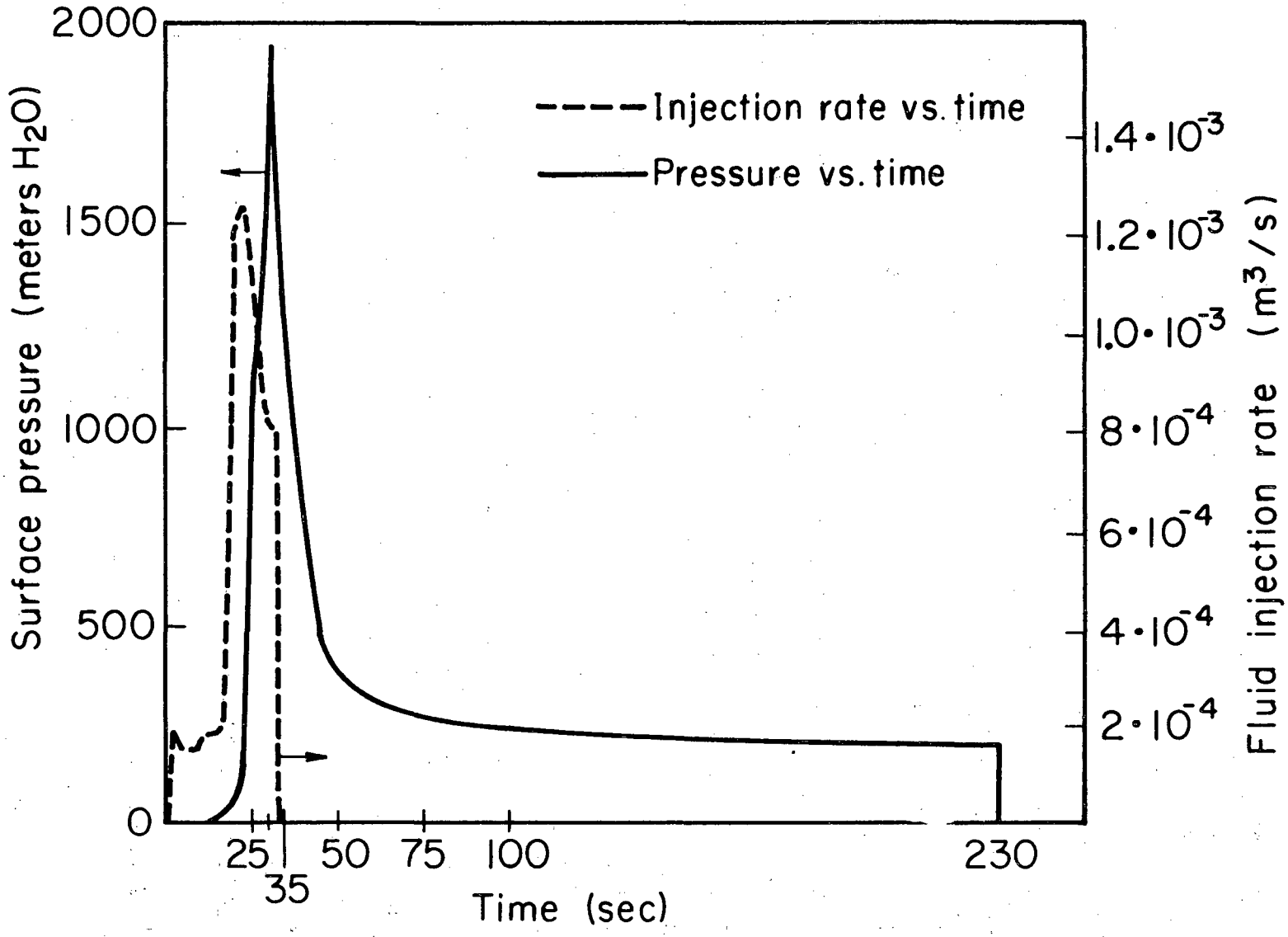

XBL807-3481

Figure 23 Monticello Data Example (after Zoback)

system but for a rigorous analysis the subsurface pressure data are needed. Unfortunately, very few field operations go to the expense of recording such data. Advances in test equipment design may allow more frequent use of downhole pressure transducers in the future.

The fluid compressibility was calculated from the estimated mixture of the oil and water emulsion used in the fracturing process. This mixture was approximately 10 parts oil to 90 parts water by volume which gave a fluid compressibility of approximately $7.6 \cdot 10^{-10}$ Pa^{-1}. While roughly twice the compressibility of pure water, this value is lower than the compressibility of the oils used in MHF applications and was considered to be a reasonable value. The surface piping and wellbore tubing were assumed to be rigid and their respective nodes were assigned material compressibilities equal to that of the fluid in the system. The compressibility and storage capacity of the packer-wellbore element was found to be much greater than the tubing elements due to the packer compliance. This wellbore compressibility was determined by trial and error involving matching the calculated pressures for any one value of packer compliance with the Monticello data during the initial pressurization period before breakdown. A reasonably good value for packer-wellbore compressibility was found to be $2.36 \cdot 10^{-9}$ Pa^{-1}. The various values for the model parameters used in the Monticello simulations are summarized in Table 2.

The Monticello experiments were conducted in a rather impermeable granite that was assumed by Zoback to be homogeneous. This same assumption was made in the present work. Consequently, the values of granite storage and permeability were relatively small but finite. Variation in these two parameters did not affect the buildup pressures in the pre-fracturing data. The granite, however, apparantly had a very high tensile strength the

Table 2 Parameters Used in Monticello Studies

Parameter	SI Units	Oilfield Units
k	10^{-17} m^2	.01 md
$(\phi c)_t$	$1.1 \cdot 10^{-12}$ Pa^{-1}	$7.6 \cdot 10^{-9}$ psi^{-1}
x_f (initial)	1.5 m	4.57 ft
w (initial)	5.0 - $7.0 \cdot 10^{-5}$ m	1.52 - $2.3 \cdot 10^{-4}$ ft
z	300 m	914 ft
h	3 m	9.14 ft
Q	0 - $1.25 \cdot 10^{-3}$ m^3/sec	0 - 20 gpm
P_b	2040 m-H_2O	2900 psi
μ	$2.35 \cdot 10^{-3}$ Pa-sec	2.35 cp
ρ_f	930 kg/m^3	0.93 gm/cc
ρ_r	2700 kg/m^3	2.7 gm/cc
β_f	$7.6 \cdot 10^{-10}$ Pa^{-1}	$5.24 \cdot 10^{-6}$ psi^{-1}
γ	100 - 1000 J/m^2	---

value of which was not available from the field data. The corrected breakdown pressure from the field data was on the order of 1800 m-H_2O (2700 psi). This value is approximately 2.3 times the value of the overburden stress at the depth of the operations so that the fracture pressure gradient Equations (6) and (7) could not be used. However, while the maximum pressure in the Monticello data was 1881 m-H_2O, a lower value of 1740 m-H_2O was used as the initiation or breakdown pressure, P_b, in the simulation as will be explained later.

Use of Monticello Data for Validation

The Monticello data was unique in that it allowed three separate physical processes to be modeled. The first was the pressurization of the wellbore which occured during the first 30 seconds and is characterized by the initial pressure rise as shown in Figure 23. The second was the initial fracture growth period between 30 and 35 seconds. This is the period corresponding to the rapid decrease in flow rate observed in Figure 23. The last phase of the process is when the pumping is terminated at 35 seconds and the pressure decays as fluid permeates into the formation. The various parameters of the model were adjusted to give the best fit to the observed data. While the record of the fluid volume vs. time served as the only true input data, there was flexibility in chosing a set of downhole parameters to match the pressure transient. Two such sets are shown for the corrected Monticello pressure data in Figure 24. The two sets differ only in the initial fracture aperture which is the size of the hairline fracture that initially extends when the fracture propagates but before the fracture pressure builds up.

From Figure 24 the data match is seen to be reasonable over most of the time span although there are some discrepencies particularly at early times. The field data indicate that there may be a fluid fillup stage before

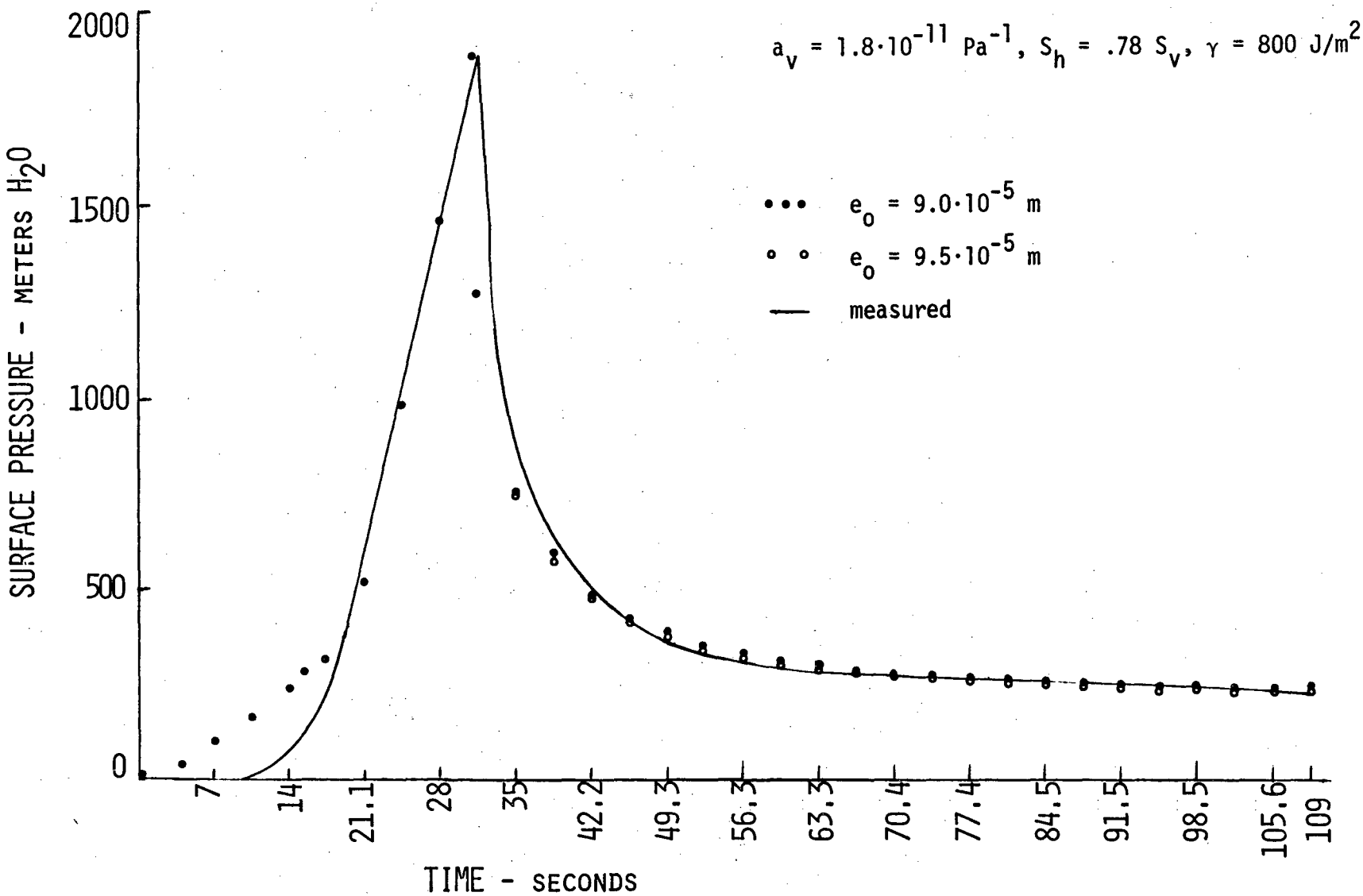

Figure 24 Monticello 2-4-1 Surface Pressure vs. time

time = 15 seconds. However, the model assumes a completeley filled system and thus the simulation pressure begins to rise immediately. Figure 24 shows that at 18 seconds there is a sharp change of the slope of the simulation pressure resulting from the sudden change in the pumping rate evidenced in Figure 23. The numerical and field results are in agreement until the breakdown is indicated. This early time data is sensitive only to the packer compliance which was matched experimentally as previously mentioned. The maximum calculated pressure of 1880 m-H_2O is nearly identical to the field indicated maximum even though the breakdown pressure P_b is 1740 m-H_2O. This indicates that the pressure continues to rise in the wellbore even though the initial fracture element is opened at the lower pressure. This effect could be related to Zoback's (1978) critical length theory but is more likely an indication that the initial model element size may be too large. This would require a finite length of time for the fluid pressure to reach the extension pressure at the end of the first fracture element.

After the maximum pressure is reached, there is a sharp decline in pressure beginning at a time equal to 32 seconds which agrees quite well with the model prediction of 31.67 seconds. At this point the fracture grows 'unstably' propagating six meters into the formation during the next four seconds. After a time equal to about 40 seconds there is no further fracture growth and the pressure transient begins to level off at a pressure of around 230 m-H_2O. Again agreement of the simulation transient and the field data is very good over this time range.

Monticello Validation - First Cycle Simulation

It will be convenient from here on to represent a specific numerical simulation using the Monticello data with a series of numbers, e.g. 2-2-1. The data were taken from two different wells in the Monticello field,

Monticello 1 and Monticello 2. The first of the three numbers represents the number of the well, although all of the data provided by Zoback comes from well number 2. More than one mini-fracture operation was performed in each well. A series of such operations was conducted at various depths. The second number refers to the particular mini-fracture operation and implies that the data is from a specific depth in the well. During each of these operations the well was repeatedly pressurized and then bled off in subsequent cycles. This technique was used by Zoback to deduce the minimum earth stress from analysis of the pressure data. The number of the cycles is the last number in the series. Thus 2-2-1 is data from the first (and initial pressurization) cycle of the second operation conducted in well number 2.

The simulation was performed for another mini-fracture operation, Monticello 2-7-1, as shown in Figure 25. The time axis of Figure 25 is marked in 3.56 second divisions corresponding to the sampling frequency of the pumping rate data. While the simulations represented in Figures 24 and 25 were both very good matches to the field data, the respective sets of simulation parameters were not the same, as can be seen by comparing the values listed on the two figures. The choice of fracture stiffness, a_v, and initial fracture opening, e_0, were 10% higher for the Monticello 2-7-1 simulation but the surface energy coefficient, γ, was 5% lower. This was somewhat disturbing since the difference in depths between the two operations was less than 15 meters and the formation properties should have been similar. However, even though it is conceivable that a 10% difference is within experimental tolerances, it is much more likely that the simulation parameters may have been over fine-tuned for the first cycle data. That is, the fit was made so exact that inaccuracies involving some of the initial assumptions may have been ignored. It is now thought

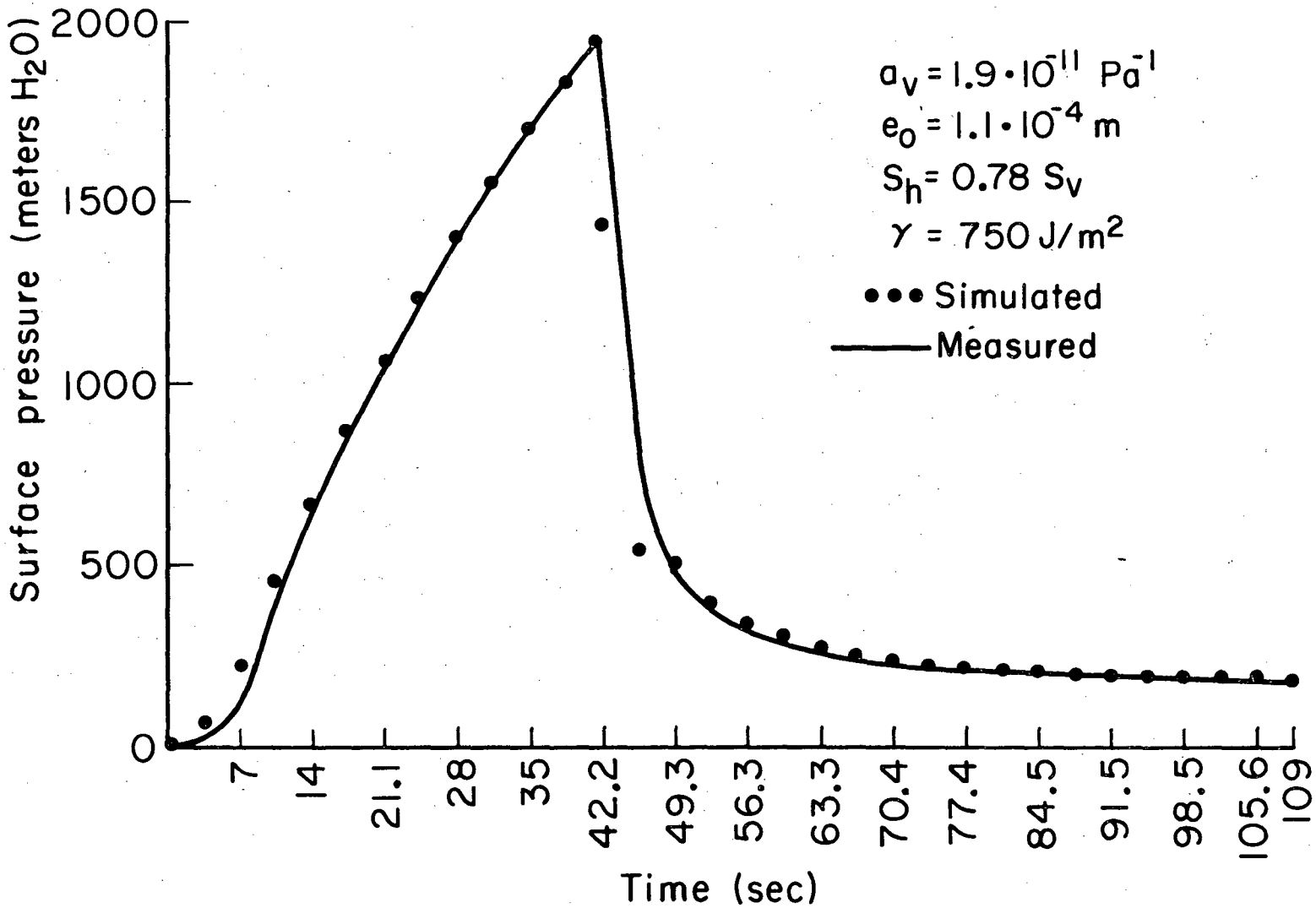

XBL807-3478

Figure 25 Monticello 2-7-1 Surface Pressure vs. Time

that it is more realistic to adjust the parameters to give a fair agreement over subsequent cycles of any one mini-fracture operation, even if the agreement with any one cycle is not as exact as in Figures 24 and 25. As will be explained later, this allows analysis of all the simulation parameters.

Monticello Validation - Consecutive Cycles

Modeling subsequent cycles for any one mini-fracture operation involved a great deal of trial and error calculation. This is partially due to the fact that the fracture growth is unstable during the initial pressurization and is not sensitive to the surface energy calculation. The fracture surface created is so small during the initial cycle that the value of γ chosen could be very high, up to 8 times the value estimatied by Aamodt (1976), before any change in the simulation occurred. The magnitude of the surface energy requirement indicated the relative insensitivity of the fracture growth to the energy calculation during the initial breakdown. Values of γ from 750 - 800 J/m^2 represent the range where the energy coefficient begins to exert influence on the initial fracture growth. A lower value of the surface energy coefficient would mean that the influence of this parameter will probably not be seen until the fracture growth becomes stable.

The consecutive cycles were all characterized by an initial pressurization phase, a growth phase where the fracture accepts fluid from the wellbore and extends, a shut-in phase when the pump was turned off, and a bleed-off stage where fluid pressure was released thereby returning a fraction of the injected fluid to the surface. This latter procedure was modeled by connecting a surface node that represented the circulation tank to the surface piping element. The simulations were continued after subtracting the energy lost, when the fluid was produced from the system, from

the available strain energy term, SURGY. The time ranges of these processes are labeled on the corrected pressure data for Monticello cycles 2-4-1, 2-4-2, and 2-4-3 shown in Figure 26. The Monticello data for these cycles was both the most complete and the longest record of the vertical fracture data provided by Zoback and was the best choice for successive cycle simulation. The numbers used beneath the time scale in Figure 26 indicate the times of fluid injection (1), shut-in times (2), and bleed-off times (3). Note that the bleed-off times have been truncated in Figure 26 due to the fact the surface pressure is always atmospheric and thus provides no information.

Consecutive Cycle Simulation Results

The radial version of the HYDFR program was used to model the Monticello data. The radial mesh was used primarily due to the assumed homogeneous nature of the granite formations in the Monticello field preventing any possible 'slip' boundaries. No conclusive statement about the true nature of the fracture system can be made from this as it is possible for almost any fracture shape to be created. However, previous researchers (Murphy and Tester, 1979) believe that radial or penny-shaped fractures will be created in similar situations. The simulation was initially conducted by a trial and error procedure involving simultaneous variation of as many as three of the parameters, e.g. a_v, e_o, and k. Later it became apparent that the change of any one of the parameters affected only specific parts of the simulation response as will be discussed in the next section.

The simulation results for the Monticello 2-4-1, 2-4-2, and 2-4-3 data are presented in Figure 27. The simulation was conducted with the 'best choice' of the various parameters that resulted in a reasonably good match to the field data. As can be seen from Figure 27 the

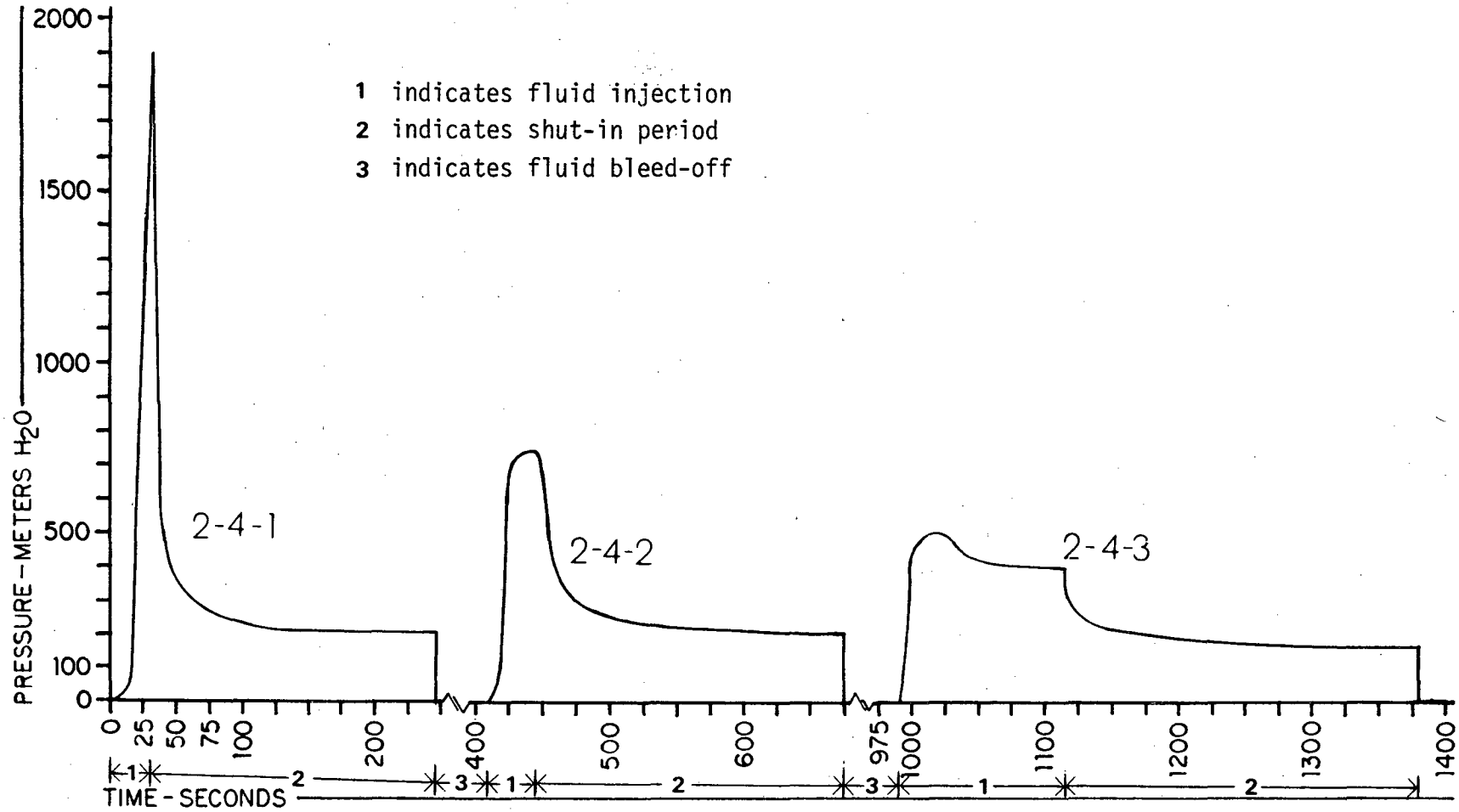

SURFACE PRESSURE VS. TIME
MONTICELLO CYCLES 2-4-1, 2-4-2, 2-4-3.

Figure 26 Subsequent Cycles in the Monticello Data

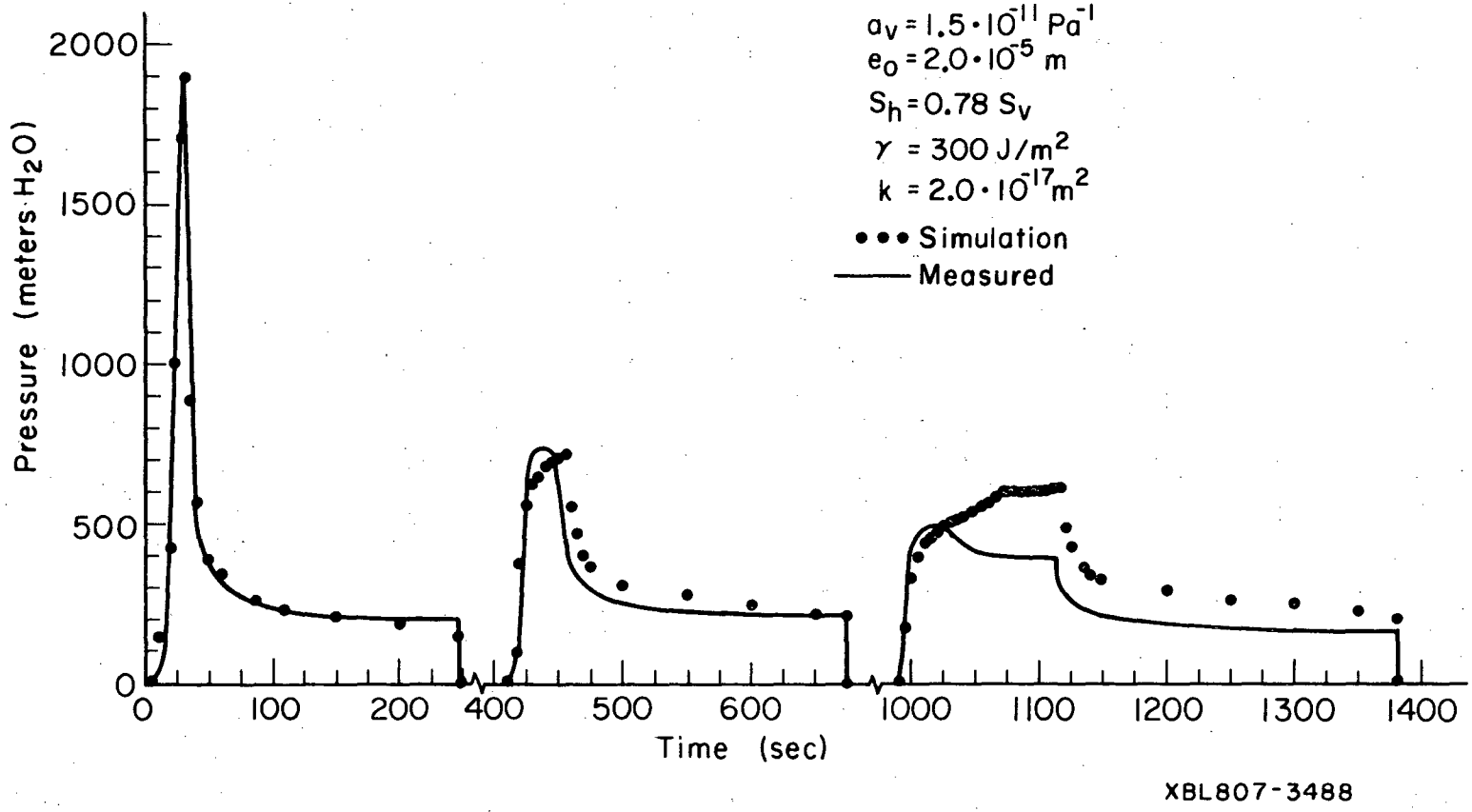

Figure 27 Monticello Simulation Results - Comparison of Field Data vs. Simulation

simulation seems to fit the Monticello data very well during the first cycle, fairly well during the second cycle, but it seems to predict higher pressures during the third cycle. The third cycle data has a region of constant pressure between 1050 and 1115 seconds where the fracture may be extending stably. However, while the simulation results also exhibit a plateau in the pressure data and thus a stable fracture extension period for the third cycle, the simulation pressure is at a relative maximum at this point. This is consistent with the model theory that requires that the pressure at the fracture tip be equal to the minimum earth stress during extension. While the Monticello 2-4-3 data indicates a maximum that is only within 100 m-H_2O of the simulation results, it is conceivable that the data reduction may have been in error or that there are other effects that have not been taken into account. These include the very real possibility that the fracture has intercepted other fractures either naturally occuring or created by other mini-fracture operations especially since the packer spacing is of the same order as r_f. The fluid may have bled off into this secondary permeability during the third cycle. This would account for the field data indicating a relative maximum before the pressure declines slightly and levels off. When designing future experiments of this type it would be desireable to use a packer arrangement that allowed simultaneous measuring of both the pressure in the cavity and the annulus above the packers. This would indicate any communication of the test fracture with the secondary fracture system or possible packer leakage. In any case while the third cycle data might not match the data identically, the overall match of the data indicates that the model can still be used to understand the processes involved in the mini-fracture operations.

C. MONTICELLO SIMULATION : PARAMETER EVALUATION

The parameters described as the 'best fit' for the simulation, i.e. $a_v = 1.5 \cdot 10^{-11}$ Pa^{-1}, $e_o = 2 \cdot 10^{-5}$ m, $S_h = .78\ S_v$, $k = 2 \cdot 10^{-17}$ m^2, and $\gamma = 300$ J/m^2, shown in Figs. 27 - 32 are not unique. The interrelations between the parameters is so great that it may be possible to generate a slightly different set of parameters that will give a similar fit to the Monticello data. The choices could be reduced if there were other field data available such as core studies that could eliminate some of the trial and error ambiguities involved in matching the pressure transients by systematic parameter variation. However, after working with the data, an understanding of how the parameters will affect the simulations may shed some light on the physical processes involved.

Effects of the Variation in Fracture Stiffness

The effect of varying the fracture stiffness is shown in Figure 28. The two values include the 'best fit' choice of $a_v = 1.5 \cdot 10^{-11}$ Pa^{-1} and a fracture stiffness of $1.7 \cdot 10^{-11}$ Pa^{-1}, a 13% increase. The fracture stiffness defined above in Equation (43) is used to relate the width of the fracture to the applied pressure. The width controls the permeability and the storage capacity of the fracture. Thus, the larger the coefficient a_v, the smaller the radius r_f needs be to encompass the same fracture volume. The final difference in the calculated fracture lengths after the third cycle was only 0.5 m for both the values of a_v, which is only 4% of the calculated fracture radius of 11.5 m and is insignificant. However, the effects on the peak pressure for the second and third cycles as a_v is varied is significant.

After the initial pressurization the fluid in the fracture is bled-off and the fracture walls close to some minimum aperture e_o'. During subsequent cycles the fluid must squeeze back into the fracture before the

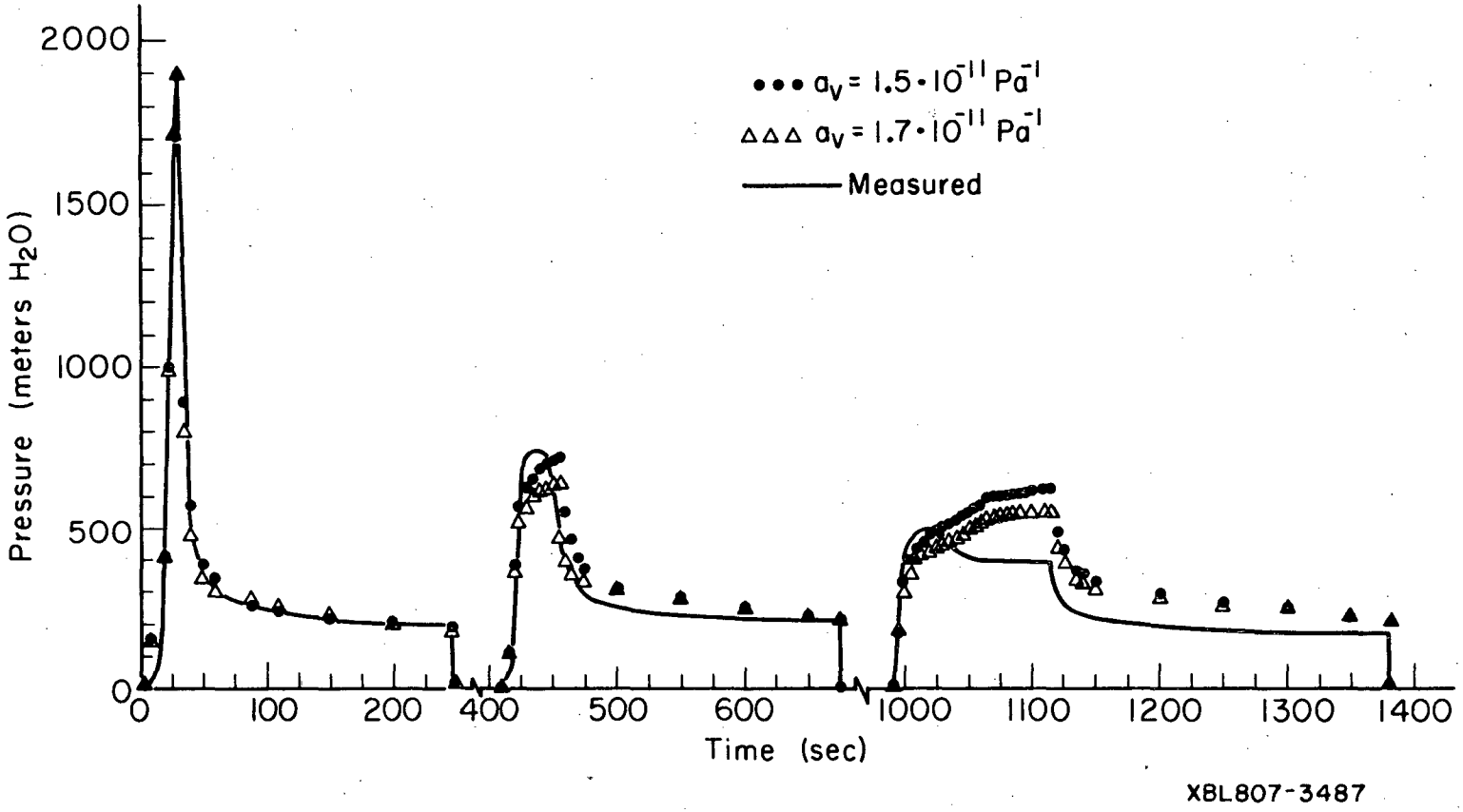

Figure 28 The Effect of Fracture Stiffness on the Monticello Simulations

fracture can continue to grow. The larger value of a_v allows the fracture walls to move apart more readily with applied pressure and thus will require lower pressures during the reopening of the fracture faces. This is indicated by the 80 m-H_2O pressure difference in the peak pressures between the two simulations for cycles 2-4-2 and 2-4-3. Once surface pumping is halted, the pressure along the fracture starts to equilibrate. Again the pressure for the more elastic fracture will equilibrate faster as the fracture walls will open at lower values of pressure. As can be seen from Figure 28 the simulation run with the larger fracture stiffness causes the initial pressure to decline much faster after the well is shut in. However the presssure in the more elastic fracture will also level off faster. This explains the fact that the simulation pressure for the smaller fracture stiffness corresponding to $a_v = 1.5 \cdot 10^{-11}$ Pa^{-1} will actually be lower during the end of the shut-in periods. The choice of one value for a_v over another was dictated by the pressure match obtained with the second cycle of the Monticello data. This match was much better for the stiffer (smaller) fracture stiffness value even though the third cycle performance may tend to favor the larger value of a_v.

Effects of Variation of Initial Aperture

Once the fracture is created, there must be initial fracture permeability, otherwise fluid flow will not occur. In the present model this is treated by using an initial fracture aperture representing a hairline fracture. This initial width, e_o, is orders of magnitude less than the final fracture aperture and controls the magnitude of the peaks in the pressure simulations. A smaller e_o would require a larger pressure drop in the first fracture element and correspondingly increase the calculated breakdown pressure. This can be seen in Figure 29 in which simulations for two values of e_o are presented, the 'best fit'

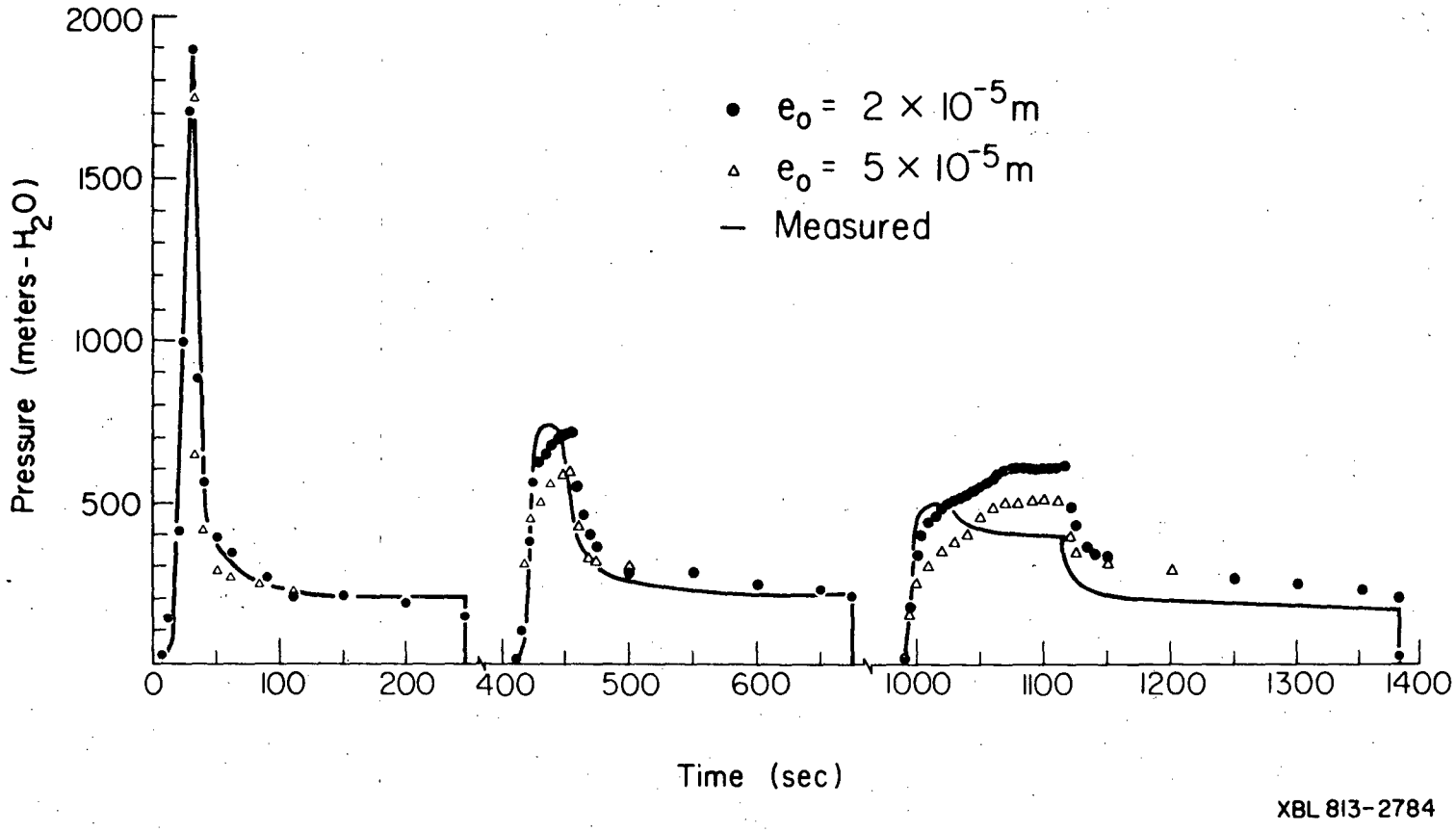

Figure 29 The Influence of the Initial Aperture on the Monticello Simulation

value of $2 \cdot 10^{-5}$ m and a larger value of $5 \cdot 10^{-5}$ m. The initial pressure peak for the latter case is more than 150 m-H_2O lower than the maximum pressure indicated by the field data.

The size of e_o correspondingly affects the size of the minimal aperture, e_o', that the fracture assumes when bled-off. The larger e_o the larger e_o' although the two values are not the same due to the hydrostatic pressure that exists in the fracture during the bleed-off phase. The larger e_o value will result in a lower pressure on subsequent cycles, since less pressure is needed to push fluid past the closed fracture walls and reopen the fracture. This effect is seen in Figure 29. Note that the effect is much the same as that of changing the fracture stiffness, however, the effect does not persist during the first cycle shut-in period. This is due to the fact that fracture flow during shut-in is controlled by the change of the fracture aperture which is a function solely of the fluid pressure and the fracture stiffness during this time.

Effect of Varying the Minimum Earth Stress

The minimum earth stress, S_h, affects the calculation of the available surface energy term SURGY. The larger the value of S_h in the simulation the more energy is required both to open the fracture and to extend it. This is due to the fact that the fluid must do work in overcoming the earth stress which is assumed to be opposing the fracture wall movement. A lower value of the earth stress will allow a larger fracture to be created due to the lower total energy required. Since the energy supplied to the system is related to the fluid pressure during injection, raising the earth stress will necessarily increase the injection pressure (as $P_{ext} > S_h$) and the energy supplied to the system, but not to a level that more than partially offsets the additional energy needed to open the fracture against the larger value of S_h.

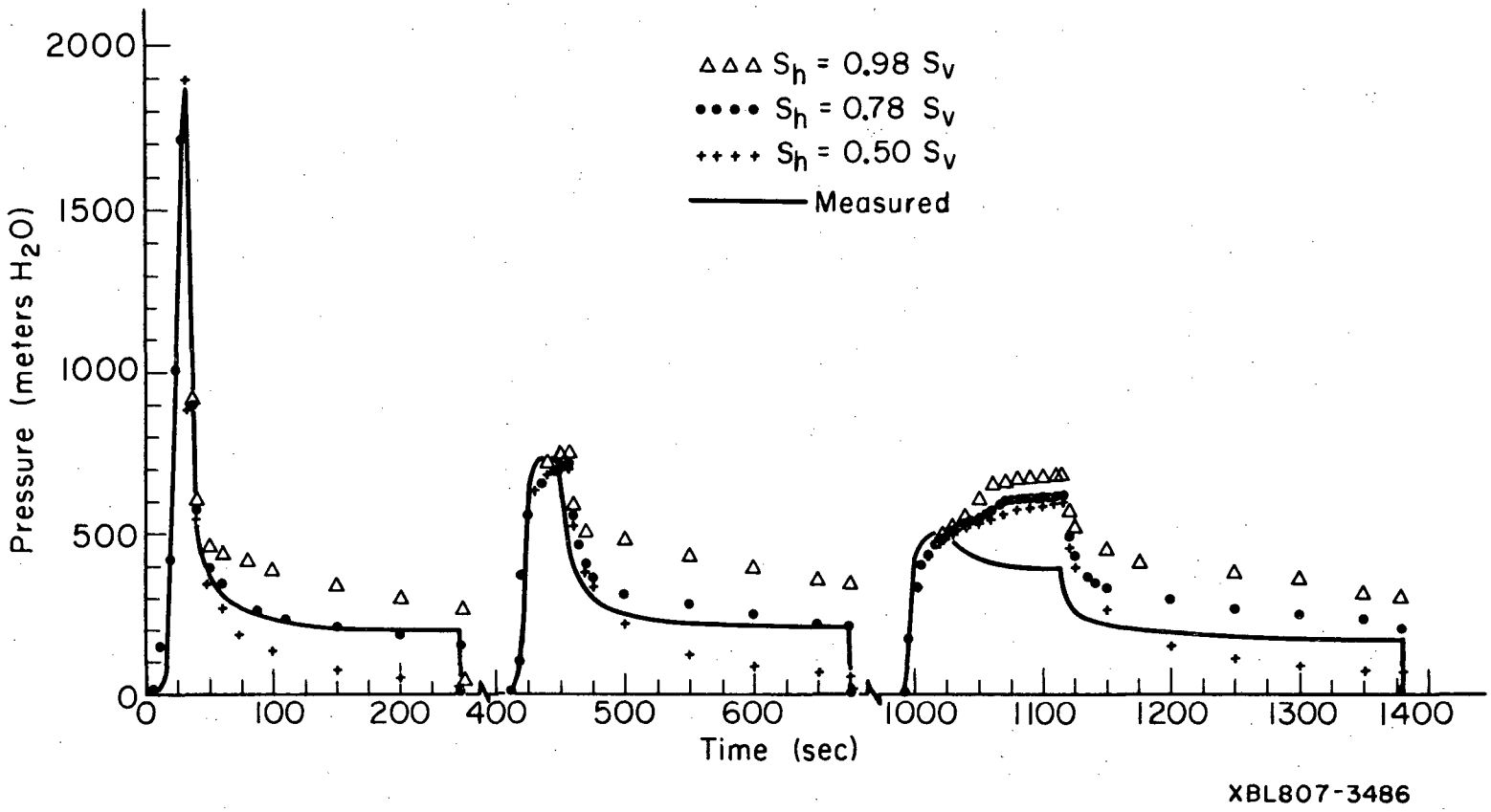

Figure 30 The Effect of the Minimum Earth Stress on the Monticello Simulation

The magnitude of S_H used in the simulations was varied as a percentage of the overburden stress S_V. The values used ranged between 0.5 S_V and 0.98 S_V; the latter value nearing the theoretical limit before the onset of horizontal fracturing. Figure 30 demonstrates the effects on the simulations of changing the minimum earth stress S_h from the 'best fit' value of 0.78 S_V to values of 0.5 S_V and 0.98 S_V. As would be expected, the lower value of S_h resulted in lower pressures over all three cycles. The only exception to the phenomenom is the brief 30 second wellbore pressurization period where the pressure is affected only by the the wellbore storage and the value of e_0. The larger value of S_h of 0.98 S_V resulted in correspondingly higher simulated wellbore pressures over the same time ranges, as seen in Figure 30.

Effect of Variation in Formation Permeability

The rock formations in the Monticello field tests are composed of granite which has relatively low values of storage capacity and permeability compared to typical petroleum reservoir rocks. Granite does exhibit secondary permeability due to micro-fractures in the matrix. Variations in rock permeability will influence the shut-in pressure after the pressure in the fracture has equilibrated. The variation in formation permeability might also affect the calculated fracture growth to a small extent by 'siphoning off' some of the available surface energy due to fluid permeation from the fracture. However, the fracture growth in this mini-fracture operation was so rapid that the effects on the surface energy term due to changes in the rock permeability were negligible. For an extremely large fracture this may not be the case as fluid permeation from the fracture may be significant. The simulations for the two permeability values shown in Figure 31 are compared to the 'best fit' value of $k = 2 \cdot 10^{-17}$ m^2 (.02 md). The lower value of 10^{-17} m^2 raises

the simulation pressures primarily during the shut-in periods by about 80 m H_2O. A larger permeability value of 10^{-16} m^2 results in a larger pressure drop when compared with the best fit simulation over most of the time range indicated in Figure 31. In fact this larger permeabilty may even act to drain entirely the fluid from the system as indicated by the atmospheric pressure in the wellbore at the end of 250 seconds. Even larger values of permeability might affect the fracture growth but were not studied since the coarseness of the reservoir mesh may begin to influence the simulation accuracy at larger values of formation permeability. For this reason the estimation of in-situ permeability by the model is probably approximate at best.

The Effect of Variation in the Surface Energy Coefficient

The last parameter varied in the simulations surface energy coefficient γ, which is a measure of the rock toughness. Results of the initial modeling described in the first cycle simulations, presented in Figures 24 and 25, indicated that a fracture surface energy coefficient from 750 to 800 J/m^2 was the minimum range that would affect the simulations. Modeling of all three cycles indicated that the minimum value of surface energy coefficient to be around 300 J/m^2. The surface energy coefficient only affects the calculation of the SURGY term and the effect of the coefficient will be seen in either reducing the fracture length or temporarily blunting the fracture growth. This blunting occurs when the value of the net available strain energy term becomes negative. As γ increases SURGY was found to oscillate around the value of zero during the stable growth period of the third cycle. As γ was further increased SURGY actually remained negative, but still oscillated, during some of the simulations. The effect of this negative surface energy value results in a much larger calculated pressure rise in the wellbore as the fracture

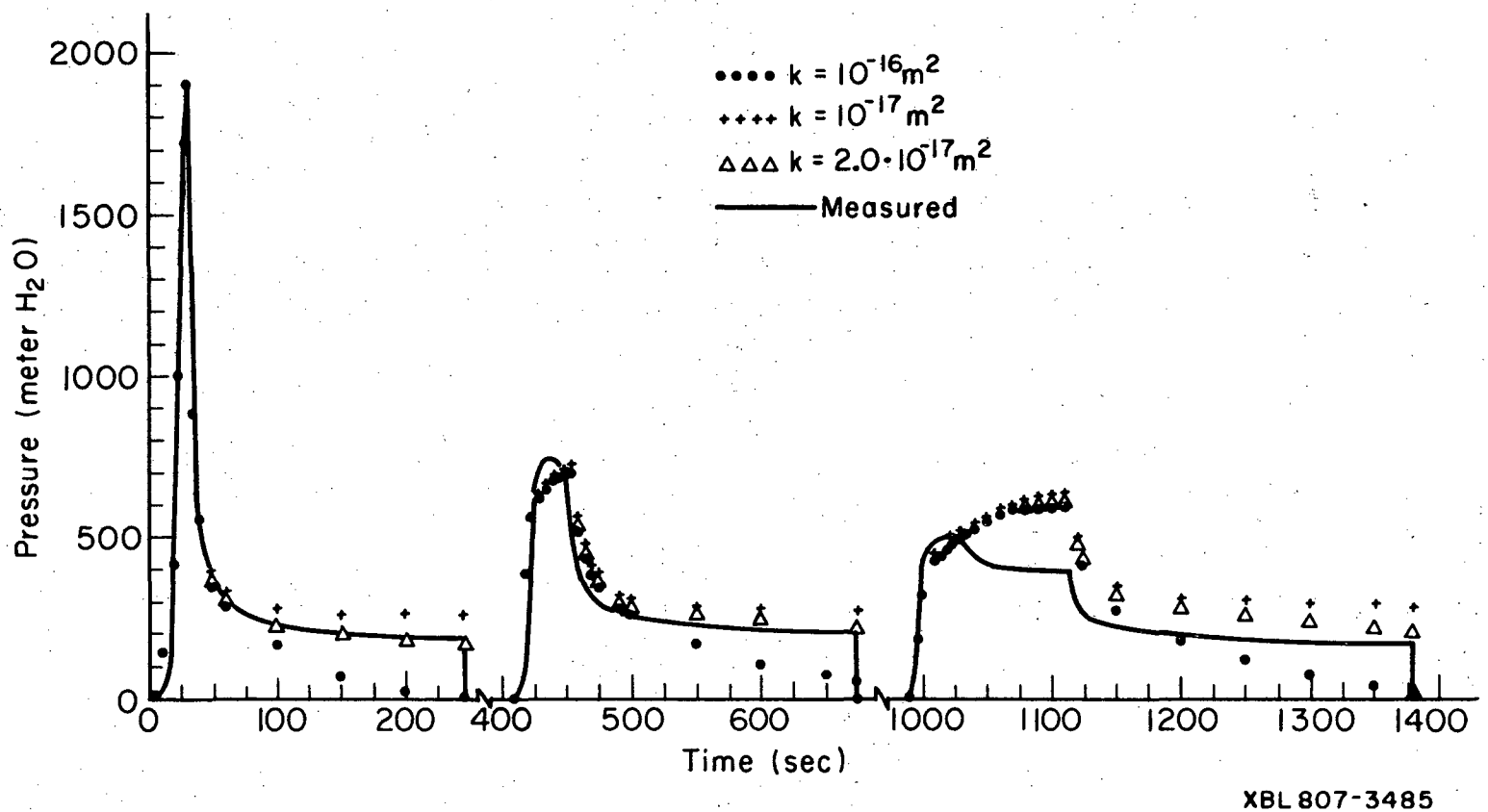

Figure 31 The Effect of the Formation Permeability on the Monticello Simulation

growth is arrested but the fluid pumping is continued. It should be pointed out that in a real situation the pumping volume is not likely be independent of the injection pressure as modeled here. The effects of the variation of surface energy coefficient are seen in Figure 32. As the magnitude of γ increases past the minimum and best fit value of 300 J/m^2 the pressure is affected at different times in the simulation. The value of γ = 350 J/m^2 increases the pressure during the last 300 seconds of the simulation. An increase in the coefficient to 500 J/m^2 begins to affect the pressure during the second cycle. In this instance the SURGY term remains negative and fracture growth is prematurely halted during the rest of the simulation. This explains the large increase in pressure observed during the third cycle. The largest value of γ = 1000 J/m^2 causes the fracture to blunt during the first cycle. It is reasonable to assume that the trend in the magnitude of the surface energy coefficient would continue as the fracture becomes larger. Thus the value of γ would become lower as the fracture growth proceeds. For this reason the value of 300 J/m^2 found for the best fit simulation is most likely anomalously high and can only be used as an upper bound to the true value.

Conclusions from the Monticello Simulations

The Monticello field study was originally designed by Zoback to analyze the data for use in estimating the magnitude of the minimum earth stress, S_h. Results from the present work indicate the minumum earth stress to be 78% of the overburden stress. Zoback (personal communication) has independently arrived at an S_h value equal to 80% of the overburden stress, which agrees with the present work. There has been no other study that would give indications of the magnitude of the other parameters used to fit the Monticello data. However, values that have been reported in the literature that have been calculated

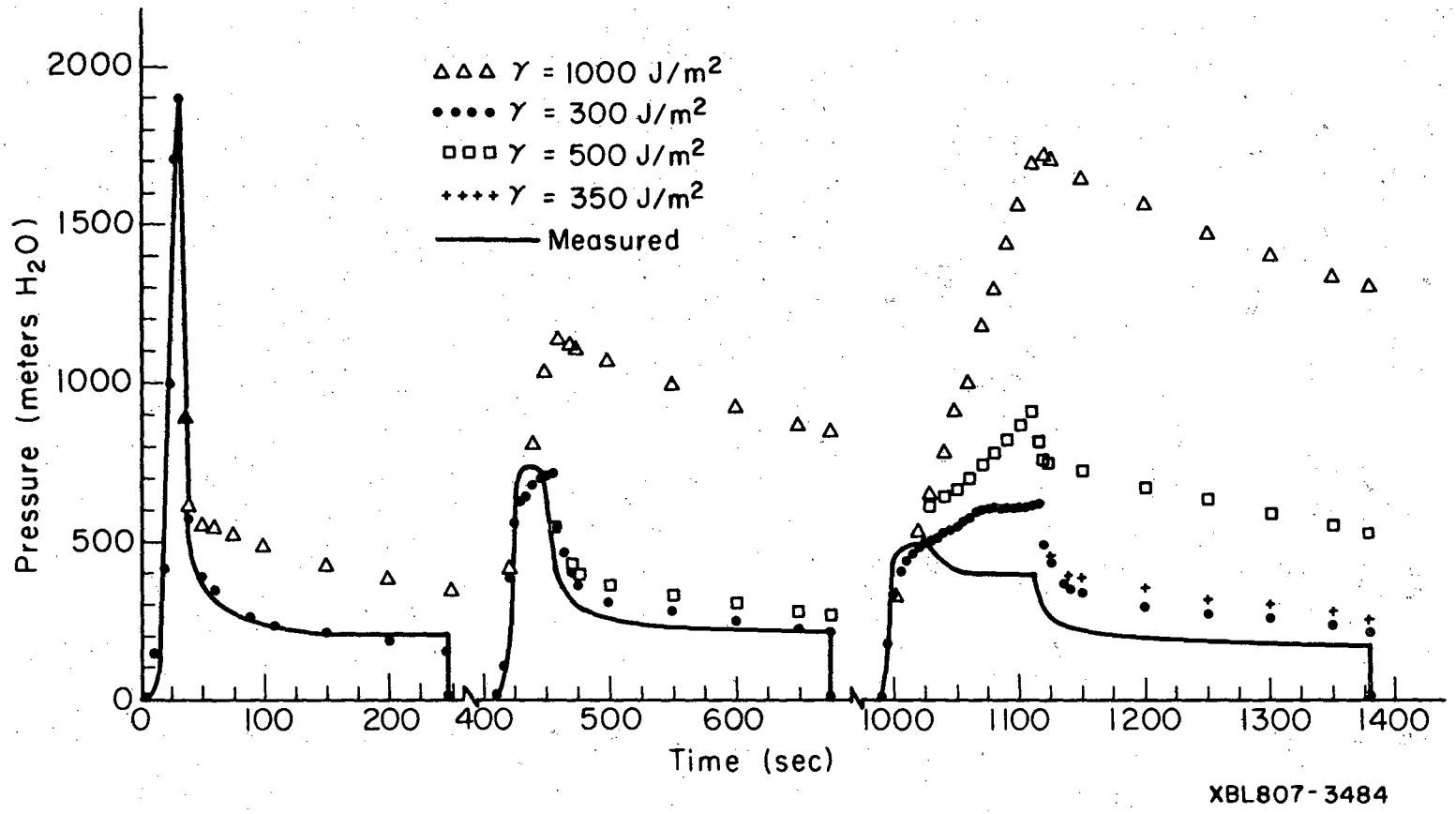

Figure 32 The Effect of the Surface Energy Coefficient on the Monticello Simulation

from field and core tests in granitic rocks may be used for comparison. Brace (1979) reports that the in-situ permeability of granite may be up to 3 orders of magnitude higher than core tests would indicate. Thus the value of $2 \cdot 10^{-17}$ m^2 is well within the range of permeabilities for granite estimated to be from 10^{-18} to 10^{-13} m^2 (.001 - 100 md). Murphy, et al., (1977) reported values for the minimum fracture aperture in granite formations on the order of 10^{-4} m which agrees with the best fit result of an e_0' of $0.65 \cdot 10^{-4}$ m. Murphy, et al., also report a rock compressibility of $2.7 \cdot 10^{-11}$ Pa^{-1} which is the same order of magnitude as the fracture stiffness a_v used in the best fit simulation, although there is no exact correspondence between a_v and rock compressibility. The value of surface energy coefficient, γ, was found to be 3 times the value reported by Aamodt (1977) and 5 times the value reported by Krech and Chamberlin (1974). As explained earlier this is to be expected since the model sensitivity increases as the product of γ and the fracture area increases. Unfortunately, the fracture area in the simulations was so small that the magnitude of γ appears anomalously high.

While the model has been used to analyze pressure transient data it could conceivably be used to predict the fracture growth and pressure variations of any arbritrary system if the system properties are known or can be estimated. This will be demonstrated in the next section. Although the values of the parameters determined to be the most representative for the Monticello experimebt may not be unique, they may still represent a reasonable range of actual field conditions. Further advances in pressure measurement techniques, i.e. downhole pressure monitoring, may provide even better data for the pressure transient analysis. This information should result more accurate understanding of these mini-fracture type experiments.

D. MODEL APPLICATIONS TO GROWTH OF RECTANGULAR FRACTURES

The HYDFR program was used to simulate the growth of rectangular fractures assumed to be generated during MHF type operations. The primary aim of this investigation is to simulate a hypothetical hydraulic fracturing operation. The range of parameters used in the simulation appear in Table 3. The analysis is done from an engineering point of view. That is, the simulation represents the behavior of a realistic hydraulic fracturing process and the calculations will be presented in real time, pressure, and distances. The factors that affect the realistic behavior of the system, i.e. the pumping rates, fluid viscosity, and use of fluid leak off control agents, will be varied in order to determine the effects on the results of the simulations. The other factors involved in the performance of the model have been discussed in the previous section. Before the simulation analysis is presented the behavior of the model itself and its effect on the simulations will be discussed.

Numerical Effects of the Scale Factor

The use of the ε factor in increasing the element sizes as the fracture propagates, affects the results of the simulations. This effect shows up most dramatically when the fracture growth is observed to change from unstable to stable and is manifested in the alteration of the slope of the x_f vs time curves. This effect is seen in Figure 33 which shows the fracture growth vs pumping time for various values of ε. There are two stages of fracture growth seen in this figure. The first growth period is due to the pressurization of the inital fracture element. The duration of this period is a function of the fluid viscosity and initial aperture dimension as discussed previously in the Monticello data section. The second stage is the unstable growth period in which the surface fluid pressure declines very rapidly as the fracture propagates into the formation. This second

Table 3 Parameters Used in Rectangular Fracture Studies

Parameter	SI Units	Oilfield Units
k	10^{-17} - 10^{-13} m^2	.01 - 100 md
k_s	10^{-17} m^2	.01 md
$(\phi c)_t$	$3.58 \cdot 10^{-10}$ Pa^{-1}	$2.47 \cdot 10^{-6}$ psi^{-1}
x_f (initial)	0.5 m	1.64 ft
w (initial)	10^{-4} m	$3.28 \cdot 10^{-4}$ ft
z	1000 m	3280 ft
h	3 m	9.84 ft
Q	0 - $8.0 \cdot 10^{-3}$ m^3/sec	4350 bbls/day
P_b	6000 m-H_2O	8500 psi
μ	1 - $1000 \cdot 10^{-3}$ Pa-sec	1 - 1000 cp
ρ_f	930 kg/m^3	0.93 gm/cc
ρ_r	2700 kg/m^3	2.7 gm/cc
β_f	$1.8 \cdot 10^{-9}$ Pa^{-1}	$1.24 \cdot 10^{-5}$ psi^{-1}
γ	20 J/m^2	---
ε	0 - 20%	---
a_v	2.5 - $50 \cdot 10^{-11}$ Pa^{-1}	1.7- $35 \cdot 10^{-7}$ psi^{-1}
S_h	0.5 - 0.98 S_v	---
formation rock	berea sandstone	---

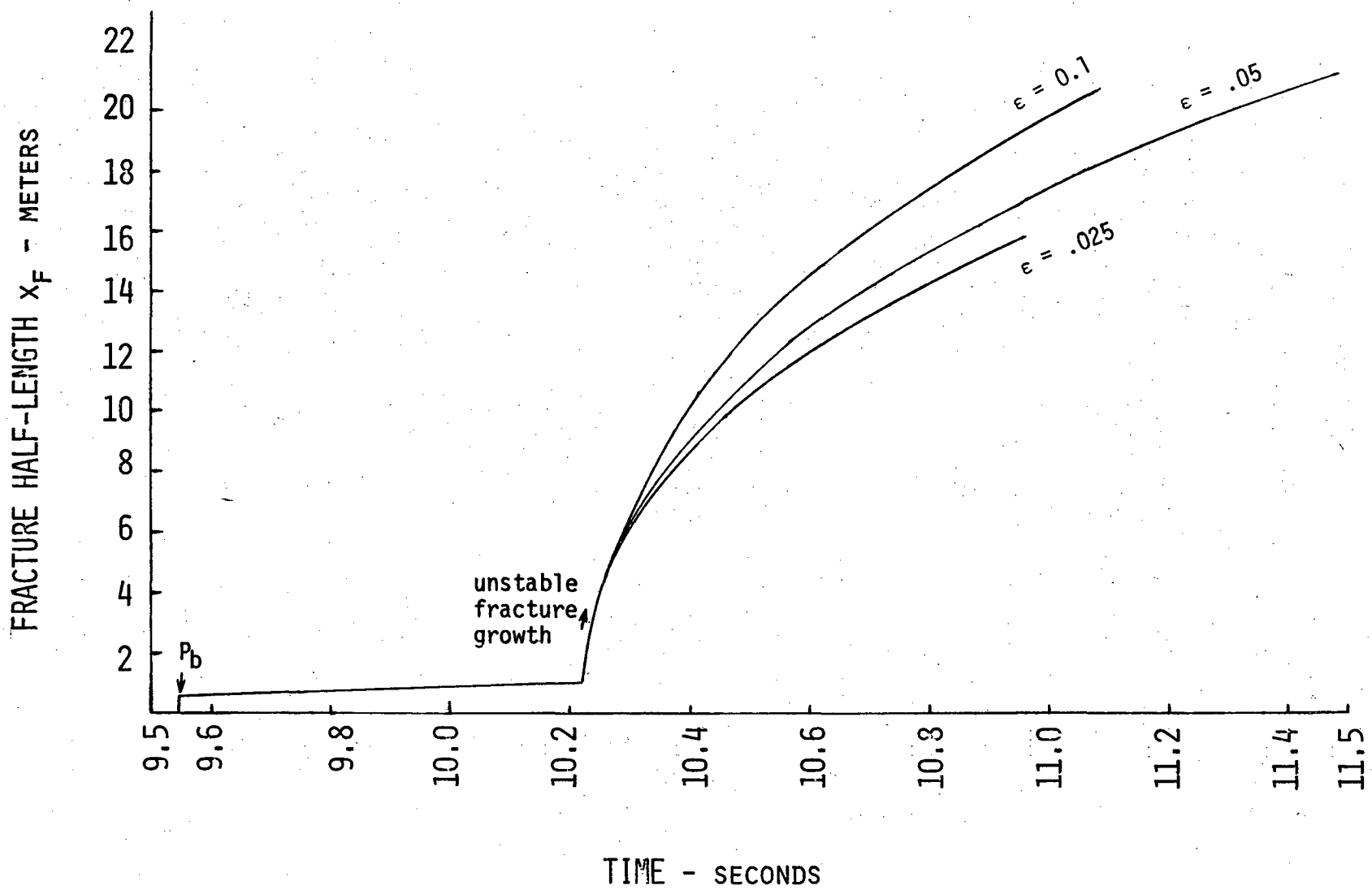

Figure 33 The Effect of Mesh Extension Factor on the Initial Fracture Growth

stage of growth begins at 10.22 seconds on Figure 33. After the fracture has grown to 6 meters the effect of the ε factor becomes increasingly apparent. As the value of ε increases the apparent slopes of the x_f vs time curves also increase. The size and spacing of the fracture elements also increases with ε. Although the results indicate that it may take less time to propagate a 16 m fracture with $\varepsilon = 0.1$ as compared to a 16 m fracture simulated with $\varepsilon = .025$ the calculated pressure in the wellbore node will drop faster the higher the value of ε. This indicates that more fluid is needed to expand the greater volume of the $\varepsilon = 0.1$ fracture mesh at any given time than is required to expand the $\varepsilon = .025$ fracture mesh at the same time. This indicates that the spacing of the mesh affects the apparent pressure gradient in the fracture. The larger mesh would have a smaller pressure gradient between the fracture tip and the wellbore nodes. Thus the larger mesh fracture could accept fluid faster than the smaller mesh fracture causing it to expand at a greater rate. This numerical effect is a necessary by-product of dealing with the limited number of elements allowed in the present computer program. The value of $\varepsilon = 0.2$ was later found to be a reasonable choice when simulating MHF type fractures reaching lengths of 250 m. This particular value of ε was used for most of the simulations and permitted the study of these large fractures with a reasonable calculation time. Even so the process was so complex that it took roughly one second of computer time to simulate 10 seconds of fracture growth. Thus $\varepsilon = 0.2$ becomes an optimum value when considering the finite resources allocated for this study. However, this will not affect the results of this section since the relationships between the various parameters of the system will be equally influenced by the effects of the ε factor. It is the understanding of the effects of these parameters on the fracture growth that is important in evaluating the usefulness of the model.

The relationship beween the width and length of the fractures and the pumping time is necessary for fracture design calculations. However, since the only indication of fracture behavior can be seen in the surface pressure transients, analysis of this transient is crucial. Results of a typical pressure vs time and a typical fracture length vs time calculation are shown in Figure 34. Two sets of curves appear in Figure 34 showing the influence of the values of ε used in the MHF simulations. The region of unstable fracture growth is indicated on the time scale and covers the first seven seconds after the maximum pressure is reached. This corresponds to the period when the wellbore pressure is rapidly dropping. After the pressure begins to build again the fracture growth is controlled by the rate of energy supplied from the surface pumps and the growth becomes stable. Again, the stable period refers to the period where fracture growth is accomplished only by an increases in pressure of the wellbore. When the wellbore pressure starts to increase, the slope of the x_f vs time curves begins to decrease markedly. The slope appears to have reached a fixed value at times greater than 60 seconds. This is only an effect of the scale of the graph as could be seen when plotting the results on log paper. Variation of the ε factor has an interesting effect on the curves shown in Figure 34. The simulation with a value of $\varepsilon = 0.2$ results in lower pressures and larger rate of fracture growth for reasons discussed previouly. It may also appear that at large times the pressure transient curves may actually parallel each other. While the pressure curves never do become parallel, their forms are nearly identical and show the effects of the scale factor only as simple displacement on the pressure axis. To reduce the effects of the mesh spacing factor on the fracture length vs time curves, it becomes necessary to reduce the magnitude of ε which correspondingly restricts the potential lengths of

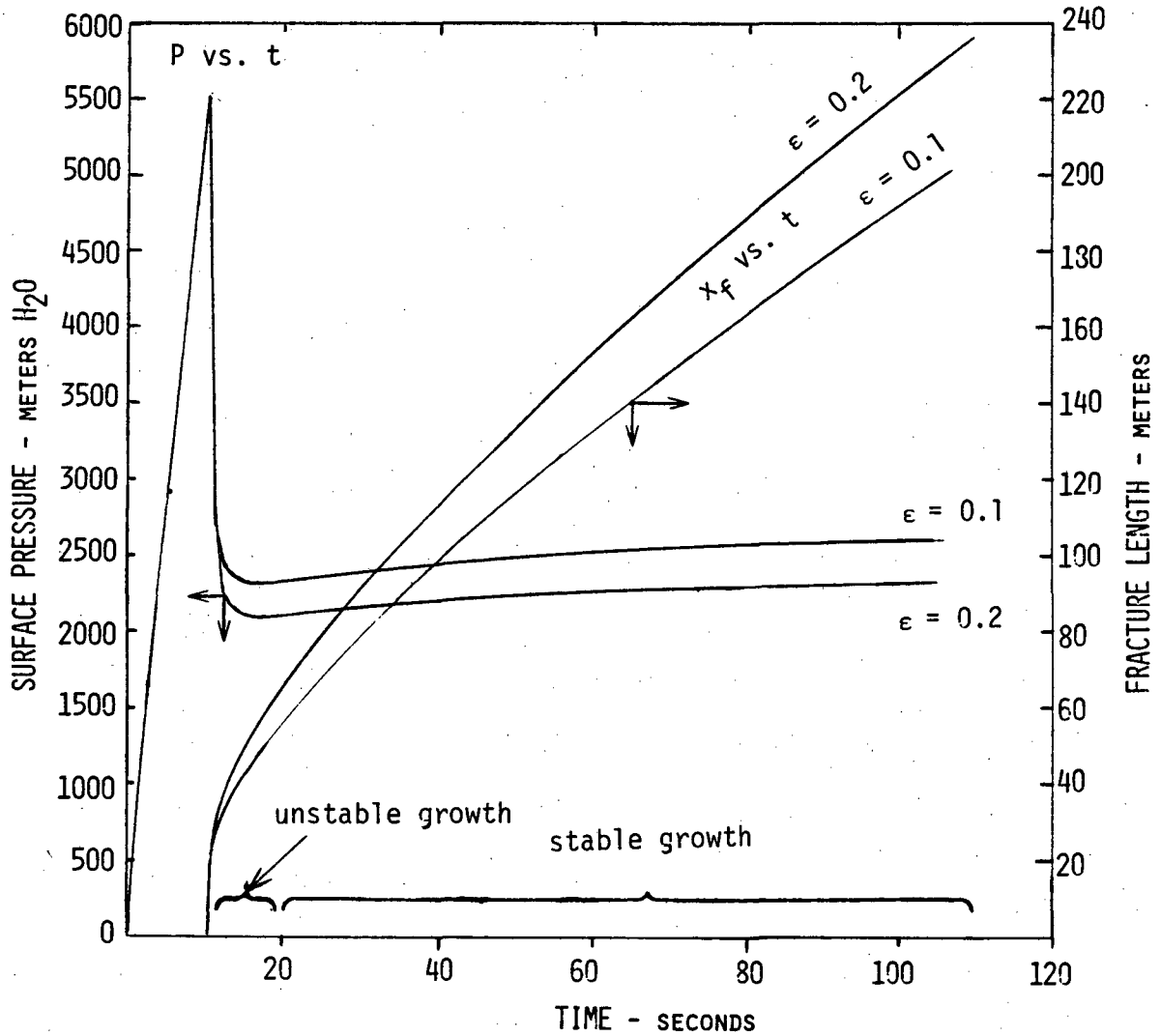

Figure 34 Pressure vs. time and x_f vs. time for a Rectangular Hydraulic Fracture

the fractures created in the simulations. In rectangular fracture growth problems a compromise to this situation was employed by reducing ε to zero after the region of stable fracture growth is reached. Since the remainder of the work will be primarily concerned with factors that will affect the stable fracture growth, initial unstable growth will be briefly covered.

Initial Fracture Growth and the Effects of Tubing Size

The assumption that the fracture does not penetrate the upper and lower boundaries formed by formations with much greater fracture toughness, should be least valid in the region near the wellbore. The pressures are higher in the near wellbore region and the initial fracture growth may be so rapid that the barrier would be penetrated despite its greater fracture resistance. Although no boundary formations are included due to the two-dimensional restrictions of the current model, the investigation of the initial fracture growth may give some insight into possible vertical migration of the fracture.

The energy stored in compressing the fluid in the tubing string is responsible for the initial unstable growth of the fracture. The energy contribution from the surface pumps may be minimal during the relatively small time period of the initial growth. The energy needed for the sudden extension can either be stored in the wellbore tubing itself or in the tubing and wellbore volume. It is also conceivable that the fracture may extend so fast that the pressure in the system will drop to the point that the total surface strain energy becomes negative and the fracture growth is arrested until the energy level builds up again. This energy, supplied by the surface pumps, can be stored as potential energy in the expansion of the fracture walls. As the value of the fracture stiffness increases, the fracture compressibility increases and the energy storage capacity of the system will also increase. This type of behavior can be thought

of as being somewhat analagous to a capacitive discharge device used in automotive ignition systems. The surface pumps supply energy to the fracture which 'discharges' after a certain saturation value is reached. The time between discharges is controlled by the rate of energy storage which is a function of the pumping rate, the stiffness of the fracture, and the rate of fluid seepage into the formation. The simulation results are presented as curves representing the average fracture growth vs time. It is very important to note that the fracture growth in this model is discrete and the points on the graphs indicate the true periodic nature of the extension process. While the average-value curve drawn through the simulation points does not indicate the discontinuous growth it does facilitate comparison of the individual curves.

Figure 35 shows a log-log plot of the calculated fracture half-length, x_f, vs time for the initial 40 m of fracture growth in a formation of typical reservoir rock (Berea sandstone). The value of the fracture stiffness coefficient is approximately 30 times the value used in the Monticello simulations for the tougher granite formations and is indicative of values that may be found in the relatively weaker rocks common in petroleum applications. The three curves repesent different values of tubing size, i.e. 8, 25.4, and 44.4 mm radii, the latter two being representative of tubing sizes used by the industry. The x_f vs time curves show two definite slopes as can be seen from inspection of Figure 35. The first slope is essentially vertical when the crack initially propagates reaching calculated tip velocities approaching 500 m/sec. At some point, the slope of the curves reduces abruptly to a value having a near linear growth rate with time. This would be expected from the form of Equation (9) which indicates that the maximum rate of growth of a rectangular fracture is linear with time if leakage from the faces can be ignored. Even though

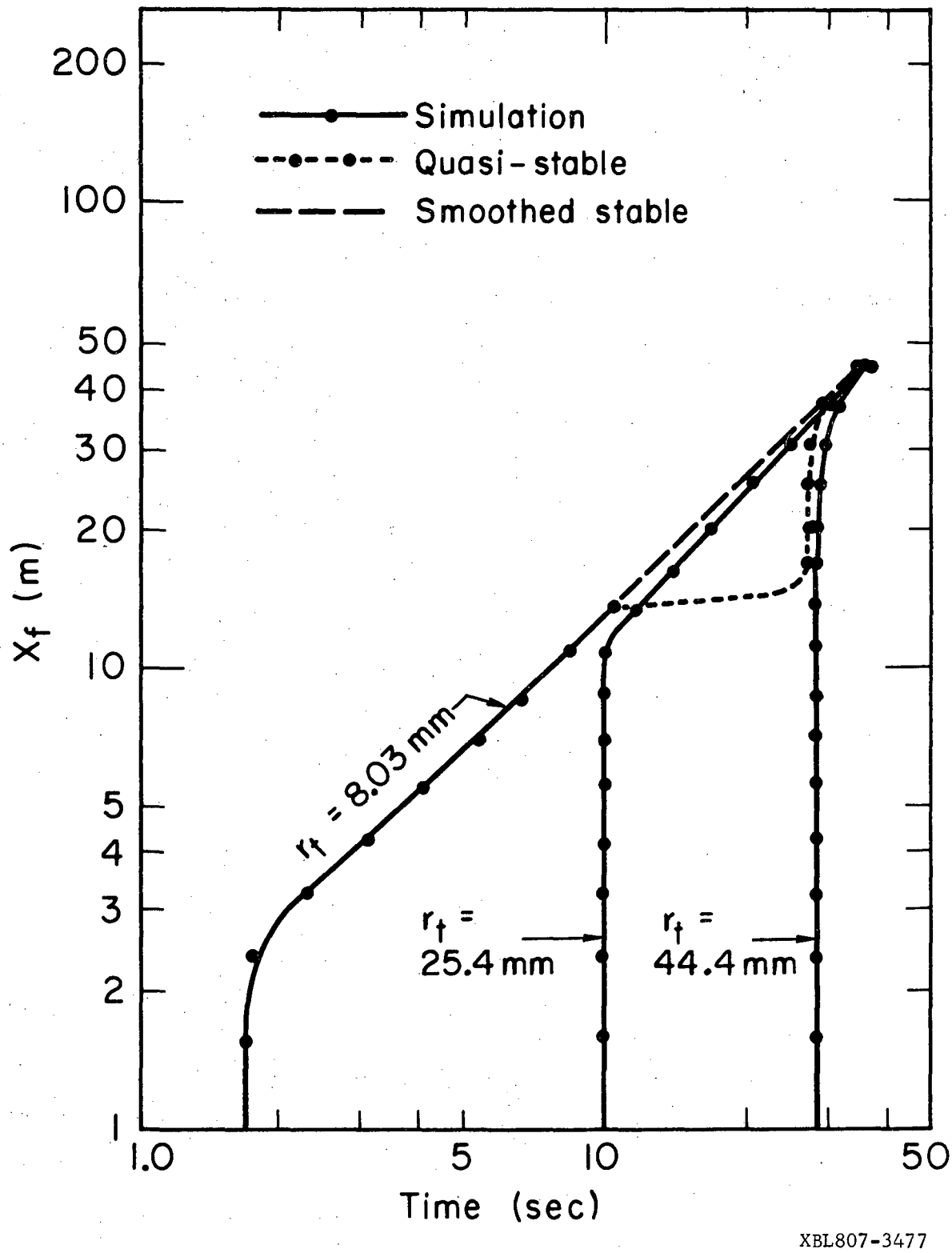

Figure 35 The Effect of Tubing Size on Unstable Fracture Length

the rock permeability was taken as 10^{-13} m^2, a skin permeability value of 10^{-17} m^2 was used to simulate the effects of a fluid loss control additive such as silica flour. However, the initial fracture growth rate was so fast that the effect of the fracture skin premeability was negligible.

In this simulation the length of the initial unstable fracture increases with the tubing size,as the system energy storage capacity also increases. For the 44.4 mm radius (3.5 in ID) tubing this unstable length reaches 30 m which is ten times the thickness of the fractured interval. The 'slip' boundary previously defined would allow the fracture walls to move apart against the top of the formation removing the stress concentration due to the fracture edge. It would seem possible that in field applications such an unstable fracture could easily penetrate into adjacent formations in the vertical direction if the 'slip boundary' is not allowed. While the use of smaller tubing sizes reduces the length of the initial unstable fracture, it does not eliminate the effect of the unstable growth period. It may prove difficult to use smaller diameter tubing to handle the flow rates used in MHF operations although annular injection after breakdown is a possibility. It is interesting to examine the curve in Figure 35 for the smallest diameter tubing used which corresponds to a tubing volume of one-tenth that of the standard 25.4 mm radius (2 in ID) tubing. This particular simulation behaves like the 'capacitive-discharge' system and exhibits two separate regions of unstable fracture growth followed by stable fracture growth, as indicated by the line marked quasi-stable in the figure. This phenomenom will simply be described as quasi-stable behavior since the majority of the points fall on the same line labeled as smoothed-stable, which is an extrapolation of the previous stable period. The quasi-stable behavior appeared in the simulations conducted with both large values of fracture stiffness and low values of μ.

The transition values for this quasi-stable behavior are $a_v > 10^{-10}$ Pa^{-1} and $\mu < .01$ Pa-sec. While this behavior may indicate that the model itself becomes periodically unstable due to the mesh spacing factor, or use of relatively large time steps, the quasi-stable behavior was nevercompletely eliminated when reducing both the ε factor and the maximum computational time steps to minuscule values of 0 and 10^{-5} seconds, respectively. It would seem that the quasi-stablebehavior is an indication that the fracture extension process may consist of a discrete series of equilibrium jumps in fracture lengths, although not to the degree indicated by Figure 35. It should be noted that such behavior has been predicted by Secor (1968) who also used an energy approach to analyse the behavior of natural fracture systems. When such quasi-stable behavior occursthe data will be smoothed.

E. LINEAR FRACTURE GROWTH - PARAMETER STUDY

The term 'fracture stiffness' as used in this work has referred to the resiliency of the fracture walls and has nodirect counterpart interms of classical elastic moduli. The value of fracture stiffness must be an in-situ measured property of the system roughly corresponding to the bulk compressibility of the rock. The properties of the rock used in these MHF type simulations are those of Berea sandstone. The range in values of permeability and porosity of Berea sandstones is fairly large. Thus the values used for this study only represent typical properties and not necessarily those of a specific rock outcrop. Accordingly, the rock permeability was varied between 10^{-17} - 10^{-13} m^2, but this wide range was found to have little effect on the simulations if the the fluid viscosity was at least 10^{-2} Pa-sec or if a fluid loss control agent was used. This latter agent is assumed to reduce the skin permeability to an arbritrary 10^{-17} m^2 which is a conservative value considering the rocks involved in

MHF operations have natural permeabilities on the order of 10^{-16} - 10^{-18} m^2. The fracture stiffness must be treated as a parameter that is not controllable but a property of the formations encountered.

Effects of Fracture Stiffness

The values used for fracture stiffness were varied by an order of magnitude from 0.25 - $5 \cdot 10^{-10}$ Pa^{-1} which corresponds roughly to the change in bulk compressibility between granites and Berea sandstones (Greenwald, 1980). Figures 36 a,b show log-log plots of fracture half-length vs pumping time for various values of fracture stiffness, a constant fluid viscosity of $2.34 \cdot 10^{-3}$ Pa-sec, and two pumping rates of $4 \cdot 10^{-3}$ m^3/sec (36a) and $8 \cdot 10^{-3}$ m^3/sec (36b). The fracture simulations were run until either 650 seconds had elapsed or a 200 m fracture length was obtained. As can be seen from the figures, the variation in fracture stiffness radically affects the growth rate of the fracture. As the stiffness of the fracture increases, i.e. a_v decreases, the growth rate increases and the difference in growth regimes becomes well defined as the contrast in slopes is more apparent. The curve for the $a_v = 2.5 \cdot 10^{-11}$ Pa^{-1} value in Figure 36a exhibits unstable growth for the first 25 m then smoothly changes to stable growth behavior. The slope of the stable fracture region of the x_f vs t curve is initially bounded by a line with a slope of 0.85 and then it is bounded by a line with a slope of 0.6 at the end of 200 m of growth as indicated on the figure. It was subsequently found for the simulation with the smallest fracture stiffness coefficient that the value of the bounding slope line actually approached a value of 0.5 when the fracture was propagated to 250 m. The values of 0.85 and 0.5 for the initial and final slopes of the fracture growth vs time curves agree well with Nordgren (1972) whose numerical model results are shown in Appendix C. The value of slope equal to 0.5 indicates fracture growth proportional to the square root of

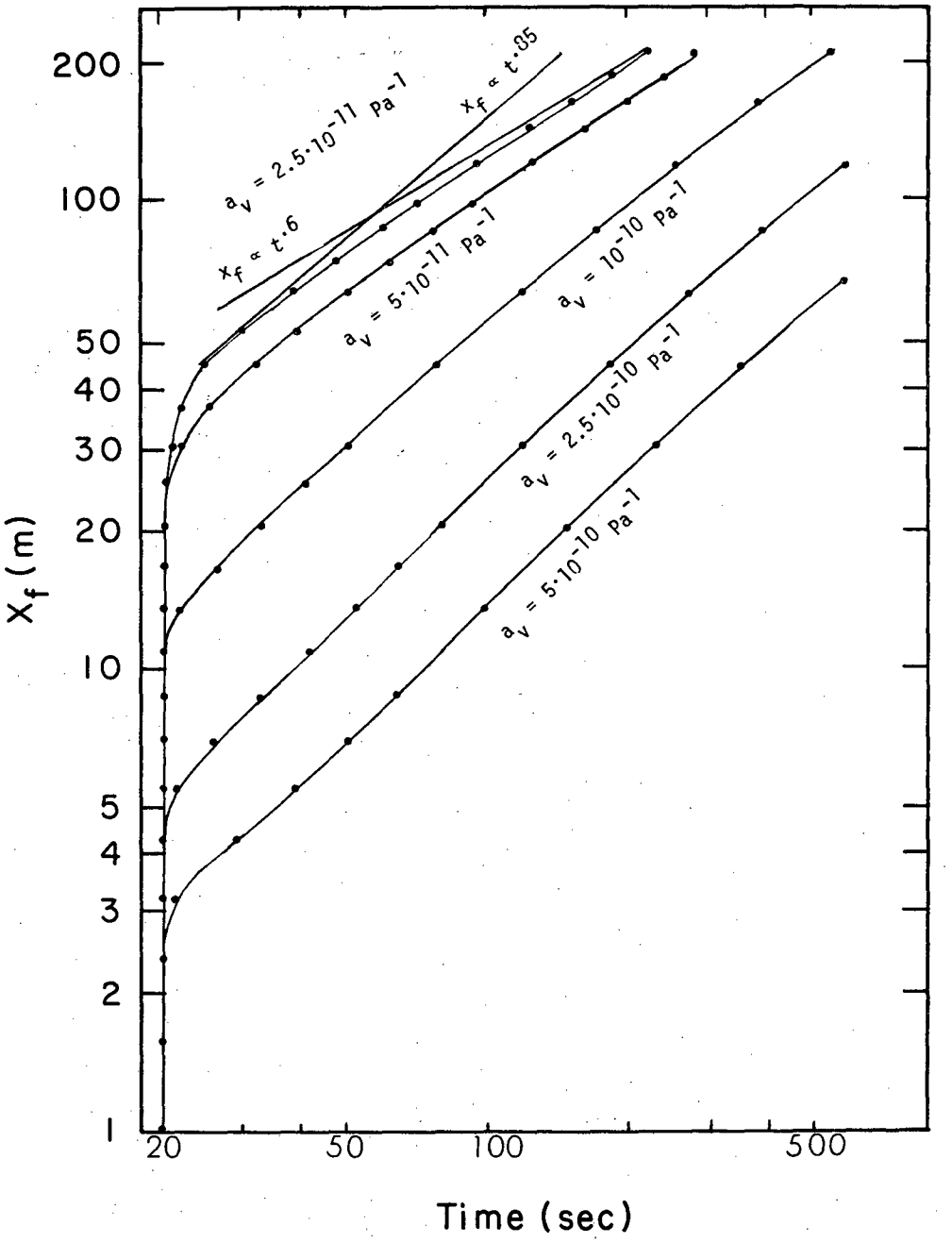

Figure 36a Log-log Plot of x_f vs. time, $Q = 4 \cdot 10^{-3}$ m^3/sec, $\mu = 2.34 \cdot 10^{-3}$ Pa-sec

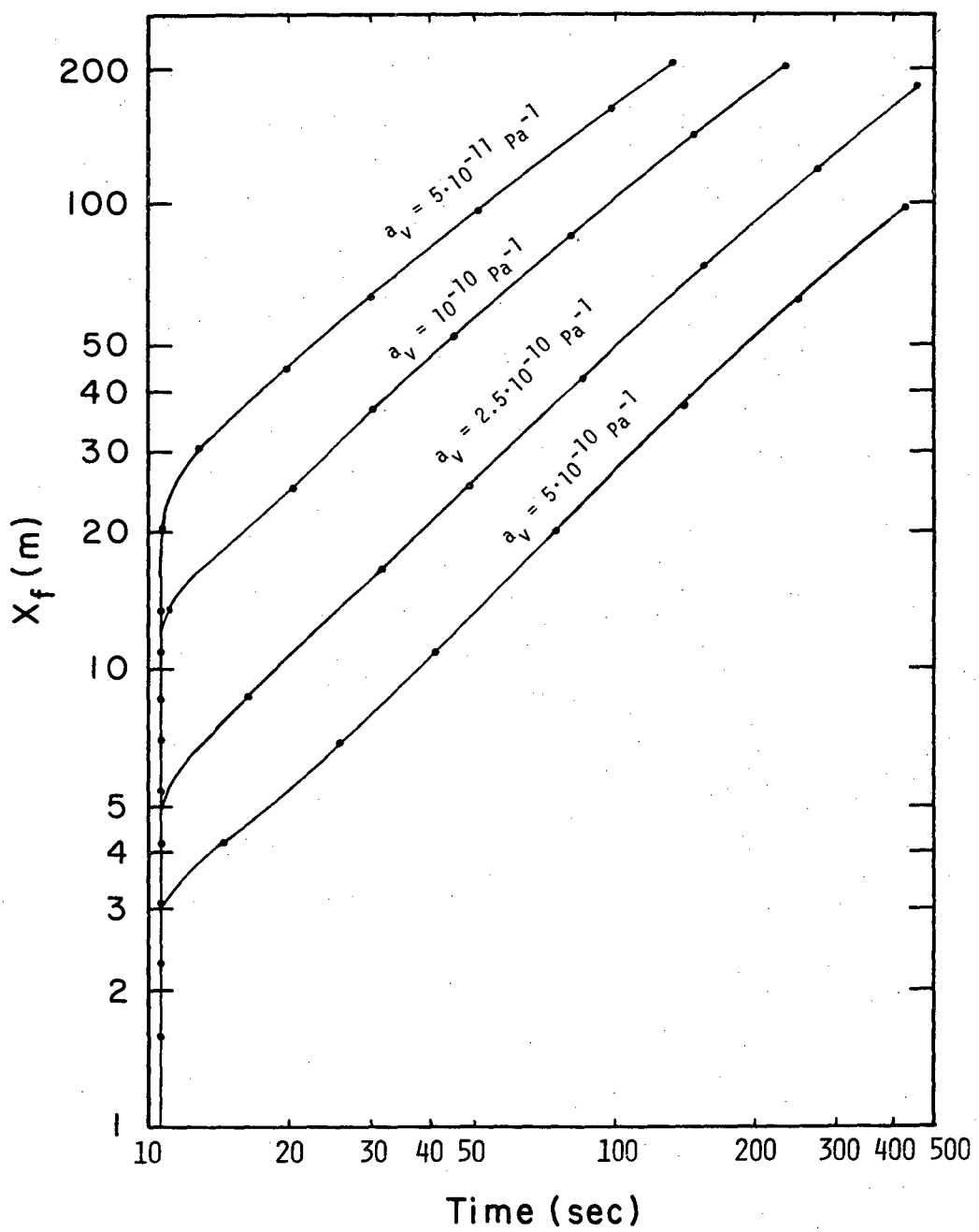

Figure 36b Log-log Plot of x_f vs. time, $Q = 8 \cdot 10^{-3}$ m^3/sec, $\mu = 2.34 \cdot 10^{-3}$ Pa-sec

time. This response agrees with Equations (13a) and (15b) which predict such a relationship for sufficiently large fractures. The slopes of the curves for simulations using larger values of fracture stiffness also decreased in magnitude but did not quite reach the square root relationship within the length of time allowed in the simulation. There is no reason to doubt that the slopes of these lines would approach a value of 0.5 after some greater fracture length (> 200 m) is reached. While it appears that the slopes of the curves in Figures 36 a,b are parallel the slope does increase with an increases in a_v. This might indicate that the valid range of the analytic approximations begins after larger elapsed times when the fracture stiffness coefficient increases.

As the fracture stiffness coefficient is increased in the simulations, the curves in Figure 36 a,b indicate that the unstable fracture length decreases which is desirable for the control of vertical migration of the fracture. The fact that the unstable fracture length increases as a_v is decreased may indicate that if the fracture stiffness of the adjacent vertical formations is lower (stiffer) than that of the fractured formation, vertical growth might actually occur.

The maximum apertures for the simulations in Figures 36 a,b are directly proportional to the fracture pressure. This varies exactly as the pressure curves shown in Figure 34. Thus the apertures will have two maxima, one during the initial unstable fracture growth period, when the wellbore pressures are highest, and the other at the end of the simulation when the fracture pressure has started to rise. The aperture results are summarized in Table 4 for various values of a_v and fluid viscosity. The calculated apertures for the simulation conducted with $a_v = 5 \cdot 10^{-11}$ Pa^{-1} ranged between values of 2.3 - .75 mm, the former value representing the initial maximum aperture and the latter the aperture at the conclusion of

Table 4 Summary of Calculated Apertures for Rectangular Fractures

$a_v \cdot 10^{10}$ (Pa^{-1})	$\mu \cdot 1000$ (Pa-sec)	$Q = 4 \cdot 10^{-3}$ m^3/sec		$Q = 8 \cdot 10^{-3} m^3$/sec	
		w_{init}	w_{final} mm	w_{init}	w_{final} mm
0.5	2.34	2.2	0.7	2.3	.75
1.0	2.34	3.5	1.3	3.5	1.3
5.0	2.34	15	6.2	15	6.2
0.5	10	2.0	.85	2.2	.99
1.0	10	2.7	1.6	2.9	1.8
5.0	10	8.3	6.2	8.2	6.2
0.5	100	3.1	1.43	3.8	1.7
1.0	100	4.0	1.8	4.7	2.1
5.0	100	7.2	6.2	7.2	6.2
0.5	1000	2.0	2.5	2.2	3.0
1.0	1000	2.7	3.1	2.9	3.65
5.0	1000	6.3	6.5	6.3	6.7

the simulation.

The increase of fracture width with time was less the one-eighth power slope predicted by Equation (15a) or by Equations (12a) and (16). This could be the result of the fracture lengths, even at 200 m, being too short to allow comparison with the analytical expressions. This lack of agreement could also result from the formulation of the model which allows w_{max} to increase only with an increase in the fracture pressure. As the fracture stiffness coefficient increases so does the maximum aperture. The maximum apertures for the $a_v = 10^{-10}$ Pa^{-1} simulation ranged between 3.5 - 1.3 mm and for an $a_v = 5 \cdot 10^{-10}$ Pa^{-1} the maximum apertures varied between 14.7 - 6.0 mm. These values are within the range expected in MHF operations.

Comparison of Figure 36a and Figure 36b indicates the effect of changing the flow rate of the system by a factor of two. While direct comparison of the two figures is difficult since the data are not presented in terms of dimensionless time, it is easy to see from the example presented in Table 5 for the $a_v = 2.5 \cdot 10^{-10}$ Pa^{-1} simulation that doubling the flow rate increases the overall growth rate by a factor of slightly more than two. This near linear response of the fracture length with the pumping rate is in agreement with Equations (13a) and (15b). The values in the table present the times required to reach different values of x_f with variation in viscosity and pumping rate. The fact that the time required to reach a given value of fracture length is reduced by a factor slightly less than two when the viscosity is low, is a result of proportionally more fluid seeping into the formation as the residence time of the fluid increases with the lower flow rate. Also note that the initial length of the unstable fracture growth, as seen by comparing the two previous figures, does not increase as the flow rate is doubled. This again indicates that the unstable fracture length is related

Table 5 Fracture Growth vs Time Calculations, $a_v = 2.5 \cdot 10^{-10}\ Pa^{-1}$

	$Q = 4 \cdot 10^{-3}\ m^3/sec$			$Q = 8 \cdot /10^{-3}\ m^3/sec$		
	$\mu \cdot 1000$ Pa-sec			$\mu \cdot 1000$ Pa-sec		
	2.34	10	100	2.34	10	100
x_f (m)	time (sec)					
5	21	23	48	10.5	13.5	33
10	38	38	48.5	19	19	33.5
20	81	78	78	40	39	38
40	160	150	145	78	77	76
60	260	245	230	125	120	115
100	460	440	420	220	213	207
150	-	-	650	350	340	330

to the release of stored energy contained in the wellbore tubing.

The Effects of Viscosity

Other sets of simulation results are presented in Figures 37 a,b for viscosity of .01 Pa-sec (10 cp) and Figures 38 a,b for viscosity of 0.1 Pa-sec (100 cp). In general the behavior of the systems at any one of these values of viscosity is similar to those discussed above. That is, as the fracture stiffness decreases, the length of the unstable fracture is reduced as is the overall growth rate. However, comparing the effects of the different viscosities indicates that as the fluid viscosity increases from $2.35 \cdot 10^{-3}$ to 0.1 Pa-sec, the overall time required to reach a certain fracture length is only slightly changed. For the example in Table 5 to reach a fracture half-length of 100 m for the case of the lower flow rate of $4 \cdot 10^{-3}$ m^3/sec, it takes 460 sec, 440 sec, and 420 sec as the viscosity changes by nearly two orders of magnitude. The final fracture length would seem to be a weak function of the fluid viscosity. Interestingly, the analytical approximation values are independent of viscosity.

The effect of viscosity on fracture width is seen in increasing the w_{max} of the fractures as shown in Table 4. This is an effect of the greater viscosity creating a larger pressure drop in the fracture. Since the pressure at the tip of the fracture is always near S_h during stable fracture growth, as the viscosity increases so does the wellbore pressures and thus the maximum fracture apertures. For example the simulation run with an $a_v = 10^{-11}$ Pa $^{-1}$ indicates that w_{max} at the end of the simulations increases from 1.3 mm to 1.6 mm when the viscosity increases from .00234 to 0.1 Pa-sec. The fracture aperture also increases with pumping rate as the viscosity increases. For a 0.1 Pa-sec viscosity fluid and fracture stiffness of 10^{-10} Pa^{-1} the range of fracture apertures increases from 4.0 - 1.8 mm to 4.6 - 2.1 mm when the flow rate

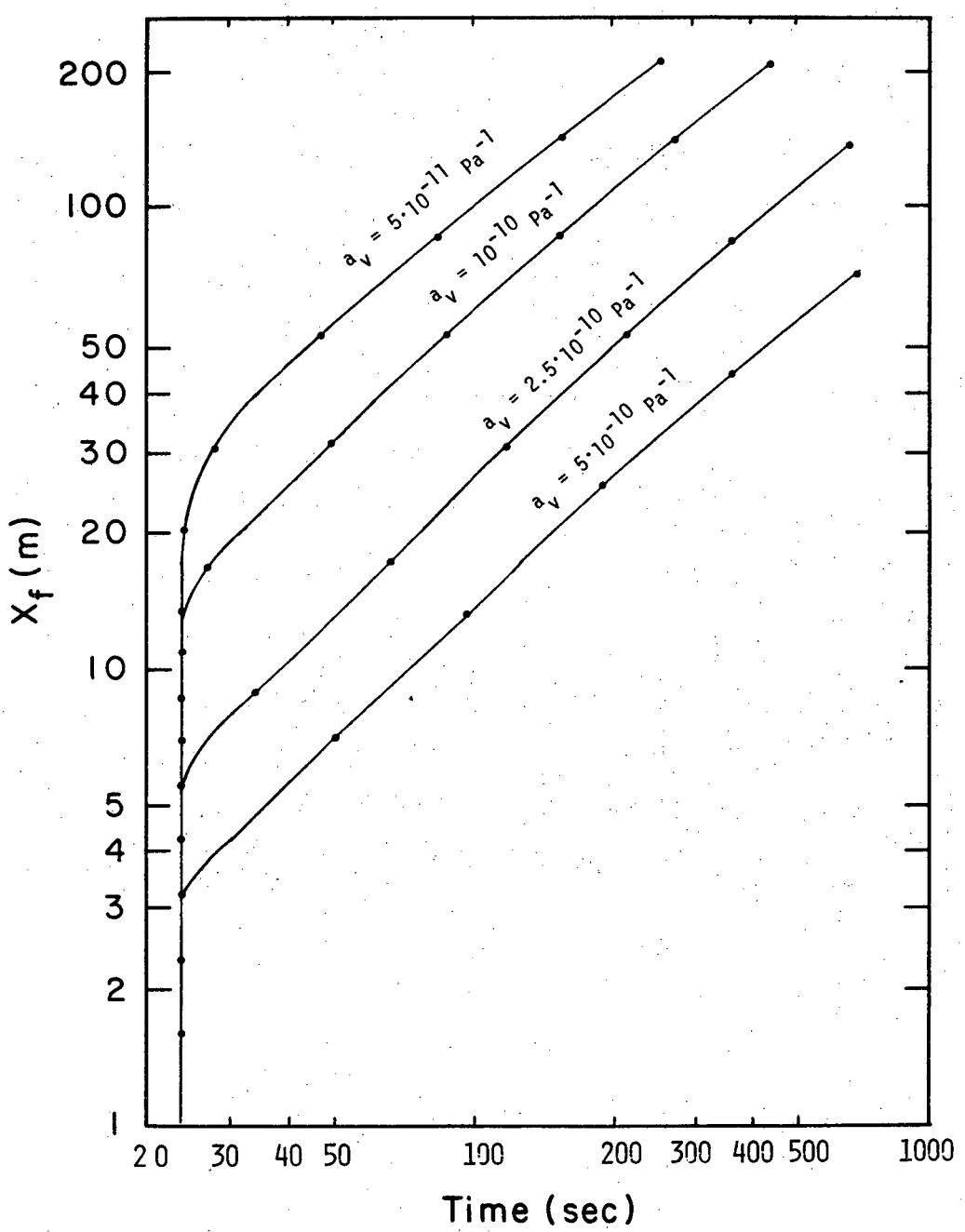

Figure 37a Log-log Plot of x_f vs. time, $Q = 4 \cdot 10^{-3}$ m^3/sec, μ = .01 Pa-sec

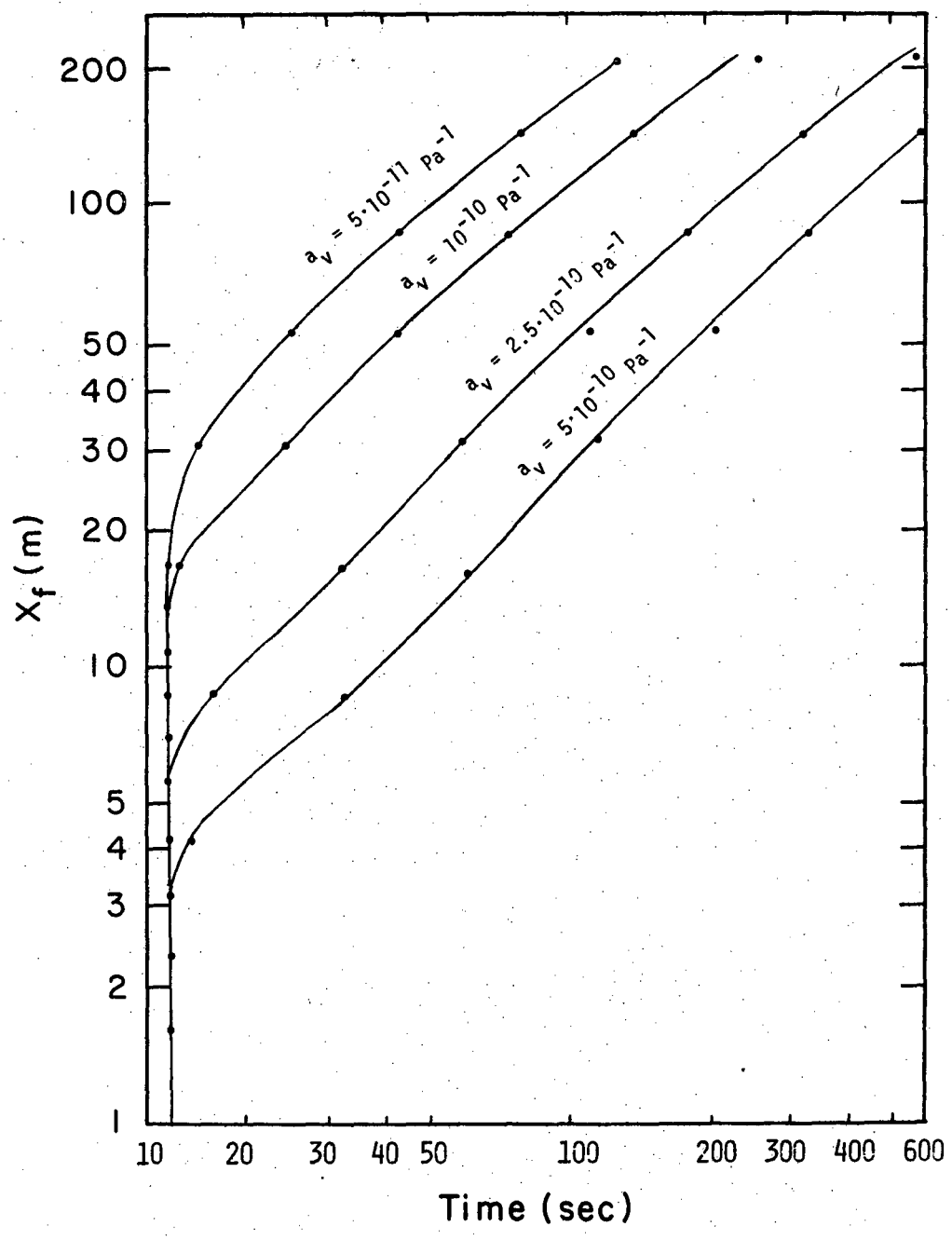

Figure 37b Log-log Plot of x_f vs. time, $Q = 8 \cdot 10^{-3}$ m^3/sec, μ = .01 Pa-sec

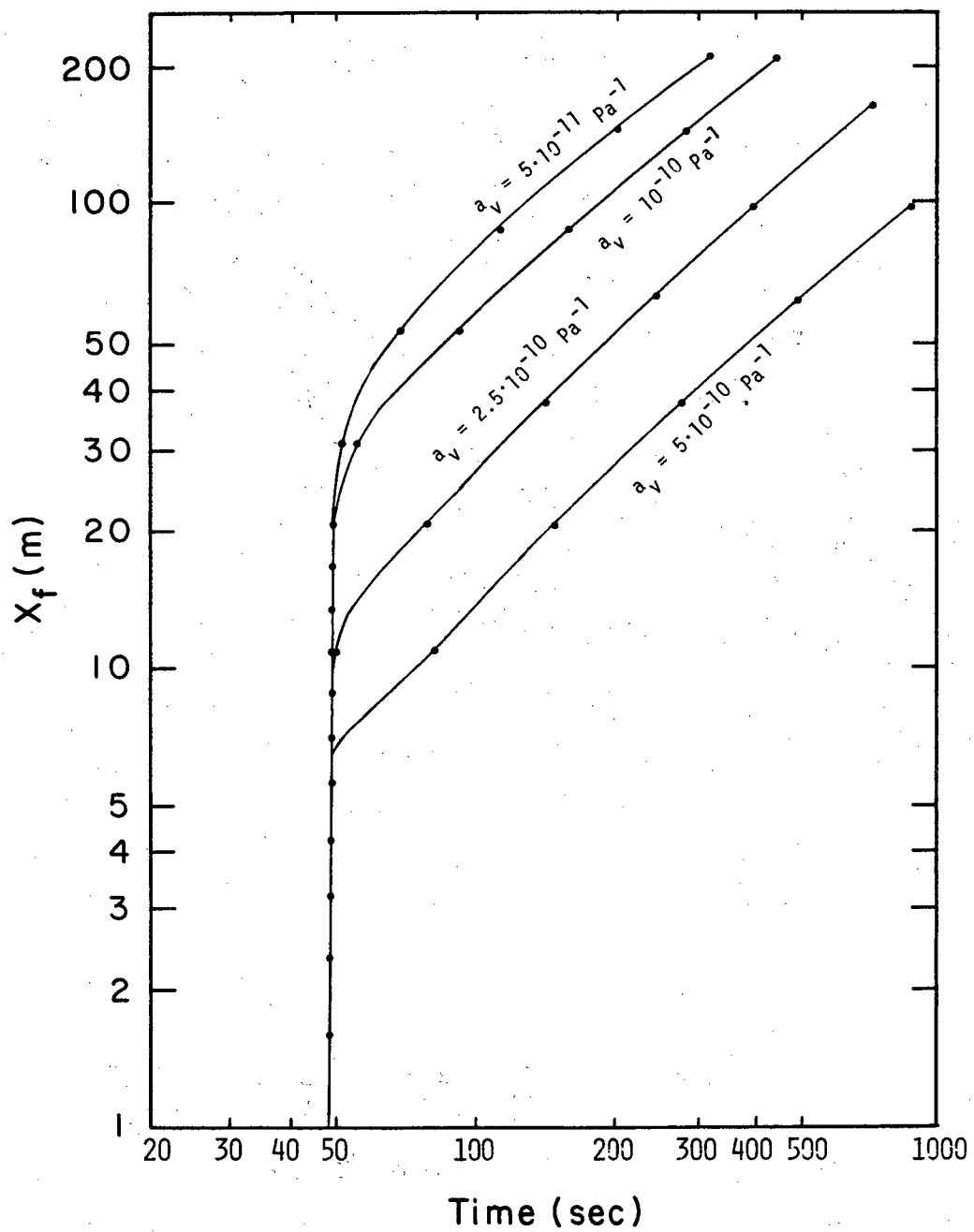

Figure 38a Log-log Plot of x_f vs. time, $Q = 4 \cdot 10^{-3}$ m^3/sec, $\mu = 0.1$ Pa-sec

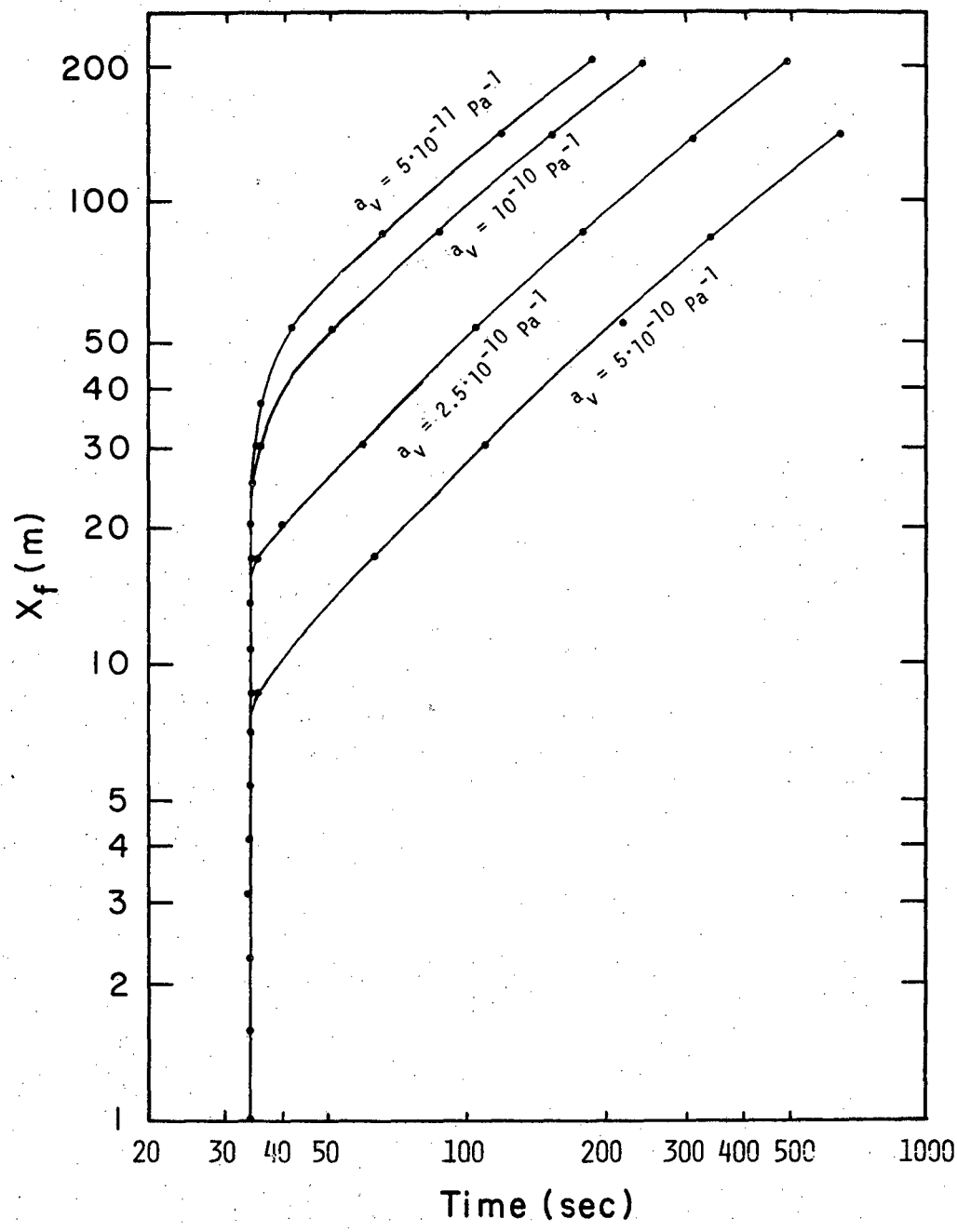

Figure 38b Log-log Plot of x_f vs. time, $Q = 8 \cdot 10^{-3}$ m^3/sec
$\mu = 0.1$ Pa-sec

is doubled. This increase is near that predicted by Equation (12a) which shows the increase in w_{max} is proportional to $Q^{1/4}$ but is below that predicted by Equation (16) which predicts a linear change in width with change in flow rate.

The aperture for the stiffer fractures increases with the viscosity increase to a much greater degree than does the apertures for the value $a_v = 5 \cdot 10^{-10}$ Pa^{-1}. The calculated w_{max} values for these latter simulations are only slightly dependent on the pumping rate. As can be calculated from the data in Table 4 there is a 3% increase in the maxixmum apertures for an $a_v = 5 \cdot 10^{-5}$ Pa^{-1} as the flow rate is doubled, and then only at a viscosity of 1.0 Pa-sec.

As the fluid viscosity increases to a value of 0.1 Pa-sec the effect of leakage in the system is reduced. A twofold increase in flow rate at this viscosity corresponds much closer to a twofold decrease in the time needed to reach a specfic fracture length for any given fracture stiffness. For example from Table 5 at a viscosity of 0.1 Pa-sec the time required to reach a 100 m length decreases from 420 seconds to 207 seconds as the flow rate was doubled. As the viscosity increases the amount of fluid lost from the system is naturally reduced and the growth rate becomes less sensitive to the leakage. If the permeability of the formation was increased the effects of the leakage should become more apparent.

The slopes of the x_f vs time curves also increases slightly with viscosity, indicating that the fracture growth becomes stable ealier in the simulation. The slopes of the curves will be somewhat higher since the results at the end of the simulations are relatively independent of viscosity, but the data departed from the vertical (unstable) portion of the curves at shorter distances requiring an increase in the overall slope.

Super Frac Simulations

The use of 'super frac' fluids with viscosities > 100 cp has been treated in the literature review chapter. The simulations conducted for these systems used a viscosity of 1.0 Pa-sec (1000 cp) and are treated somewhat differently than for the previous simulations. The origin of the time scale for the previous simulations represents the point of fracture extension of the second element and not the time when the first element is opened, which is the fracture initiation time. The time lag between the initiation and extension times was so great during the the 1.0 Pa-sec simulations that the initial aperature e_0 was increased by a factor of ten to prevent needless waste of computer time. Thus while the time origins on the previous figures increased with viscosity, the time origin appears lower for the 1.0 Pa-sec simulations shown in Figures 39 a,b. As can be seen from these figures the unstable length is not clearly distinguished from the stable growth range. This indicates that the release of energy from the wellbore volume is affected by the viscosity of the fluid. This effect of viscosity could be used to help control the unstable fracture growth. However, like the concept of reducing the tubing size, the horsepower requirements for the surface pumps would be excessive. The use of this high viscosity fluid also results in a large pressure gradient in the fracture. This is apparent in that the wellbore pressures and apertures increase with time. This latter observation can be noted in Table 5 where the apertures at 1.0 Pa-sec increase by as much as 40% over the time of the simulation for the lower values of a_v.

It is also interesting to note that the fracture aperture for the stiffest (lowest a_v) simulations increase 400% over the total range of viscosities (.00234 to 1.0 Pa-sec) although w_{max} for the most resilient fracture increases by only 8%. This would tend to support the need for

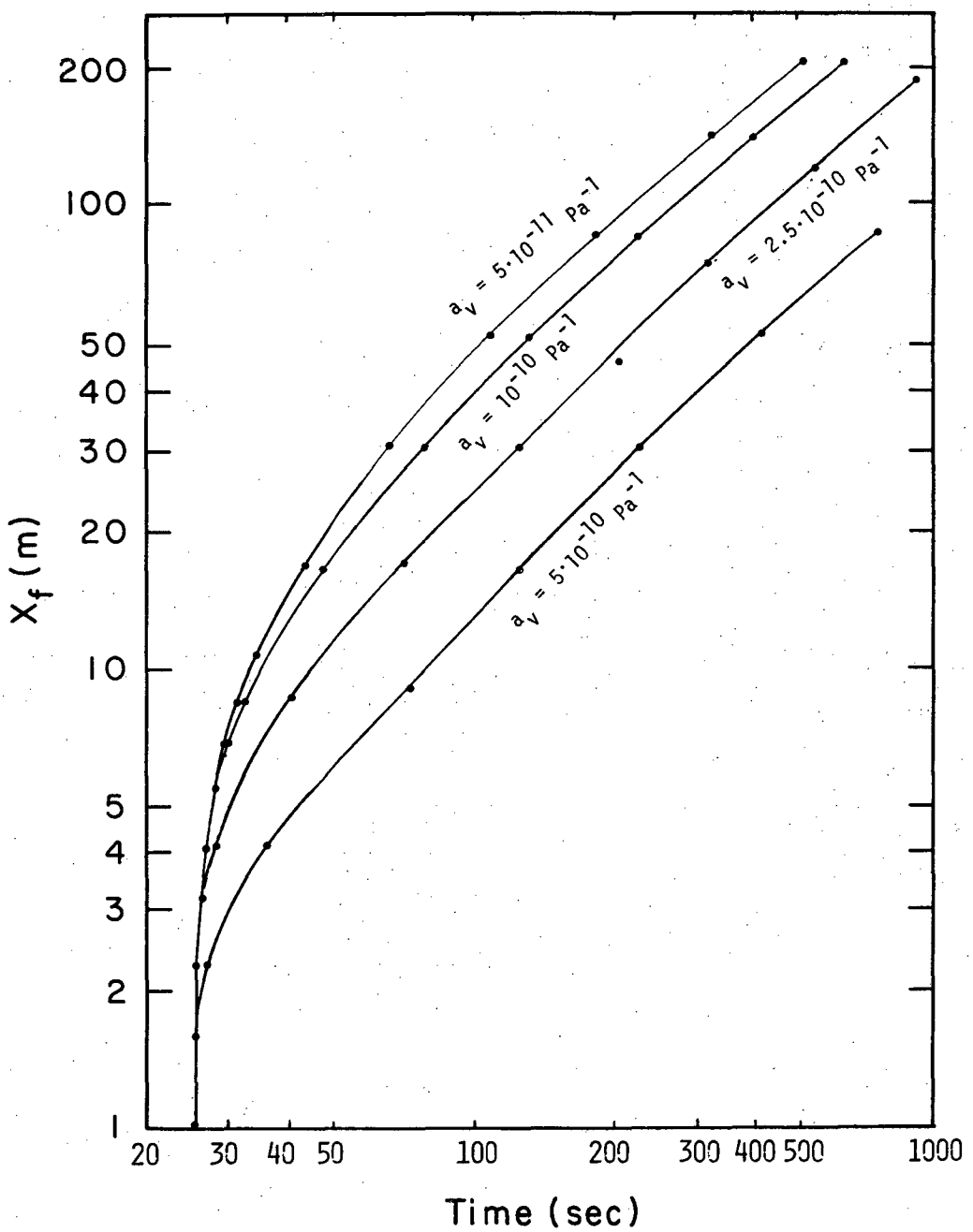

Figure 39a Log-log Plot of x_f vs. time, $Q = 4 \cdot 10^{-3}$ m^3/sec, $\mu = 1.0$ Pa-sec

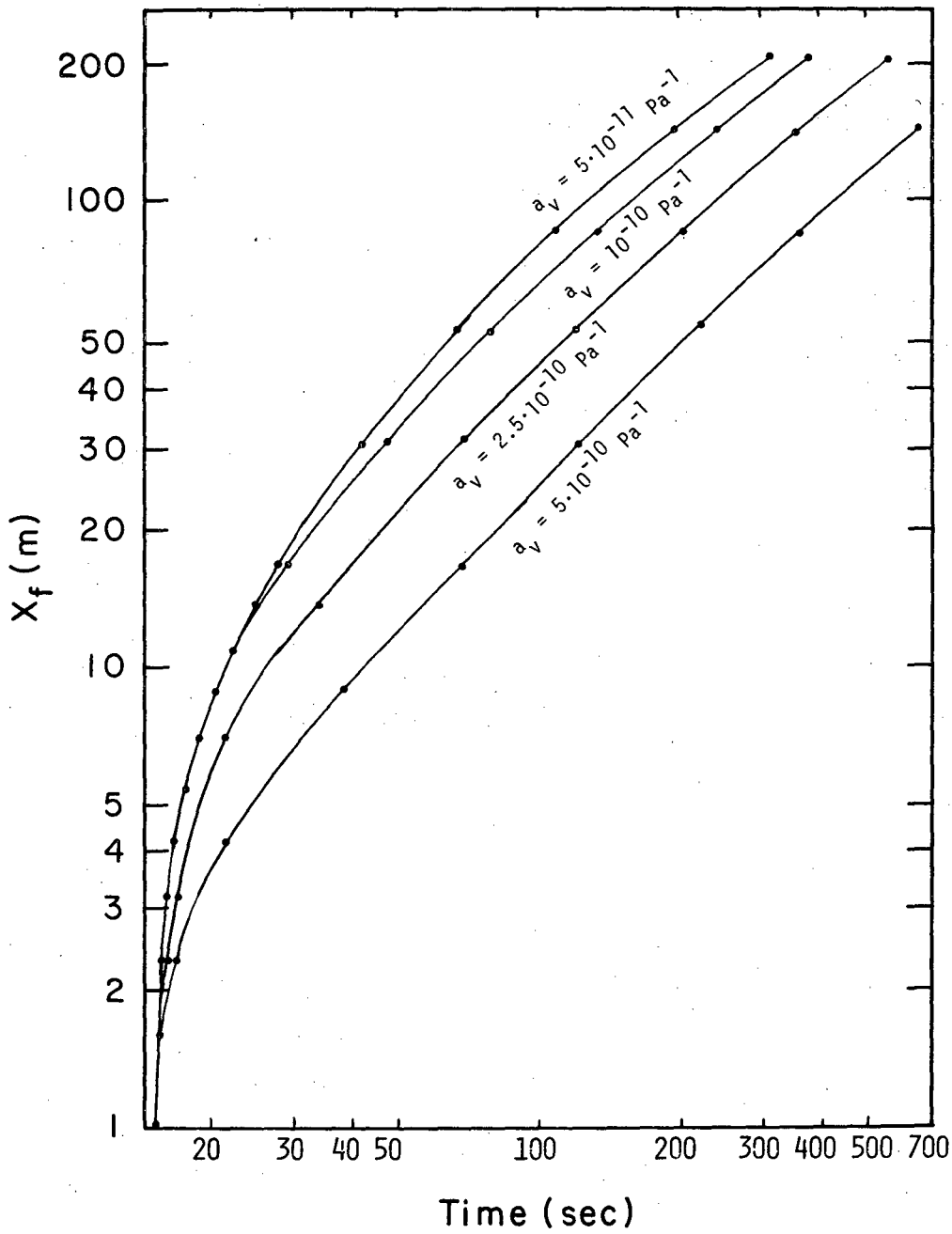

Figure 39b Log-log Plot of x_f vs. time, $Q = 8 \cdot 10^{-3}$ m^3/sec, $\mu = 1.0$ Pa-sec

inclusion of a shear modulus in the approximate solutions presented for the estimation of the fracture width since the aperture must be a function of the elastic properties of the system. However, while the fracture length has also been seen to depend on the fracture stiffness, it is interesting to note that only Nordgren (1972) includes any rock properties in the equation for the calculation of fracture length.

Fracture Control : Variation in Flow Rate

The last parameter studied in regards to its effect on fracture growth was variation in the flow rate. Figures 40 a,b present the effects of five different flow rates on the log-log plots of x_f vs time for two different fracture stiffnesses. Two of the flow rates can be visualized as ramp functions, one monotonically increasing with time, the other linearly decreasing with time from an initial peak value. The total volume injected in these latter cases is equivalent to the volume injected with a constant rate of $8 \cdot 10^{-3}$ m^3/sec over the 650 seconds of the simulation. This constant rate case is also presented for comparison. Figure 40a shows that regardless of the surface pumping rate the unstable fracture length is similar for these three cases, in the range of 20-25 m. Note that these three curves indicate possible convergence at a length greater than that allowed for the simulations. This would indicate that the final fracture dimensions are a function of the total volume injected and are insensitive to the rate of injection. This convergence is slightly better defined in Figure 40b for a more resilient fracture system. However, it appears that while the ultimate length of these three constant volume simulations might be the same, the unstable fracture length calculated using the growing rate function is only half as long as the unstable fracture lengths of the other two cases, i.e. 5m for the former and 10 m for the latter, as seen in Figure 40 b. This indicates the possibility that

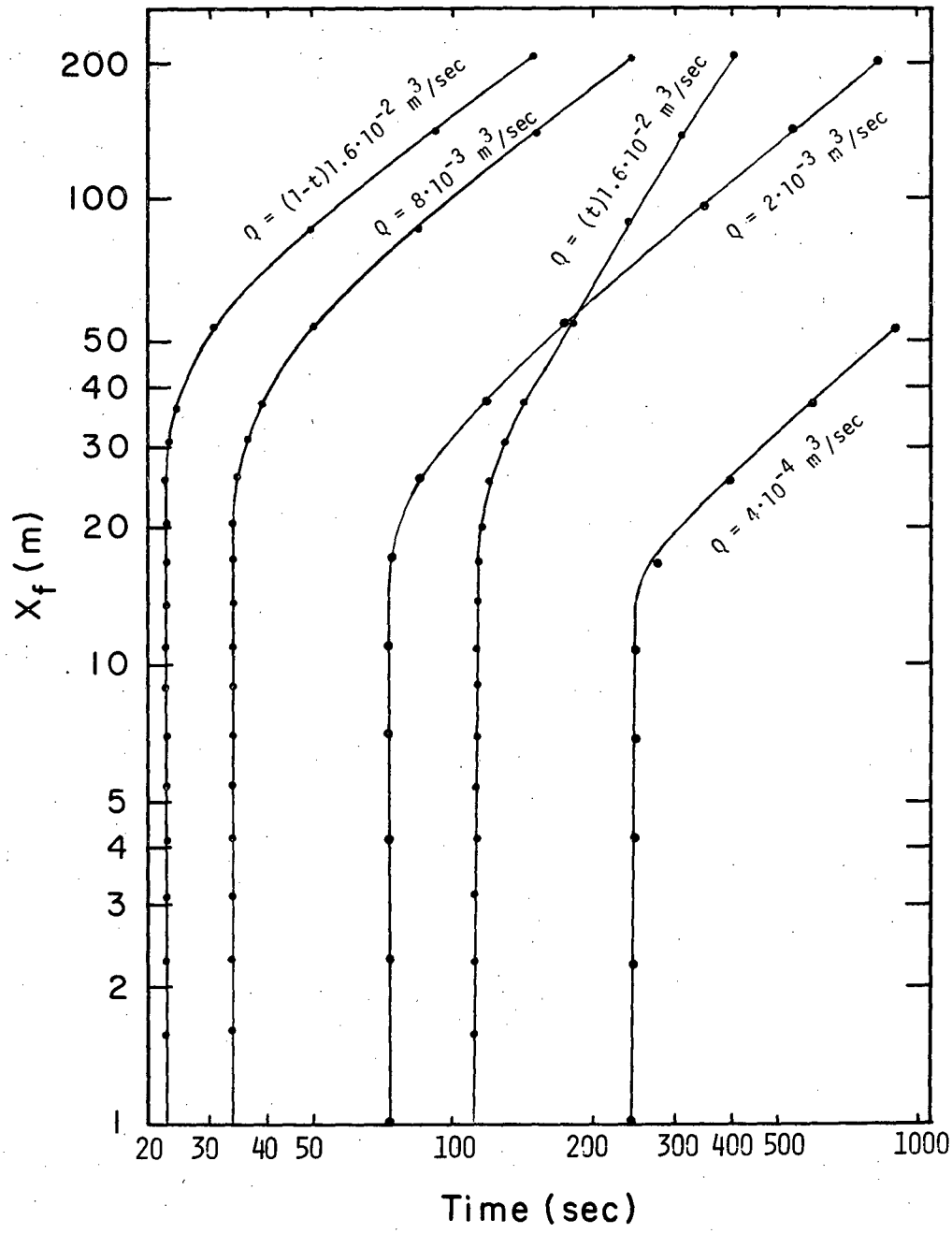

Figure 40a Log-log Plot of x_f vs. time, variable flow rates, $a_v = 10^{-10}$ Pa^{-1}, $\mu = 0.1$ Pa-sec

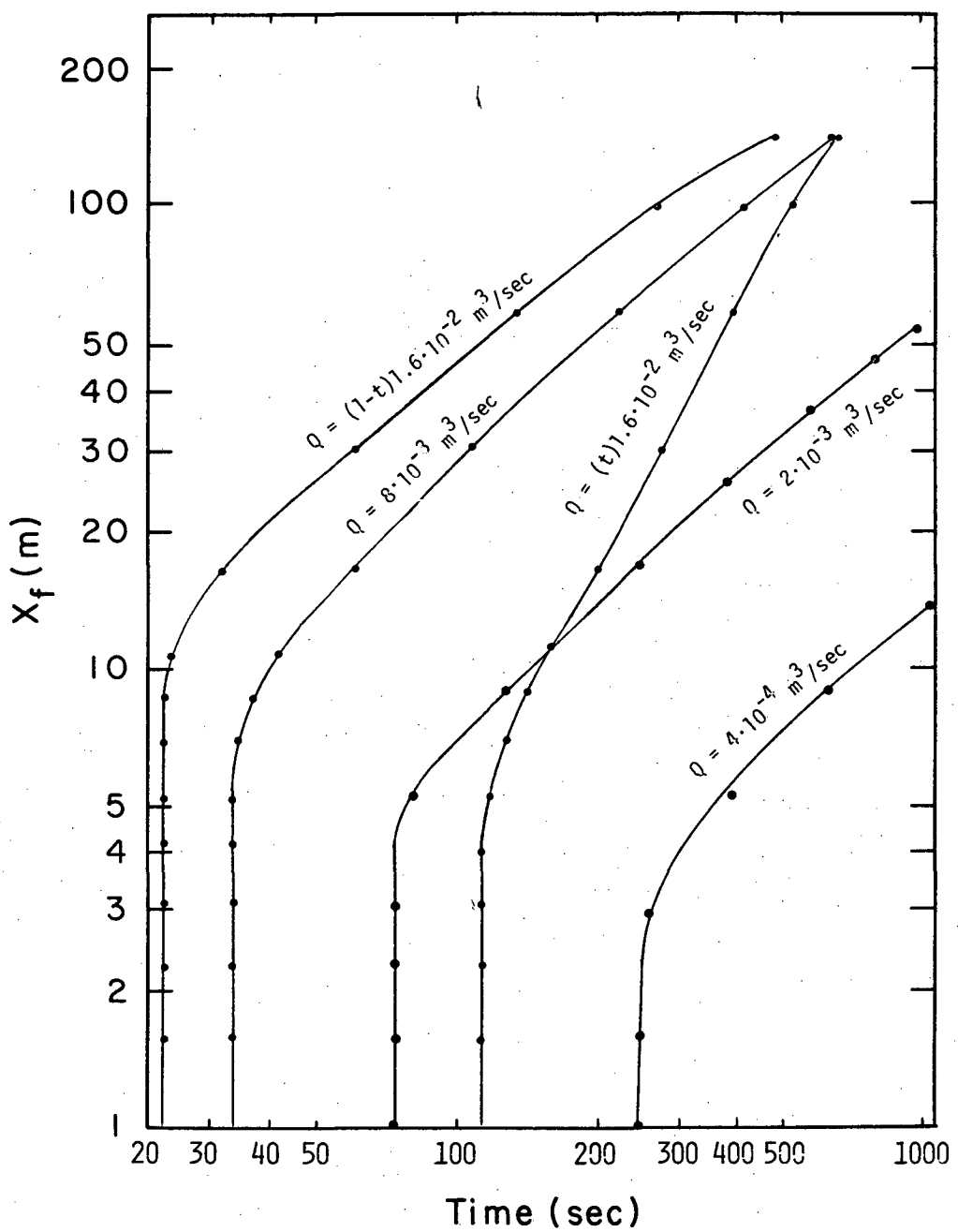

Figure 40b Log-log Plot of x_f vs. time, variable flow rates, $a_v = 5 \cdot 10^{-10}$ Pa^{-1}, $\mu = 0.1$ Pa-sec

another method may be employed to control the growth of the fracture in the vertical direction for more elastic formations. This would involve a slow pressurization rate of the wellbore so that any contribution from the pumps to the unstable fracture growth is minimized. The pumping volume would be increased only after the fracture growth becomes stable so that the energy supplied to the system may be more efficiently used in extending the vertical fracture in the horizontal direction.

The other two curves of Figures 40 a,b are for minimal flow rates, one-tenth those used for the previous simulations in Figures 36 - 39. These curves indicate that there is some contribution from the surface pumps during the unstable fracture growth as their unstable lengths of 3 - 10 m are the lowest of any of the simulations. However, the use of these minimal flow rates may also permit the effects of fluid leakoff to affect the fracture growth and result in a loss of fracturing efficiency.

Summary of the Rectangular Hydraulic Fracture Simulations

This section has dealt with hydraulic fracture simulation and the factors that control unstable fracture growth. These factors affect the storage of compressible energy in the wellbore tubing before the onset of fracture breakdown and include the fluid compressibility, the tubing volume, and the pumping rate. The values of fracture length and aperture calculated with the analytic approximations were compared with the simulation results. However, the restriction that the fracture length be much larger than the fracture height restricts the use of these values to fracture half-lengths greater than 250 meters, which is the maximum practical length used in the present form of the model. The analytical calculations may be useful for estimating limiting values of the fracture geometry, but only during stable fracture growth. Nordgren (1972) presents an expression for the rate of fracture growth at small fracture lengths that agrees with the

results of this study, but these values are also limited to stable fracture growth. All the analytical treatments have assumed that the vertical growth of the fracture will be contained within the reservoir rock formation. However, this assumption may be inaccurate if the adjacent vertical formations are thin and conditions favor a large period of unstable fracture growth.

The calculated fracture length is seen to depend directly in the pumping rate and be relatively independent of the fluid viscosity as long as fluid seepage is minimal. The fracture length does depend inversely on the value of fracture stiffness but the fracture aperture increases as the value of a_v increases. While the simulations presented in this section were designed to explore the use of the model in predicting realistic hydraulic fracture behavior the model could be improved for use as a field simulator. These improvements are beyond the present scope of this work and will be covered in the next section.

Future Work

The formulation of the present model employs a one-dimensional approach to calculate the fracture deformation. Realisticall, a two or three-dimensional approach should be used in treating the fracture mechanics. The incorporation of the two or three-dimensional stress calculation is not trivial and may be best accomplished by re-formulating the IFDM framework or by expanding the calculations to take into account simultaneous solution of both the equation of mass conservation and the stress-strain tensor. This would necessitate greater array storage space. The array dimensions would also need to be enlarged to permit a greater number of fracture elements.

The increase in well depths and geothermal applications would require that the model be modified to include heat transfer and thermal effects.

These thermal effects include temperture dependent properties and development of an excess surface energy calculation that would include energy exchange when the fluid temperature changes and/or the rock contracts when cooled by pad fluids. A computer code, CCC (Bodvarsson, et al., 1979), presently uses the IFDM formulation to solve problems of non-isothermal fluid flow in porous media. This program could be adapted for modeling the non-isothermal hydraulic fracturing process by incorporating the modifications made in program HYDFR, but this would involve substantial effort.

A provision could be made in the present model to study vertical growth of the fracture in multi-layered systems. This would involve the use of a predesigned mesh with different formation properties, S_h, a_v, k, etc., in each layer. The direction of fracture growth could be calculated on a least energy principle, that is, the fracture growth would be in the direction that maximizes the SURGY term. The complex fracture mesh needed in the study could be used in conjunction with only a few layers of reservoir elements, to minimize computational time, since the small time needed for the initial fracture growth would restrict the fluid seepage from the fracture faces.

Proppants could be modeled in the fracture by specifying a minimum aperture the fracture walls would return to after the initial breakdown period, when the fracture aperture is at a relative maximum. This value would have to come from laboratory measurements and would require modifying the excess surface energy calculation.

While any of the above modifications would improve the present model, it is still flexible enough to simulate or analyse a wide range of fracture stimulations if the formation properties of fracture stiffness and surface energy requirement are known. Future work should also entail developing techniques for measuring these properties.

V. SUMMARY AND CONCLUSIONS

The process of hydraulic fracturing is important in many Earth Science related fields including: petroleum reservoir stimulation, geothermal energy extraction, in-situ coal gasification, and in-situ measurement of tectonic stresses. A literature review has revealed a better need for understanding the relationship between pore-fluid pressure, fluid flow, and the propagation of a hydraulic fracture. This understanding is at least partially derived from a pressure transient analysis of the fracture-reservoir system. A concept is developed that explains the hydraulic fracturing process in terms of the transmission of energy supplied by the surface pumps to pressurizing the fracture system, and to create new fracture surface. The process involves a complex relationship between the earth stress, S_h, the formation permeability, k, the stiffness or resiliency of the fracture, a_v, the initial aperture of the fracture, e_o, and the specific surface energy coefficient, γ. The parameters are interrelated through a highly non-linear partial differential equation which neccesitates a numerical approach for its solution.

A numerical approach, involving modification of the IFDM computer code TERZAGI, is first introduced and applied to the analysis of pressure transients in a well intercepting a single vertical fracture. The model uses a cubic law relating fracture aperture to permeability.

The method has been validated against known analytical solutions and has been used to investigate the effects that possible field conditions may have on well test data. Results indicate that the usefulness of the dimensionless fracture conductivity parameter, C_r, in the utilization of type curve analysis is severely restricted when any one of a

combination of factors may vary. These include wellbore storage, fracture storage, fracture damage in the form of a fracture skin or restricted fracture flow capacity, asymmetric fracture geometry, or deformable proppant-fracture systems.

The model has been extended by the use of a modified Griffith crack energy approach and a self-generating mesh to represent the growth of a hydraulic fracture as a series of discrete macroscopic extensions. The resultant computer program HYDFR has been developed for application to the analysis of pressure transients recorded during the hydraulic fracturing process.

The model used for circular fracture extension successfully matched data from field experiments involving repeated mini-fracture operations conducted in the Monticello field in South Carolina. These experiments were conducted by the US Geological Survey to measure in-situ tectonic stresses in seismically active region.

Analysis of the mini-fracture data indicate that the parameters determined through 'best fit' choices agree well with data available in the literature. The 'best fit' choice of parameters is so interrelated, however, that these values cannot be uniquely determined and should only be used to estimate representative properties of the system. These parameters include: the mimimum earth stress, S_h, the fracture stiffness coefficient a_v, the surface energy requirement, γ, the in-situ rock permeability, k, and the initial fracture opening, e_o.

The use of a mesh acceleration factor, ε, allowed a model for rectangular fracture extension to be used successfully in the simulation of the massive hydraulic fracturing process. In these simulations fracture half-lengths exceeded 200 m and maximum fracture apertures ranged between 0.7 - 6.7 mm, depending on the value of a_v.

Results from the MHF simulations indicate that it is possible that the initial fracture growth may be unstable and violent enough to penetrate into adjacent formations above and below. This effect may be mitigated by the use of lower or variable pumping rates, higher fluid viscosity, and reducing the initial internal energy of the system by the use of lower compressibility pad fluids such as water or the use of smaller wellbore tubing.

Results from the simulation indicate that after the initial unstable period, characterized by rapid wellbore depressurization during the fracture growth, the growth becomes stable. This stable growth is characterized by a gradually increasing or constant wellbore pressure. However, the possibility exists that for larger values of fracture stiffness coefficient and lower values of fluid viscosity the fracture may extend in a quasi-stable fashion with repeated periods of rapid growth combined with periods of relative inactivity.

Analysis of the rate of the fracture growth has been compared with approximations derived for extremely long fractures. The numerically calculated rate of the fracture growth is slightly larger than the analytical approximations and approachs a $t^{1/2}$ relationship only at fracture lengths exceeding 250 m. The calculated values of fracture aperture do not agree as well with the earlier approximations. This may be due to the restriction of the one-dimensional fracture wall deformation used in the model.

The analytical assumptions of a constant fracture extension pressure do not hold for the use of extremely viscous fracturing fluids (> 1.0 Pa-sec). The pressure in the fracture will increase with time, for a constant pumping rate, independent of the value of the fracture stiffness at large values of fluid viscosity.

VI. NOMENCLATURE

a	is a constant = $1 - C_r/C_b$, also a microscopic crack length (L)
a_v	is the fracture stiffness (LT^2/M)
$a_{l,m}$	are elements in the conductance matrix $\overline{A_{l,m}}$ (L/T)
A	is the surface area of the fracture (L^2)
$A_{l,m}$	is the interfacial area beween elements l and m (L^2)
$\overline{A_{l,m}}$	is the matrix of conductance terms relating the amount of fluid flow from the elements with unit change in fluid potential (1)
ΔA_{fi}	is the area of each fracture element (L^2)
c	is the wellbore storage coefficient equal to the amount of fluid stored per unit height of the wellbore (L^2)
c_t	refers to the total compressibility of the formation (LT^2/M)
C	is the fluid loss coefficient, constant of integration ($L/T^{1/2}$)
C_r, C_b	are the matrix, bulk rock compressibilities (LT^2/M)
$D_{l,m}$	is the normal separation distance beween the interface $A_{l,m}$ and node l and is also expressed as $d_{l,m}$ (L)
D	is the mean depth to the formation (L)
e	is the void ratio, also the fracture aperture used in strain energy calculations (1), (L)
e_o	is the initial fracture aperture (L)
e_o'	is the minimum fracture aperture after closure (L)
E	is the Young's modulus (LT^2/M)
F_f	is a constant (1)
g	is the acceleration of gravity (L/T^2)
G	is the formation shear modulus (LT^2/M)
h	is the formation or fracture height or thickness (L)
h_e	is the effective fracture height (L)
k	is the rock permeability, spring constant (L^2), (M/T^2)
k'	is an equivalent spring constant for a fracture (M/T^2)
k_f	is the fracture permeability (L^2)

K_s is the skin permeability (L^2)

K_C is the fracture toughness constant (M/LT^2)

K_I is the stress intensity factor for Mode I behavior (M/LT^2)

L is the instantaneous fracture length (L)

$\overline{MC_l}$ is the mass capacity matrix (1)

$\tilde{n}$ is the unit vector normal to the fracture surface (1)

P is the fluid pressure (M/LT^2)

P_b is the breakdown pressure for impermeable or slightly permeable rock (M/LT^2)

P_l is the pressure at any time in node l (M/LT^2)

P_e is the static reservoir pressure, pore pressure in the fracture at a void ratio e (M/LT^2)

P_o, P_p is the initial pore pressure in the formation (M/LT^2)

P_{ext} is the minimum fracture pressure required for extension (M/LT^2)

$\overline{P_{ext}}$ is the static equivalent pressure acting in the fracture during extension (M/LT^2)

P_{ws}, P_{wf} are the shut-in, flowing well pressures (M/LT^2)

P_b^p is the breakdown pressure for a very permeable rock (M/LT^2)

$\tilde{P}_l$ is the vector containing the pressures of the l nodal elements (M/LT^2)

q, q_1 is the fluid seepage rate into the formation, production rate (L^3/T)

Q, Q_1 is the surface injection rate (L^3/T)

r is the pipe radius (L)

r_e is the radius of the outer reservoir boundary (L)

r_f is the fracture radius for a vertical penny-shaped fracture (L)

r_w is the wellbore radius (L)

r_{we} is the effective wellbore radius (L)

$\tilde{r}$ is the unit vector in the direction normal to the wellbore axis (L)

Δr is the incremental fracture radius of each fracture element (L)

R is the instantaneous fracture radius (L)

R is the instantaneous fracture radius (L)

S_h is the minimum horizontal earth stress (M/LT^2)

S_H is the maximum horizontal earth stress (M/LT^2)

S_V is the vertical stress due to the weight of the overburden (M/LT^2)

S_l is the volumetric generation term in node l (M/LT^2)

$\tilde{S}_l$ is the vector containing the generation terms for the l nodal elements (1)

t is the time (T)

$\Delta t_{l,stable}$ is the size of the largest stable time step for element l (T)

T_{LA}, T_{LB} are time lags from an observation well before, after stimulation (T)

T_o is the formation tensile strength (M/LT^2)

T_o^v is the formation tensile strength in the vertical direction (M/LT^2)

V is the wellbore volume (L^3)

V_f is the volume of the fracture (L^3)

V_l is the volume of nodal element l (L^3)

w is the fracture width (L)

w_f is the fracture width as a function of x_f (L)

w_s is the skin thickness (L)

w_{max} is the maximum fracture width (L)

W_e is the energy required for an incremental extension of the fracture (L)

W_s is the total system energy available for fracture extension (L)

x is the coordinate along the direction of fracture propagation (L)

x_{ch} is the length of the choked region in the fracture (L)

x_e is the characteristic dimension of a square drainage area (L)

x_f is the fracture half-length (L)

x_{fe} is the effective fracture half-length (L)

z_l is the elevation of node l (L)

Dimensionless Parameters

$\overline{C}$ is the dimensionless wellbore storage coefficient

C_r is the dimensionless fracture conductivity

P_{wD} is the dimensionless pressure

S_{fs} is the dimensionless fracture skin

T_D is the conventional dimensionless time

T_{Df} is the dimensionless time defined with x_f

Greek Letters

α_i are stress related coefficients (1)

β is the angle between the axis of the wellbore and the stress S_h, also the argument of the error function (1)

β_f is the fluid compressibility (LT^2/M)

γ is the surface energy coefficient (ML^2/T^2)

ε is the mesh extension factor (1)

θ is the angle between the directions of S_h and $\sigma_{\theta\theta}$ (1)

μ is the fluid viscosity (M/LT)

ν is the dynamic Poisson's ratio (1)

ρ is the density, also the radius of curvature (M/L^3), (L)

σ is the stress applied at the end of a sharp edged crack (M/LT^2)

σ_{max} is the maximum stress acting on a sharp edged crack (M/LT^2)

σ_θ is the tangential stress component at the wellbore face (M/LT^2)

$\sigma_{\theta\theta}, \sigma_{rr}, \sigma_{zz}$ are the principal stresses at the wellbore face (M/LT^2)

τ is the adiabatic surface of an arbritrary volume, also an angle (1)

ϕ is the porosity, angle between σ_θ and S_h (1)

Ψ is the fluid pressure potential

REFERENCES

Aamodt, R. L.; "Hydraulic Fracture Experiments in GT-1 and GT-2" report LA-6712, Los Alamos Scientific Laboratory, February 1977

Abé, H., Keer, L. M., and Mura, T.; "Theoretical Study of Hydraulically Fractured Penny-Shaped Cracks in Hot, Dry Rocks", Int. J. for Numerical and Analytical Methods in Geomechanics, (vol. 3, 1979) 79-96

Agarwal, R. G.; Carter, R. D.; and Pollock, C. B.; "Evaluation and Performance Prediction of Low-Permeability Gas Wells Stimulated by Massive Hydraulic Fracturing", J. Pet. Tech. (March, 1979) 362-372

Anderson, R. A., Ingram, D. S., and Zanier, A. M.; "Determining Fracture Pressure Gradients from Well Logs", J. Pet. Tech. (November, 1973) 1259-1268

Biot, M. A.; "General Solutions of the Equations of Elasticity and Consolidation for a Porous Media", J. Appl. Mech. (vol. 23, 1956) 91-96

Bodvarsson, G. S., Lippman, M. J., and Narasimhan, T. N.; "Recent Modifications of the Numerical Code CCC", Annual Report of the Earth Sciences Division, Lawrence Berkeley Laboratory 1979

Brace, W. F.; "Permeability of Crystalline and Argillaceous Rock: Status and Problems", submitted to Int. J. Rock Mech. and Min. Sci. August, 1979

Christman, S. A.; "Offshore Fracture Gradients", J. Pet. Tech. (August 1973) 910-914

Cinco-Ley, H., and Samaniego, F.; "Effect of Wellbore Storage and Damage on the Transient Behavior of Vertically Fractured Wells", SPE 6752 presented at the 52nd Annual SPE Fall Technical Conference, Denver, Colorado Oct. 9-12, 1977a

Cinco-Ley, H., and Samaniego, F.; "Determination of the Orientation of a Finite Conductivity Vertical Fracture by Transient Pressure Analysis", SPE 6750 presented at the 52nd Annual SPE Fall Technical Conference, Denver, Colorado Oct. 9-12, 1977b

Cinco-Ley, H., Samaniego, F., and Dominguez, A.; "Transient Pressure Behavior for a Well with a Finite Conductivity Vertical Fracture", Soc. Pet. Eng. J. (August, 1978) 253-264 .

Cleary, M. P.; "Rate and Structure Sensitivity in Hydraulic Fracturing of Fluid-Saturated Porous Formations", presented at the 20th U.S. Symposium on Rock Mechanics, Austin, Texas June 4-6, 1979

Cooke, C. E. Jr.; "Conductivity of Fracture Proppants in Multiple Layers", J. Pet. Tech. (September, 1973) 1101-1107

Cooke, C.E. Jr.; "Effect of Fracturing Fluids on Fracture Conductivity", J. Pet. Tech. (October, 1975) 1273-1282

Cornet, F.H.; "Comparitive Analysis by the Displacement-Discontinuity Method of Two Energy Criteria of Failure", J. Appl. Mech. (vol. 46, 1979) 349-355

Corten, H. T.; "Fracture Mechanics of Composites", chapter 9 vol. VII of Fracture edited by H. Leibovitz, Academic Press 1972

Coulter, G. R., and Wells, R. D.; "The Advantages of High Proppant Concentrations in Fracture Stimulation", J. Pet. Tech. (June, 1972) 643-650

Cummings, R. G., Morris, G. E., Tester, J. W., and Bivins, R. L.; "Mining Earth's Heat: Hot Dry Rock Geothermal Energy", Tech. Review (February, 1979) 58-78

Daneshy, A. A.; "Mechanics and Direction of Hydraulic Fracturing" Petroleum Engineer (October, 1973a) 17-20

Daneshy, A. A.; "A Study of Inclined Hydraulic Fractures", Soc. Pet. Eng. J. (April, 1973b) 61-68

Daneshy, A. A.; "Experimental Investigation of Hydraulic Fracturing Through Perforations", J. Pet. Tech. (October, 1973c) 1201-1206

Daneshy, A. A.; "On the Design of Vertical Hydraulic Fractures", J. Pet. Tech. (January, 1973d) 83-97

Dinsmoor, B., Galland, J. M., and Edgar, T. F.; "The Modeling of Cavity Formation During Underground Coal Gasification", J. Pet. Tech. (May, 1978) 695-704

Duff, I. S.: "MA28 - a Set of Fortran Subroutines for Sparse Unsymmetric Linear Equations", Harwell report AERE-R-87 (July, 1977)

Dusseault, M. B.; "A Conceptual Model for Hydraulic Fracture in the Athabasca Oil Sands", in print, University of Alberta 1979.

Edwards, A. L.; "TRUMP Computer Program: Calculation of Transient Laminar Flow in Porous Media," Rept. UCRL-50664, Lawrence Livermore Laboratory, California, 1969

Evers, J. F.; "Transient Tests and Long-Range Performance Predictions in Stress-Sensitive Gas Reservoirs", J. Pet. Tech. (August, 1977) 1025-1030

Fast, C. R., Holman, G. B., and Covlin, R. J.; "The Application of Massive Hydraulic Fracturing to the Tight Muddy "J" Formation, Wattenburg Field, Colorado", J. Pet. Tech. (January, 1977) 10-16

Felsenthal, M., and Ferrel, H. H.,;",Fracturing Gradients in Waterfloods of Low-Permeability, Partially Depleted Zones", J. Pet. Tech. (June, 1971) 727-730

Forman, S. E., and Secor, G. A.; "The Mechanis of Rock Failure Due to Water Jet Impingement", Soc. Pet. Eng. J. (February, 1974) 10-18

Free, D. L., Frederick, A. F., and Thompson, J. E.; "Fracturing With a High-Viscosity, Cross-Linked Gel — Continuous Fracturing Technique", J. Pet. Tech. (January, 1978) 119-122

Geertsma, J., and de Klerk, F.; "A Rapid Method of Predicting Width and Extent of Hydraulically Induced Fractures", J. Pet. Tech. (December, 1969) 1571-1581

Gidley, J. L., Mutti, D. H., Nierode, D. E., Kehn, D. M., and Muecke, T. W.; "Stimulation of Low-Permeability Gas Formations By Massive Hydraulic Fracturing — A Study of Well Performance", J. Pet. Tech. (April 1979) 525-531

Greenwald, R. F.; Volumetric Response of Porous Media to Pressure Variations, Ph.D. Dissertation, University of California, 1980

Gringarten, A. L., and Ramey, H. J.; "The Use of Green's Functions in Solving Unsteady-Flow Problems in Reservoirs", Soc. Pet. Eng. J. (October, 1973) 285-296

Gringarten, A. L., and Ramey, H. J.; "Unsteady-State Pressure Distributions Created by a Well with a Single Horizontal Fracture, Partial Penetration, or Restricted Entry", Soc. Pet. Eng. J. (August, 1974) 413-426

Gringarten, A. L., Ramey, H. J., and Raghavan, R.; "Unsteady-State Pressure Distributions Created by a Well With a Single Infinite Conductivity Vertical Fracture", Pet. Eng. J. (August, 1974) 347-360

Gringarten, A. L., Ramey, H. J., and Raghavan, R.; "Applied Pressure Analysis for Fractured Wells", J. Pet. Tech. (July, 1975) 887-892

Haimson, B., and Fairhurst, C.; "Hydraulic Fracturing in Porous-Permeable Materials", J. Pet. Tech. (July, 1969) 811-817

Haimson, B., and Fairhurst, C.; "In-Situ Stress Determination at Great Depth by Means of Hydraulic Fracturing", Published in Rock Mechanics-Theory and Practice : proceedings of the eleventh symposium on rock mechanics, conducted at the University of California, Berkeley; edited by W. H. Somerton, July 16-19, 1969, published 1970

Holditch, S. A., and ELy, J.; "Succesful Stimulation of Deep Wells Using High Proppant Concentrations", J. Pet. Tech. (August, 1973) 959-964

Holditch, S. A., and Morse, R. A.,; "The Effects of Non-Darcy Flow on the Behavior of Hydraulically Fractured Gas Wells", J. Pet. Tech. (October, 1976) 1169-1179

Holditch, S. A.; "Factors Affecting Water Blocking and Gas Flow From Hydraulically Fractured Gas Wells", J. Pet. Tech. (December, 1979) 1515-1524

Howard, G. C., and Fast, C. R.; "Optimum Fluid Characteristics for Fracture Extension", API Drilling and Production Practice, 1959 261-270

Howard, G. C., and Fast, C. R.; Hydraulic Fracturing SPE Monograph Volume 2, 1970

Hubbert, M. K., and Willis, D. G.; "Mechanics of Hydraulic Fracturing", Pet. Trans. AIME (vol. 210, 1957) 153-163

Hunsbedt, A., Kruger, P., and London, A. L.; "Energy Extraction From a Laboratory Model Fractured Geothermal System", J. Pet. Tech. (May, 1978) 712-718

Iwai, K.; Fundamental Studies in Fluid Flow Through a Single Fracture, Ph.D dissertation, University of California, 1976

Jennings, A. R., and Sprawls, B, T.; "Successful Stimulation in the Cotton Valley Sandstone — A Low-Permeability Reservoir", J. Pet. Tech. (October, 1977) 1267-1276

Jones, F. O.; "A Laboratory Study of the Effects of Confining Pressure on Fracture Flow and Storage Capacity in Carbonate Rocks", J. Pet. Tech. (January, 1975) 21-27

Kehle, R. O.; "Determination of Tectonic Stresses through Analysis of Hydraulic Well Fracturing", J. Geophys. Res (vol. 69, 1964) 259

Kiel, O. M.; "A New Hydraulic Fracturing Process", J. Pet. Tech. (January, 1970) 89-96

Komar, C. A., Shuck, L. Z., Overbey, W. K., and Anderson, T. O.; "Delineating a Subsurface Fracture System in a Petroleum Reservoir — An Experiment", J. Pet. Tech. (May, 1973) 531-537

Kretch, W. E., and Chamberlin, P. G.; "New Techniques for Measuring Rock Fracture Energy", Soc. Pet. Eng. J. (June, 1974) 237-242

Krueger, R. F.; "Advances in Well Completion And Stimulation During JPT's First Quarter Century", J. Pet. Tech. (December, 1973) 1447-1462

Mathias, J. P.; "Successful Stimulation of a Thick, Low-Pressure, Water-Sensitive Gas Reservoir by Pseudo-Limited Entry", J. Pet. Tech. (February, 1971) 185-190

Medline, W. L., and Massé, L.; "Laboratory Investigation of Fracture Initiation Pressure and Orientation", Soc. Pet. Eng. J. (April, 1979) 129-144

Morse, R. A., and Von Gonten, W. D.; "Productivity of Vertically Fractured Wells Prior to Stabilized Flow", J. Pet. Tech. (July, 1962) 807-811

Murphy, H. D., Lawton, R. G., Tester, J. W., Potter, R. M., Brown D.W., and Aamodt, R. L.; "Preliminary Assessment of a Geothermal Energy Reservoir Formed by Hydraulic Fracturing", Soc. Pet. Eng. J. (August, 1977) 317-326

Murphy, H. D. , and Tester, J. W.; "Heat Production from a Geothermal Reservoir Formed by Hydraulic Fracturing — Comparison of Field and Theoretical Results", SPE 8265 presented at the 54th Annual SPE Technical Conference held in Las Vagas, Nevada, September 23-26, 1979

Narasimhan, T. N.; A Unified Numerical Model for Saturated-Unsaturated Groundwater Flow, Ph.D dissertation, University of California, Feb., 1975

Narasimhan, T. N., Witherspoon, P. A., and Edwards, A. L.; "Numerical Model for Saturated-Unsaturated Flow in Deformable Porous Media, Part II: The Algorithm" Submitted to Water Resources Research LBL-5932, (March, 1977)

Narasimhan, T. N., and Witherspoon, P. A.; "Recent Developments in Modeling Groundwater Systems", LBL-5209, (May, 1977)

Narasimhan, T. N., and Palen, W. A.; "A Purely Numerical Approach for Analyzing Flow to a Well Intercepting a Vertical Fracture", SPE 7983 presented at the 48th West Coast Regional Meeting of the SPE at Ventura, California, April 18-20, 1979

Nordgren, R. P.; "Propagation of a Vertical Hydraulic Fracture", Soc. Pet. Eng. J. (August, 1972) 306-314

Novotny, E. J.; "Prediction of Stimulation from Acid Fracturing Treatments Uing Finite Fracture Conductivity", J. Pet. Tech. (September, 1977) 1186-1194

Palen, W. A.; The Effects of Temperature, Pressure, and Saturation on the Sonic Velocities and Dynamic Elastic Moduli of Reservoir Sandstones, M.S. thesis, University of California, 1978

Peng, S. S., and Ortiz, C. A.; "Crack propagation and fracture of rock specimens loaded in compression", published in proceedings of an inernational conference on Dynamic crack propagation, edited by G. C. Sih, Lehigh University, 1972

Perkins, T. K., and Krech, W. W.; "Effect of Cleavage Rate and Stress Level on Apparent Surface Energies of Rocks", Soc. Pet. Eng. J. (December, 1966) 308-314

Pierce, A. E., Vela, S., and Koonce, K. T.; "Determination of the Compass Orientation and Length of Hydraulic Fractures By Pulse Testing", J. Pet. Tech. (December, 1975) 1433-1438

Pinder, G. F., and Frind, E. O.; "Application of Galerkin's Procedure to Aquifer Analysis", Water Resources Res., (vol 8, 1972) 108-120

Power, D. V., Schuster, C. L., Hay, R., and Twombly, J.; "Detection of Hydraulic Fracture Oientation And Dimensions in Cased Wells", J. Pet. Tech. (September, 1976) 1116-1124

Raghavan, R.; "Some Practical Considerations in the Analysis of Pressure Data", J. Pet. Tech. (October, 1976) 1256-1268

Raghavan, R.; "Pressure Transient Analysis of a Vertically Fractured Well Produced by Solution Gas Drive", Soc. Pet. Eng. J. (October, 1977a) 369-376

Raghavan, R.; "Pressure Behavior of Wells Intercepting Fractures", Proceedings of the First Invitational Well-Testing Symposium, October 19-21, 1977, LBL-7027 117-160

Sandhu, R. S., and Huang, S. W.; "Application of Griffith's Theory to Analysis of Progressive Fracture Failure", Int. J. of Fracture. (vol. 2, February, 1975)

Secor, D. T.; "Mechanics of Natural Extension Fracturing at Depth in the Earth's Crust", Geological Survey of Canada Research in Tectonics (March, 1968) 3-49

Seidel, W. R., and Stahl, E. J.; "Gas Well Stimulation with a Viscous Water-Base Fracturing Fluid", J. Pet. Tech. (November, 1972) 1385-1390

Sinclair, A. R.; "Rheology of Viscous Fracturing Fluids", J. Pet. Tech. (June, 1970) 711-719

Sinclair, A. R., Terry, W. M., and Kiel, O. M.; "Polymer Emulsion Fracturing", J. Pet. Tech. (July, 1974) 731-738

Smith, M. B., Holman, G. B., Fast, C. R., and Covlin, R. J.; "The Azimuth of Deep, Penetrating Fractures in the Wattenburg Field", J. Pet. Tech. (February, 1978) 185-193

Spilhaus, A. F., "Hot Dry Rock at Fenton Hill", Trans. Am. Geophys. (November 27, 1979)

Sneddon, I. A.; Fourier Transforms, McGraw-Hill, 1951

Strubhar, M. K., Fitch, J. L., and Glenn, E. E.; "Multiple, Vertical Fractures From an Inclined Wellbore — A Field Experiment", J. Pet. Tech. (May, 1975) 641-647

Tannich, J. D.; "Liquid Removal From Hydraulically Fractured Gas Wells", J. Pet. Tech. (November, 1975) 1309-1317

Tetleman, A. S., and McEvily, A. J.; Fracture of Structural Materials, John Wiley and Sons, 1967

Thomas, P. D., and Lombard, C. K.; "Geometric Conservation Law and its Application to Flow Computations on Moving Grids", AIAA Journal (vol. 17, no. 10) 1030-1037

Uraiet, A., Raghavan, R., and Thomas, G. W.; "Determination of the Orientation of a Vertical Fracture by Interference Tests", J. Pet. Tech. (January, 1977) 73-80

Vairogs, J., and Rhoades, V. W.; "Pressure Transient Tests in Formations Having Stress-Sensitive Permeability", J. Pet. Tech. (August, 1973) 965-970

van Everdingen, A. F., and Meyer, L. J.; "Analysis of Buildup Curves Obtained After Well Treatment", J. Pet. Tech. (April, 1971) 513-525

van Domselaar, H. R., and Visser, W.; "Proppant Concentration in and Final Shape of Fractures Generated by Viscous Gels", Soc. Pet. Eng. J. (December, 1974) 531-536

van Poolen, H. K.; "Productivity vs. Permeability Damage in Hydraulically Produced Fractures", API Drilling and Prod. Pract. 1957 103-110

von Schonfeldt, H, and Fairhurst, C.; "Field Experiments in Hydraulic Fracturing", Soc. Pet. Eng. J. (February, 1972) 69-77

White, F. M., Viscous Fluid Flow, McGraw-Hill, 1974

Williams, B. B.; "Fluid Loss from Hydraulically Induced Fractures", J. Pet. Tech. (July, 1970) 882-888

Williams, B. B., and Nierode, D. E.; "Design of Acid Fracturing Treatments", J. Pet. Tech. (July, 1972) 849-859

Williams, B. B., Nieto, G., Graham, H. L., and Leibach, R. E.; "A Staged Fracturing Treatment for Multisand Intervals", J. Pet. Tech. (August, 1973) 897-904

Zoback, M. D., Healy, J. H., and Roller, J. C.; "Preliminary Stress Measurements in Central California Using the Hydraulic Fracturing Technique", Pure and Applied Geophysics (vol. 115, 1977) 135-152

Zoback, M. D.; "A Simple Hydraulic Fracturing Technique for Determining Fracture Toughness" Science, 1978

Zoback, M. D., and Pollard, D. D.; "Hydraulic Fracture Propagation and the Interpretation of Pressure-Time Records for In-situ Stress Measurements", 19th U.S. Symposium on Rock Mechanics, University of Nevada, 1978 14-22

Zoback, M., Roller, J., Svitek, J., and Seeburger, D.; "Hydraulic Fracturing Stress Measurements and the Magnitude of Shear Stress on the San Andreas Fault in Southern California", in press, J. Geophys. Res. 1980

APPENDICES

A. Derivation of the Fluid Leakoff Coefficient

The solution to the problem of one-dimensional transient fluid flow into a semi-infinite solid with an initial condition, $P(y,0) = P_b$, and boundary conditions, $P(0,t) = P_{ext}$; $P(\infty,t) = P_b$, is given by Equation (A1) (Carslaw and Jaegar, 1959)

$$P(y,t) = (P_{ext} - P_b)\ \mathrm{erfc}\{y/(2\sqrt{kt/\phi\mu c})\} + P_b \tag{A1}$$

where the complementary error function, $\mathrm{erfc}(\beta)$, is defined as $1 - \mathrm{erf}(\beta)$ and $\mathrm{erf}(\beta) = 2/\sqrt{\pi} \int_0^{\beta} \exp(-u^2)\, du$. The flow into the formation face is found by application of Darcy's law

$$q = -\frac{k}{\mu}\frac{\partial P}{\partial y}\Big)_{y=0} = -\frac{k}{\mu}\nabla P \tag{A2}$$

Taking the derivitive of Equation (A1) and substituting into Equation (A2) yields

$$q = \frac{k}{\mu}\frac{(P_{ext} - P_b)}{\{\pi kt/\phi\mu c\}^{1/2}} = \frac{C}{\sqrt{t}} \tag{11}$$

For the range of values used in Table 3 the value of C varies between $4.475\cdot10^{-8} - 9.25\cdot10^{-5}$ m/$\sqrt{\text{sec}}$ ($1.13\cdot10^{-6} - 2.35\cdot10^{-3}$ ft/$\sqrt{\text{min}}$) which are in the low range of values given by Williams (1970). Note this equation will holds only if $(p_{ext} - P_b)$ is constant. Variable fluid pressure in the fracture makes the fluid leakoff coefficient only an approximation.

B. Kiel's Equations

Kiel (1970) derived the following equations to express the aperture of the fracture as a function of the fracture length

$$w = \frac{4L(1-\nu^2)\,\overline{P_{ext}}}{\pi E}\left(\cos\Theta \ln\left\{\frac{\sin(\Theta - \Theta_o)}{\sin(\Theta + \Theta_o)}\right\} + \cos\Theta_o \ln\left\{\frac{\tan\{(\Theta + \Theta_o)/2\}}{\tan\{(\Theta - \Theta_o)/2\}}\right\}\right) \quad \text{(A3)}$$

where $x/l = \cos\Theta$

and $\Theta_o = \pi/2(1 - S_h/\overline{P_{ext}})$.

The equation relating the fracture length with total fracture volume can be expressed as

$$L = \left(\frac{V_f E}{2(1-\nu^2)h\overline{P_{ext}}\sin(\pi S_h/\overline{P_{ext}})}\right)^{.5} \quad \text{(A4)}$$

where V_f is the volume of the fracture.

C. Nordgren's Equations

Nordgren's (1972) dimensionless constants for length, L_D, time, t_D, and aperture, w_D, are

$$L_D = \pi \left[\frac{(1 - \nu)\,\mu\, Q^5}{256\, C^8\, G\, h^4}\right]^{1/3} \times L \quad \text{(A5)}$$

$$t_D = \pi^2 \left[\frac{(1 - \nu)\,\mu\, Q^2}{32\, C^5\, G\, h}\right]^{2/3} \times t \quad \text{(A6)}$$

$$w_D = \pi \left[\frac{16\,(1 - \nu)\,\mu\, Q^5}{C^2\, G\, h}\right]^{1/3} \times w \quad \text{(A7)}$$

Nordgren's approximate solutions for fracture growth as a function of time are for the case of no fluid loss (or small T_D)

$$L_D(T_D) = 1.32\ T_D^{4/5}\ ,\quad w_D(0,T_D) = T_D^{1/5} \qquad \text{(A8), (A9)}$$

and for large fluid loss (or large T_D)

$$L_D(T_D) = .637\ T_D^{1/2}\ ,\quad w_D(0,T_D) = .798\ T_D^{1/8} \qquad \text{(A10), (A11)}$$

D. Gringarten's Solutions

The analytical solution for the pressure drop in a well intercepting an infinite conductivity vertical fracture is given by Equation (A12) (Gringarten, et al., 1974)

$$P_{wD} = {}^1/_2\ \sqrt{\pi T_{Df}}\ \left(\mathrm{erf}\{\frac{.134}{\sqrt{T_{Df}}}\} + \mathrm{erf}\{\frac{.866}{\sqrt{T_{Df}}}\}\right) - .067\ E_i\{-\frac{.018}{T_{Df}}\} - .433\ E_i\{-\frac{.75}{T_{Df}}\} \qquad \text{(A12)}$$

where $E_i(\beta)$ is the exponential integral defined as $-E_i(\beta) = \int_0^\beta \exp(-u)/u\ du$.

The solution for the pressure drop of a well intercepting a uniform flux vertical fracture located in a semi-infinite reservoir is

$$P_{wD}(T_{Df}) = \sqrt{\pi T_{Df}}\ \mathrm{erf}(1/2\sqrt{T_{Df}}) - {}^1/_2\ E_i(-1/4T_{Df}) \qquad \text{(A13)}$$

where all terms are as defined above.

E. Development of the Integral Finite Difference Method

The potential or diffusion equation is a parabolic partial differential equation. For porous media the general form of the diffusion equation can be expressed as

$$S + \nabla\left(\frac{k}{\mu}\right)\nabla\Psi = \phi c \frac{\partial\Psi}{\partial t} \tag{A14}$$

where Ψ is the fluid potential,

S is a volumetric source or sink term,

P is the fluid pressure,

g is the acceleration of gravity,

ρ is the fluid density,

z is the elevation,

k is the rock permeability,

ϕ is the porosity,

μ is the fluid viscosity, and

c is the total compressibility of the saturated porous media.

Integrating Equation (A14) over the volume of an arbritrary volume element located in the flow region gives

$$\iiint_V S\, dV + \iiint_V \nabla\left(\frac{k}{\mu}\right)\nabla\Psi\, dV = \phi c \iiint_V \frac{\partial\Psi}{\partial t}\, dV \tag{A15}$$

For a fixed volume size neither the source term or the time derivative are dependent on the volume integration and can be taken outside of the integral sign. The Green's theorem expresses the volume integral with an equivalent surface integral as

$$\iiint_V \nabla\left(\frac{k}{\mu}\right)\nabla\Psi\, dV = \frac{k}{\mu} \iint_S \nabla\Psi \cdot d\tilde{s} \tag{A16}$$

where $d\tilde{s} = \tilde{n}ds$, and $\tilde{n}$ is the outward normal from the surface area ds.

Equation (A15) becomes substituting for the volume integration

$$SV + \iint_s \frac{k}{\mu} \nabla\Psi \cdot d\tilde{s} = dcV \frac{\partial\Psi}{\partial t} \tag{A17}$$

Substituting Darcy's law in the form of Equation (A2) the equation becomes

$$SV + \iint_s q.nd\tilde{s} = \phi cV \frac{\partial\Psi}{\partial t} \tag{A18}$$

Equation (A18) states, in integral form, that the time rate of change in the fluid potential, Ψ, averaged over an elemental volume, V, is equal to the sum of both the normal flux of fluid over the area of the volume element and the fluid generated by source terms located within the element. This is a mathematical statement of the principle of mass conservation. Using the finite difference linear approximation of the gradient of fluid potential and for the change in fluid potential in the nodal element , 1, over the time Δt Equation (A18) can be expressed for the nodal volume. The integral finite difference equation becomes Equation (26)

$$S_1V_1 + \sum_{i=1}^{n} \frac{k_i(P_i - P_1 + \rho g(z_i - z_1))A_{i,1}}{\mu_i \; D_{i,1}} = \frac{(\phi c)_1 V_1 (P_{1_{t+\Delta t}} - P_{1_t})}{\Delta t} \tag{26}$$

where all terms are defined as above.

ACKNOWLEDGEMENT

This work was supported by the Assistant Secretary for Conservation and Renewable Energy, Office of Renewable Technology, Division of Geothermal and Hydropower Technologies of the U.S. Department of Energy under Contract W-7405-ENG-48.

This report was done with support from the Department of Energy. Any conclusions or opinions expressed in this report represent solely those of the author(s) and not necessarily those of The Regents of the University of California, the Lawrence Berkeley Laboratory or the Department of Energy.

Reference to a company or product name does not imply approval or recommendation of the product by the University of California or the U.S. Department of Energy to the exclusion of others that may be suitable.

TECHNICAL INFORMATION DEPARTMENT
LAWRENCE BERKELEY LABORATORY
UNIVERSITY OF CALIFORNIA
BERKELEY, CALIFORNIA 94720